SOVIET PHYSICS USPEKHI VOLUME 7, NUMBER 4 JANUARY-FEBRUARY 1965
538.113

ELECTRON PARAMAGNETIC RESONANCE IN SILICON AND GERMANIUM

L. D. BOGOMOLOVA, V. N. LAZUKIN, and I. V. CHEPELEVA

Usp. Fiz. Nauk 83, 433-502 (July, 1964)

THE nature of the solid state is one of the most important problems of modern physics. Its solution is approached by physicists along different paths and by different methods.

During the last decade and a half solids have been extensively investigated by radio-spectroscopy methods, particularly by electron paramagnetic resonance (EPR) and electron nuclear double resonance (ENDOR). The study of crystal semiconductors by the EPR method began in 1953. The EPR and double-resonance methods have made it possible to study many interesting properties of semiconductor crystals and the physical processes occurring in them. Thus, for example, the EPR of shallow donors and acceptors has provided the answer to several questions connected with the position of the impurity atom in the crystal lattice, and with the structure of the energy bands in these substances. Experiments on the EPR of shallow donor and acceptor states constitute the basis of the theory of Kohn and Luttinger which has made it possible to map out wave functions for these states. The EPR of shallow donors in silicon helps solve one of the most interesting problems in solid state—that of the interaction between the crystal-lattice waves and the magnetic moments of the electrons in the nuclei. A combination of experiments on the EPR of shallow donors in silicon with experiments on photoconductivity has answered several questions connected with the kinetics of the transitions between impurity atoms. EPR and ENDOR were used to study the interaction between impurities and vacancies in lattices and the structure and production of radiation defects in silicon crystals bombarded by high-energy electrons and fast neutrons. Interesting results were obtained by observation of EPR with the crystal deformed or placed in an electric field.

In this survey we discuss EPR of impurities that produce shallow and deep levels in silicon and germanium, and also the EPR of radiation defects resulting from irradiation of crystals. It must be noted, however, that the EPR method is already in use for the investigation of binary and vitreous semiconductors. It will undoubtedly play an important role in research on the nature of semi-conductivity of noncrystalline semiconductors. A study of the EPR of semiconducting crystals is of interest in quantum radioelectronics.

This article reviews work published up to 1963. It is impossible to discuss here the techniques and the capabilities of EPR in general. Those interested are referred to the books "Electron Paramagnetic Resonance" by S. A. Al'tshuler and B. M. Kozyrev, "Paramagnetic Resonance in Solids" by W. Low, "Masers" by Singer, etc., and also to the collection "Electron Paramagnetic Resonance in Semiconductors" (IL. 1962).

I. FIRST EXPERIMENTS ON THE EPR OF SHALLOW DONORS IN SILICON. THE THEORY OF KOHN AND LUTTINGER

In 1953 Portis et al[1] first observed EPR of the conduction electrons of n-type silicon crystals: the resonance spectrum consisted of one line with a g-factor close to that of the free electron. Somewhat later Fletcher et al[2,3] succeeded in observing EPR of electrons localized on donors.

In Fletcher's experiments, which were made at liquid-helium temperature with crystals of silicon doped with arsenic (nuclear spin $I = 3/2$) and phosphorus ($I = 1/2$), the spectrum hyperfine structure due to the magnetic interaction of the unpaired electrons with the spins of the donor nuclei was resolved. The widths of the hyperfine structure lines ($2I + 1$ in number) and the distances between them were measured. These experiments, as well as later ones on silicon doped with lithium[4], were devoted to the inhomogeneous resonance line broadening, due to the interaction of the donor electron with the nuclei of the silicon magnetic isotope Si^{29} ($I = 1/2$, natural abundance 4.68%). Experiments on samples of silicon with increased content of Si^{28} (99.88% ± 0.08%) have shown that the broadening of the resonance lines is due to the above-mentioned interaction, since the width of the EPR lines of the phosphorus donors in the purified silicon amounted to 0.22 Oe, whereas for ordinary crystals it amounted to 2.5 Oe[5].

These first experiments yielded the following qualitative picture: when elements of group V are introduced into the crystal of the tetravalent silicon, the introduced atoms, occupying the lattice sites, form four covalent bonds with the neighboring Si atoms. Participating in the production of these bonds are four of the five valence electrons of the impurity atom, while the fifth remains with unpaired spin and makes paramagnetic resonance absorption possible. At low temperatures, the unpaired electron is more strongly bound to the donor atom, whose nuclear magnetic field produces the slight splitting of the EPR line, observed in the experiment as a hyperfine structure. A weaker interaction of the unpaired electrons with the Si^{29} nuclei produces only an inhomogeneous broadening of the resonance line.

At room temperatures the donor is ionized and the electron is in the conduction band; however, if the impurity atom concentration exceeds 10^{17}—10^{18} cm^{-3}, a considerable part or even all the donor electrons will be in the impurity conduction band at helium temperatures. They will produce an EPR spectrum consisting of a single line with a g-factor close to that for the free electron. The effect of the transition of the unpaired electrons from the donor levels to the impurity conduction band on the character of the EPR spectrum was investigated in[6,7].

If the impurity concentration is sufficiently high (above 10^{16} cm^{-3}), the impurity atoms, being close to one another, can form pairs whose electron spins are strongly bound by exchange forces. In this case two electrons act like a single effective electron situated in the average field of two nuclei. Consequently an additional line, of lower intensity, will be observed between the hyperfine structure lines. With increasing impurity concentration, more and more complicated groups of impurity atoms are formed. Accordingly, the number of additional lines increases (Fig. 1). When the impurity concentration reaches 10^{18} cm^{-3} and more, the intermediate lines merge into one, and the components of the hyperfine structure vanish completely, thus offering evidence that the majority of electrons go over from the donor levels into the impurity conduction band.

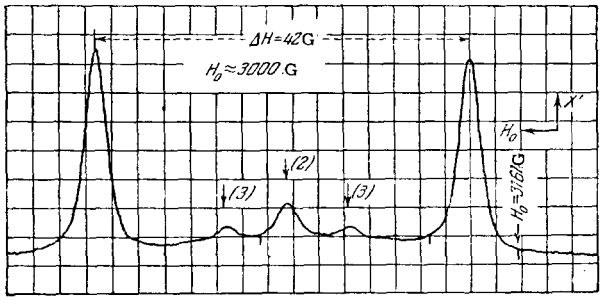

FIG. 1. Spectrum of P donors in Si at T = 1.2° K (P concentration ≈ 10^{17} cm^{-3}). Three weak lines due to exchange interaction are seen between the two intense hyperfine structure lines. The parentheses contain the number of the atoms whose exchange interaction leads to the appearance of the corresponding line.

EPR in semiconductors is characterized by very large relaxation times, which reach tens of minutes or even hours in some cases. These times are strongly influenced by many factors, such as impurity concentration, temperature, magnetic field intensity, number of electrons in the conduction band, etc. The EPR line intensities and the relaxation times depend to a great degree on the purity of the specimen, on its surface finish, and on various lattice defects. Exposure to light exerts an appreciable influence.

The qualitative picture of the EPR in silicon with shallow donor impurities, disclosed by the first experiments, was subsequently convincingly verified in the theoretical papers of Kohn and Luttinger[8,9-11]. The theory they developed for the donor states in silicon and germanium with impurity atoms of low ionization energy (0.10—0.05 eV) (P, As, Sb, etc.) has made it possible to determine the wave functions and the energy spectrum of the unpaired electrons of the donor atoms, and prepare the ground for further calculations of such spectral characteristics as the hyperfine splitting, g-factor, and also the relaxation times. The shallow donor states in Si and Ge are described by hydrogen-like wave functions with large effective radii. Thus, for silicon the "Bohr" radius a* is equal to 21 Å (lattice constant a = 5.42 Å), and for germanium the values are a* = 45 Å and a = 5.62 Å. These large dimensions of the region of localization of the impurity states are due to the high dielectric constant of the crystals (κ_{Si} = 12, κ_{Ge} = 16) and the low effective masses of the carriers. As is well known, the state of the conduction electrons in an ideal crystal can be described with the aid of the Bloch functions, which are solutions of the Schrödinger equation with the periodic potential V(r) produced by the crystal lattice. For localized impurity electrons the Schrödinger equation is written in the form

$$\left[-\frac{\hbar^2}{2m}\nabla^2 + V(\mathbf{r}) + U(\mathbf{r}) - E\right]\Psi(\mathbf{r}) = 0, \qquad (1.1)$$

where U(r)—additional potential resulting from replacing the silicon atom by a donor atom. If the orbit of the donor electron is sufficiently large compared with the lattice constant, then the perturbing potential U(r) can be represented in the Coulomb form

$$U(\mathbf{r}) = -\frac{e^2}{\varkappa r}, \qquad (1.2)$$

where κ—static dielectric constant* and the origin is at the donor nucleus.

Expression (1.2) is not applicable near the impurity-atom nucleus (for small r). It is likewise not completely correct at large r, owing to the screening caused by the interaction of the electrons with one another. The effect of the donor-ion Coulomb field on the donor electron is greatly weakened by the large dielectric constant of the medium. Owing to the large dimensions of the region of their localization, we can apply to the impurity states the effective-mass method, in which the effect of the lattice is taken into account by introducing the electron effective-mass tensor in place of its free-space mass m.

The wave functions of the localized electron, which are solutions of (1.1), are constructed from the Bloch functions for the bottom of the conduction band. It is known that the conduction band in Si has in wave-vector space six equivalent energy minima, located on the six [100] axes. If the coordinates of the point of the

*It is shown in [11] that the use of the static dielectric constant is perfectly admissible because of the slower motion of the impurity electron, compared with the other electrons of the crystal.

minimum on the [100] axis are denoted by $\mathbf{k}_1(\mathbf{k}_0, 0, 0)$, then the equation of the equal-energy surface in the vicinity of this point can be written in the form

$$E_j = E_0 + \frac{\hbar^2}{2m_1}(k_{jx} - k_0)^2 + \frac{\hbar^2}{2m_2}(k_{jy}^2 + k_{jz}^2), \quad (1.3)$$

where the effective masses are $m_1 = 0.98m$ and $m_2 = 0.19m$. These surfaces are ellipsoids, with principal axes directed along [100], [101], etc.

Assuming that (1.2) and (1.3) hold, Eq. (1.1) has as solutions

$$\chi_j = F_j(\mathbf{r})\,\psi(\mathbf{k}_j, \mathbf{r}). \quad (1.4)$$

Here $\psi(\mathbf{k}_j, \mathbf{r}) = u(\mathbf{r})\exp(i\mathbf{k}\cdot\mathbf{r})$ is the Bloch function corresponding to the minimum of energy at the point $\mathbf{k}_j$ (it is assumed that this minimum is not degenerate); the modulating function F_j is the solution of the hydrogen-like Schrödinger equation with effective masses m_1 and m_2, which is transformed from (1.1) with the aid of (1.3). This equation enables us to obtain the spectrum of the eigenvalues ϵ_n^* which characterize both the bound ground state and a whole series of excited states.*

The functions $F_j(\mathbf{r})$ change little within the unit cell. The normalization integral for the functions $F_j(\mathbf{r})$ is taken over the entire space (for the Bloch functions—over the unit cell). Only in the case of small variation of the function $F_j(\mathbf{r})$ can the effective-mass approximation be used in this problem. A solution in the form

$$F_j(\mathbf{r}) = (\pi\tilde{a}^2\tilde{b})^{-1/2}\exp\left[-\left(\frac{x_j^2}{\tilde{b}^2} + \frac{y_j^2 + z_j^2}{\tilde{a}^2}\right)^{1/2}\right] \quad (1.5)$$

with corresponding choice of the parameters $\tilde{a}$ and $\tilde{b}$ for all $m_2/m_1 < 1$ makes it possible to account sufficiently well for the experimental results. Owing to the anisotropy of the effective mass, the functions $F_j(\mathbf{r})$ have no spherical symmetry and are slightly elongated in the y_j and z_j directions, compared with x_j, to which a heavier effective mass m_1 corresponds. The phases of the functions χ_j are chosen all real and equal at the origin.

Let us consider the ground state. Inasmuch as there are six equivalent minima, there are six solutions of the form (1.4), corresponding to six different k_j but belonging to the same eigenvalue ϵ_0^*. The complete solution is given by a linear combination of these six degenerate solutions:

$$\Psi_0(\mathbf{r}) = \frac{1}{\sqrt{6}}\sum_{j=1}^{6}\chi_j(\mathbf{r}) = \frac{1}{\sqrt{6}}\sum_{j=1}^{6}F_j(\mathbf{r})\,\psi(\mathbf{k}_j, \mathbf{r}). \quad (1.6)$$

The six-fold degeneracy of the ground state is partially lifted by introducing corrections to the effective-mass method. Purely formally, however, without account of the corrections, the remaining degeneracy can be established uniquely from the symmetry of the Hamiltonian of the impurity states, which is invariant under the transformations of the point group of the tetrahedron T_d with the donor atom at the center. Obviously, the six degenerate functions χ_j form a basis for the representation R of the group T_d, which has five classes.* Comparison of the characters of the representation {1s} and of the indicated five irreducible representations shows that {1s} breaks up into a sum of three representations (1-, 2- and 3-dimensional):

$$\{1s\} = A_1 + E + T_1. \quad (1.7)$$

Thus, owing to the symmetry properties of the intracrystalline field, the six-fold degeneracy of the ground state is partially lifted and singlet, doublet, and triplet states arise. According to the Kramers theorem, the singlet state is doubly degenerate in the spin, and, as shown by EPR experiments, is the ground state. The linear combinations corresponding to the different irreducible representations (1.7) are written in the form

$$\Psi_{0i} = \sum_{j=1}^{6}\alpha_i^{(j)}\chi_j \quad (i = 1, 2, \ldots, 6), \quad (1.8)$$

where $j = 1, \ldots, 6$ corresponds to different minima $(k_0, 0, 0)$, $(-k_0, 0, 0)$ ... $(0, 0, -k_0)$, and the coefficients $|\alpha^{(j)}|^2$ characterize the probability of finding the electron at the j-th minimum. Out of the six 1s wave functions, only the nondegenerate function Ψ_{01} has a finite value on the donor nucleus ($r = 0$). Because of this, the greatest hyperfine splitting should be observed for the singlet state, as is indeed confirmed experimentally.

In order to check how well the wave function Ψ_{01} [which coincides with (1.6)] describes the ground state, the hyperfine splitting was calculated in [8]. The total hyperfine splitting (i.e., the distance over the field between the extreme lines of the multiplet) is

$$(\Delta H) = \frac{16\pi}{3}|\Psi_{01}(0)|^2\mu_D. \quad (1.9)$$

If the moment μ_D of the donor nucleus is known, then the determination of the hyperfine splitting reduces to a calculation of $|\Psi_{01}(0)|^2$. On the other hand, knowing (ΔH) from experiment, we can find the experimental value of $|\Psi_{01}(0)|^2$. The values of $|\Psi_{01}(0)|^2$ were estimated approximately from the experimental values of the ionization energy. The calculations thus yielded a phosphorus donor $|\Psi_{01}(0)|^2 \approx 0.4 \times 10^{24}$ cm^{-3}, whereas the measurements yielded $|\Psi_{01}(0)|^2 = 0.44 \times 10^{24}$ cm^{-3}. The good agreement shows that the ground state is a singlet one and is described by the function Ψ_{01}. Inasmuch as only the singlet state has a finite probability of being located at the point of the nucleus, it is separated in energy from the doublet and triplet states. This splitting depends on the type of impurity [12,13]. The

*The existence of excited states was confirmed by infrared absorption experiments [10].

*This representation reduces to five irreducible representations A_1, A_2, E, T_1, and T_2 of group T_d: $R = n_1A_1 + n_2A_2 + n_3E + n_4T_1 + n_5T_2$, where the integers n represent the number of levels with degeneracy of the corresponding multiplicity.

corresponding term in the Hamiltonian $\mathcal{H}_{e0}$, which gives rise to the interaction that leads to the splitting (essentially a spin-orbit interaction), has been represented in the form of a matrix, which we do not reproduce here (see[29]). Its matrix elements Δ_c characterize the splitting due to the spin-orbit interaction for an electron situated in the k-space region near one minimum. If this matrix is made to operate on different linear combinations of the wave functions (1.8), we find that the spacing between the singlet and doublet is $E_{12} = 6\Delta_c$, and the splitting between the doublet and triplet is much smaller, $E_{23} = 2\delta\Delta_c$ (δ is small and positive). The excited doublet and triplet states play an important role in different phenomena in silicon at low temperatures, for example, in interactions between the spin system and the lattice phonons.

II. SOME DISTINGUISHING FEATURES OF SEMICONDUCTOR EPR RESEARCH PROCEDURES

EPR can be observed in a semiconductor crystal containing some impurity, as a rule, only at helium temperatures. However, even at such temperatures semiconducting materials have a rather high conductivity, and this leads to large dielectric losses of microwave power and to a corresponding reduction in the Q of the radiospectroscope cavity. This imposes very stringent requirements on the construction of the radiospectroscope, and particularly on its sensitivity.

The sensitivities of different radiospectroscope systems were estimated by Feher[14]; we shall indicate only briefly what spectroscope systems were used in EPR experiments on semiconductors.

A comparison of the different types of spectroscopes shows that the greatest sensitivity is possessed by: a) balanced-bridge spectrometers with bolometer detectors operating at low magnetic-field modulation, and b) superheterodyne spectroscopes with crystal detectors operating both with and without magnetic-field modulation. The use of a balanced bridge as the essential spectroscope element in either type makes it possible to operate both in absorption (χ'') and dispersion (χ'),[15] depending on whether the bridge is balanced in phase or in amplitude. This is a very valuable property when working with semiconductors, which as already noticed, show rather long relaxation times. If the spin-spin and spin-lattice relaxation times are long, the bridges are usually tuned for dispersion and the signal is observed under conditions of fast adiabatic passage. This is readily realized with either spectroscope type. In many experiments, particularly in double-resonance experiments where higher sensitivity is required, the method of low modulation of the magnetic field is used, with a frequency 100—1000 cps and an amplitude 0.5—1.0 Oe. To reduce the noise at this frequency, rigid coupling with the resonator is used when tuning for absorption.

In most work with semiconductors, the unloaded Q of the cavity was not less than 5000, reaching 20,000 in individual cases. In many cases the cavity construction affords a possibility of exposure to light, which exerts an appreciable influence on the relaxation time. Many investigations were made by the double resonance method, where the semiconductors must be acted upon by magnetic fields with frequencies that stimulate both electronic and nuclear transitions. The radio-frequency field for the nuclear transitions is applied with a loop or a small coil[12] through an opening in one of the cavity walls.

Cavities were built[16] in the form of quartz cylinders coated on the inside with a thin layer of silver; a helix of very small pitch was cut over this layer with a diamond cutter. The generator leads are soldered to the end of the silver helix. The radio-frequency field produced in the cavity by such a helix is somewhat weaker than that produced by a copper coil of equal size.

An essential factor in the success of the experiment is a correct relation between the dimensions of the specimen and the cavity. An increase in the volume of the specimen leads, on the one hand, to an increase in the signal, since the number of paramagnetic centers is increased, and on the other hand to increased losses, lower cavity Q, and by the same token a weaker signal. Calculations show that the optimum specimen volume is such that the cavity Q is 2/3 of its unloaded value. The investigated semiconductor specimens usually were of the order of 100 mm^3.

The choice of the spectroscope operating frequency was based on the following considerations. It is known that higher frequencies lead to an increase in sensitivity, since the minimum number of spins observed with the spectroscope is usually inversely proportional to $\omega^{7/2}$. At the same time, the power output of a microwave source decreases rapidly with increasing frequency, and this cancels out the gain due to the increased frequency. On the other hand, to obtain very narrow lines, which are usually used in the case of semiconductors, high stability and homogeneity of the magnetic field are necessary, and these are much easier to realize at low frequencies. The most useful spectroscope turned to operate at 9000 Mcs ($\lambda \approx 3$ cm); some of the investigations were made at 14,000 Mcs ($\lambda \approx 2$ cm) and 24,000 Mcs ($\lambda \approx 1.25$ cm).

The long semiconductor relaxation times and the appreciable dielectric losses make it necessary to carry out the EPR observation at helium temperatures (1.25—4.2° K) and (much less frequently) at hydrogen temperatures (14—20° K).

In most cases the observation of EPR is at a slow passage[17], where the time necessary to pass through the resonance line is much longer than the relaxation time. Then, if the apparatus is of sufficiently good quality, the shape of the observed resonance signal duplicates the shape of the distribution of the spin packets. In the examined semiconductor materials,

which give inhomogeneously broadened lines, and also many other cases, the picture becomes much more complicated if the long relaxation time makes the passage through the resonant line "fast," i.e., occurring within a time much shorter than the relaxation time. It is then necessary to account for many factors to interpret the experimental results correctly.

In connection with the timeliness of this problem, a thorough study was made both of the possible methods of observing EPR, and of the associated "passage effects"[18,19]. In[19] are considered different methods of observing EPR lines in a system described by Bloch's equations (i.e., for which spin diffusion etc. can be neglected). It was shown that to interpret the shape and amplitude of an inhomogeneously broadened line, observed if the magnetic field varies like $H = H_0(t) + H_m \cos \omega_m t$, it is necessary to know not less than seven parameters (with dimension of frequency):

$$\frac{1}{T_1}, \quad \frac{1}{T_2}, \quad \gamma \Delta H, \quad \gamma H_1, \quad \gamma H_m, \quad \omega_m, \quad \frac{1}{H_1}\frac{dH_0}{dt},$$

where T_1 and T_2—spin-lattice and spin-spin relaxation times, γ—gyromagnetic ratio, ΔH—half-width of the resonance curve, H_1—amplitude of the high-frequency field, H_m and ω_m—amplitude and frequency of the modulation field. The signal shape depends on the ratio of these parameters and can be very complicated. An analysis of the solutions of Bloch's equations for different ratios of these parameters shows that 11 methods of observing EPR signals are possible, most of them already realized experimentally (the investigations were carried out with a silicon sample, doped with phosphorus of concentration 1.7×10^{16} cm^{-3}, at various temperatures, microwave power levels, modulation frequencies, etc.). An estimate was made of the form and magnitude of the χ' and χ'' signals for these cases, and various "passage effects" were also considered, as well as the conditions under which the "unperturbed" lines were observed and the resonant signals had a maximum. Which method is the most effective depends on what information it is desired to obtain in the particular case.

It was noted[19] that in the observation of EPR it is important to distinguish between truly physical effects, explained in terms of the theory of fast passage (when tuning to χ' in adiabatic fast passage, for example, such effects are various phase shifts of the dispersion curves relative to the modulating field, a line shape similar not to the dispersion derivative but to the absorption line shape, etc.), from false passage "effects" (for example, the broadening and splitting of the lines if the speed of passage, characterized by H_m or by dH_0/dt, is incorrectly chosen), which can be eliminated in most cases.

Without stopping to discuss all possible methods of observation and the "passage effects," let us consider only those which were used and allowed for[12,20] for the EPR of donors in silicon. Let us dwell briefly on the effect of line broadening.

In semiconducting materials with large relaxation times, EPR is usually observed, using adiabatic fast passage (AFP)[17], by registering the dispersion signal χ', i.e., the magnetization component in phase with the microwave field H_1 (the absorption signal is negligibly small under such conditions[19]). If the AFP is effected by varying the magnetic field, then the following condition should be satisfied

$$\frac{dH_0}{dt} \ll \gamma H_1^2. \tag{2.1}$$

In adiabatic variation of the field, the angle between the magnetic moment and the effective magnetic field acting on the spins remains invariant in the coordinate system which rotates at microwave frequency ω.[21] Because of this, AFP is accompanied in the ideal case by total inversion of the level populations, and the direction of the magnetization vector is reversed, its absolute magnitude remaining constant.*

If this method is used to observe inhomogeneously broadened lines, their experimentally-obtained shape may differ appreciably from the distribution of the spin packets†, which can be described[1] by means of a function h satisfying the normalization condition

$$\int_{-\infty}^{+\infty} h(H_i - H_0)\, dH_i = 1. \tag{2.2}$$

Here H_i—resonant magnetic fields for different spins, due to the magnetic interaction between donor electrons and different aggregates of Si^{29} nuclei situated inside the electron orbits and responsible for the broadening. In[12] is given an expression for the projection of the magnetization $M_x(H)$ (due to all the spins) on the H_1 direction in a coordinate system that rotates around H_0 with angular velocity ω[21] (this corresponds to registration of the dispersion under the AFP conditions). An analysis of this expression for the case when the distribution curve $h(H_i - H_0)$ is a Gaussian function (with half-width ΔH) shows that for very small fields H_1 the envelope of $M_x(H)$ also has a Gaussian form. The larger H_1 (i.e., the better the condition (2.1) is satisfied), the more the observed line shape differs from the spin-packet distribution, and the closer H_1 is to ΔH. Calculation of the broadening has shown, for example, that for $\Delta H/H_1 = 10^3$ the observed line width ΔH_{obs} is 8% larger than the width of the curve describing the distribution of the spin packets, and for $\Delta H/H_1 = 10^{10}$ it is approximately 30% larger.‡

*A detailed explanation of AFP is given in J. R. Singer's book "Masers," N.Y. 1959.

†A spin packet is an aggregate of spins with close resonant fields, with the absorbed energy uniformly distributed within the aggregate. Consequently, the inhomogeneously broadened line can be regarded as consisting of a set of narrow homogeneously broadened lines corresponding to the aggregate of spin packets.

‡It must be noted that this line-broadening effect does not occur in the case of AFP of homogeneously broadened lines.

Depending on the relaxation time, Feher[12] realized two methods of observing signals under AFP conditions, nonstationary and stationary. The first was used in ENDOR investigations, and the second for a study of EPR line shape and width.

After a certain number of passages (i.e., modulation cycles), saturation causes the magnetization to tend to a stationary value; the condition for this is the equality $M_i(N-1) = M_i(N+1)$, where N—number of modulation cycles, and M_i—magnetization produced by spins whose resonant fields are equal to H_i. If this condition is not satisfied (for example, at the instant when the microwave power is turned on), then the magnetization does not reach its equilibrium value.

When a signal was registered, in both cases the AFP conditions were satisfied for the modulating field ($\omega_m H_m^2 \ll \gamma H_1$, $\omega_m \gg 1/T_2$), and the amplitude of this field was much smaller than the spin-packet line width ($H_m \gg H_1$). If the resonant line passage time is shorter than the relaxation time (dH_0/dt is so small that the stationary-state condition is satisfied for each value of H_0), then at sufficiently small H_1 the susceptibility $\chi'(H)$ (for a Gaussian distribution of the spin packets) can be written in the form

$$\chi'(H) = \frac{2\chi_0}{\pi}\frac{H}{\Delta H}\left(\frac{0.69}{\pi}\right)^{1/2} \times \exp\left[-\left(\frac{H_i - H_0}{H}\right)^2\right] \cdot 0.69\,(\cos\omega_m t)\ln\left(\frac{1.7\,\Delta H}{H_1}\right) \quad (2.3)$$

(χ_0—static susceptibility). This expression was used for a comparison of the experimental and theoretical EPR line shapes. For samples with large relaxation times, the stationary method could be used by exposing the specimen to light so as to reduce the relaxation time.

On the other hand, if the passage time is longer than the relaxation time, the shape of this nonstationary signal remains the same as in (2.3), and the signal amplitude decreases by a factor $2/\pi$. It must be noted that the output signal does not depend on the modulation-field amplitude so long as $H_m > H_1$; when H_m approaches H_1, the signal starts to decrease.

In the derivation of (2.3) it was assumed that there is no spin-spin interaction and that in the case of AFP through the line the absolute value of the magnetization remains unchanged. This assumption is in good agreement with the experimental data (see Ch. III).

The ENDOR method has been extensively used in investigations of paramagnetic resonance in semiconductors. It was first used to investigate phosphorus donors in silicon and to produce nuclear orientation in such a system[22,23]. The method makes it possible to determine the hyperfine splitting and the g-factor[12] very accurately. It was also used to determine the nuclear spins and to study the anomalies of the hyperfine structure[12,24-26].* In recent years this method was used to investigate impurity centers in silicon, producing deep levels[16].

The possibility of using the method of double electron-nuclear resonance is based on the fact that the inhomogeneously broadened line can be saturated in parts. If the spin diffusion is insignificant, then the saturation of the lines of one group of spin packets does not cause any change in the remaining groups, since their resonant frequencies are different.

To observe electron-nuclear double resonance it is necessary to apply to the specimen not only two magnetic fields (constant and microwave), but also a small radio-frequency magnetic field H_r, perpendicular to the constant field, and with a frequency that can be varied over the required range. This field induces transitions between the levels due to the interactions with the nuclei [see (3.3), (3.4), and Fig. 2], thereby changing the electron level populations. This changes the magnitude of the EPR signal. Thus, if some definite EPR level is fixed in the instrument and the frequency ν_r of the field H_r is varied, then peaks above the fixed level will be observed at certain frequencies

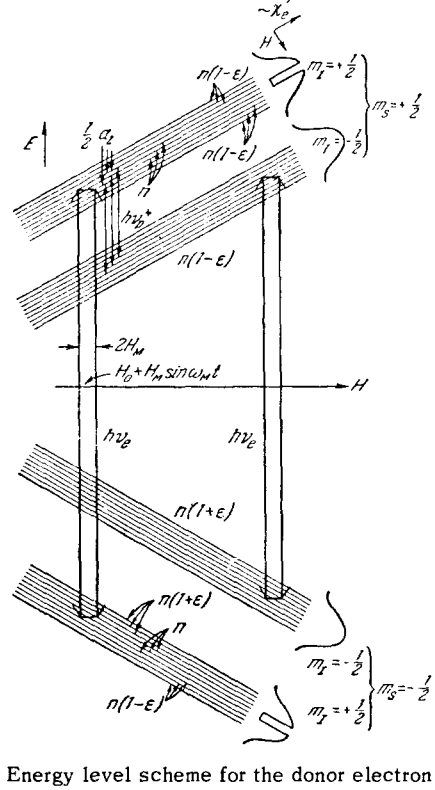

FIG. 2. Energy level scheme for the donor electron in phosphorus doped silicon in a magnetic field. For simplicity we assume that the microwave field completely saturates the part of the line corresponding to $m_I = +\frac{1}{2}$.

*For more details, for example, see W. Low, Paramagnetic Resonance in Solids, Solid State Physics Suppl. 2, Academic Press N.Y. 1960.

ν_r corresponding to certain nuclear transitions. The aggregate of these peaks constitutes the double-resonance spectrum, which makes it possible to ascertain the structure of the EPR lines and by the same token the interactions that occur in the system. Double resonance experiments are carried out on highly sensitive superheterodyne spectroscopes with magnetic-field modulation at helium temperatures (usually at 1.25°K). The double-resonance line width is small, approximately 10 kcs, whereas the EPR lines are ~10 Mcs wide. Thus the use of double resonance increases the resolution by three orders of magnitude.

III. ELECTRON PARAMAGNETIC RESONANCE OF DONORS AND ACCEPTORS IN SILICON AND GERMANIUM, FORMING SHALLOW IMPURITY LEVELS

1. EPR of Donors in Silicon

Before we discuss the experimental data on EPR of shallow donors in Si and the procedure used to obtain these data, we must examine the types of interactions in such systems.

1. Hamiltonian. Energy Level Scheme. The various interactions in the systems under consideration (when an external field H_0 is applied)[12] can be described by the Hamiltonian

$$\mathcal{H} = -\mu_e H_0 - \mu_D H_0 - \left(\frac{8\pi}{3}\right)\mu_e\mu_D |\Psi_{01}(0)|^2 + \frac{8\pi}{3}\sum_l \mu_e\mu_l |\Psi_{01}(\mathbf{r}_l)|^2 - \sum_l \mu_l H_0 + \sum_l \frac{1}{(\mathbf{r}-\mathbf{r}_l)^3} \times \left\{\mu_l\mu_e - \frac{3[\mu_l(\mathbf{r}-\mathbf{r}_l)][\mu_e(\mathbf{r}-\mathbf{r}_l)]}{(\mathbf{r}-\mathbf{r}_l)^2}\right\}, \quad (3.1)$$

where μ_e—electron magnetic moment, μ_D—magnetic moment of the impurity atom nucleus, μ_l—magnetic moment of the Si^{29} nuclei in the different sites l of the silicon lattice, and $\Psi_{01}(\mathbf{r}_l)$—electron wave function in the site l. The distance r is measured from the donor nucleus. The third and fourth terms of the Hamiltonian describe the interaction between the magnetic moment of the donor electron and the magnetic moments of the donor and Si^{29} nuclei. The last term is the dipole interaction due to the donor electron and to the Si^{29}, and vanishes when the electron wave function has strict cubic symmetry. Owing to the symmetry properties of the wave function, the dipole and quadrupole interactions vanish for the site where the donor is located.

In ordinary EPR experiments one induces the transitions $\Delta m_S = \pm 1$, $\Delta m_D = 0$, $\Delta m_{Si} = 0$, where m_S, m_D, and m_{Si} are the magnetic quantum numbers for the electron, donor, and the Si^{29} nuclei. This gives rise to a series of allowed hyperfine structure lines, for which

$$h\nu_e = g\beta H_0 + a_D m_D, \quad (3.2)$$

where g—electronic g-factor, β—Bohr magneton, a_D—constant of hyperfine interaction with the donor nucleus, m_D assumes values I, I − 1, . . . , −I, and ν_e—microwave frequency (see Fig. 2; for simplicity we consider here a phosphorus donor with nuclear spin I = 1/2).

In the ENDOR technique, transitions for which $\Delta m_S = 0$ are induced, i.e., one flips either the donor ($\Delta m_D = \pm 1$) or the Si^{29} nuclei ($\Delta m_{Si} = \pm 1$)*.

In the first case we observe lines with frequencies given by

$$h\nu_D^{\pm} = \left|\frac{1}{2}a_D \mp \frac{\mu_D}{I_D H_0}\right|, \quad (3.3)$$

the upper sign corresponding to $m_S = \pm 1/2$ and the lower to $m_S = -1/2$ (Fig. 2). The frequencies ν_D range from several dozen megacycles to several megacycles. In the second case (when the Si^{29} nuclei located in the sites l are flipped), the transition frequencies are given by

$$h\nu_e^{\pm} = \left|-\left(\frac{\mu_{Si}}{I_{Si}}\right)H_0 \pm \frac{1}{2}a_l \mp \frac{1}{2}b_l(1-3\cos^2\theta)\right|, \quad (3.4)$$

where a_l and b_l—constants of hyperfine isotropic and anisotropic interaction with the Si^{29} nuclei. This equation describes two series of lines centered around the unperturbed Larmor frequency of a Si^{29} nucleus in the field H_0 ($\nu_H \sim 2.6$ Mcs at $H_0 \approx 3000$ Oe). The hyperfine splitting due to the Si^{29} nuclei ranges from several megacycles to zero, depending on the distance of the Si^{29} nuclei from the donor (on Fig. 2 the corresponding values of the energies are drawn for the sake of simplicity as discrete levels, although the width of each level is actually larger than the spacing between levels). Let us consider the main characteristics of the EPR spectrum, namely the g-factor, the hyperfine interaction, the line shape, and the line width.

2. Line Shape and Width. a) Theoretical estimate. The EPR line shape was investigated theoretically by Kohn. He showed[10] that if the wave function of the donor electron spans a large number of Si^{29} lines, then the EPR line shape can be described by a Gaussian function. For a Gaussian line shape, the ratio

$$\Gamma = \frac{M_4}{(3M_2^2)^2} \quad (3.5)$$

is equal to unity (M_4 and M_2 are the fourth and second moments of the line, respectively). The value of Γ is very close to unity if the line shape is described by expression (2.4). The fewer the Si^{29} nuclei spanned by the electron orbit, the more Γ deviates from unity; this should take place, in particular, for a donor with maximum ionization energy.

As mentioned earlier, the EPR line width of the donors in silicon is due essentially to the hyperfine interaction between the donor electron and the Si^{29} nuclei. To estimate this width, the hyperfine interactions a_l were calculated for different lattice sites l occupied by the Si^{29} nuclei. The line width (character-

*We shall call the corresponding lines ENDOR lines.

ized by the second moment of the line M_2) is equal to

$$\Delta H_{av}^2 = \sum_{l=0}^{\infty} f n_l \left(\frac{a_l}{2}\right)^2, \qquad (3.6)$$

where f—natural abundance of the Si^{29} isotope and n_l—number of equivalent atoms in the "shell" l. In estimating the line width, the sum in (3.6) was divided into two parts, one made up of the first four largest experimentally determined interactions with the nearby Si^{29} nuclei (see Table II; this part accounts for 80% of the observed line width), and another with the remaining interactions corresponding to the 24 nearby Si^{29} "shells", and calculated on the basis of (3.7) with $k_0/k_{max} = 0.85$. Owing to the exponential attenuation of the wave function, it is sufficient to include only the first 24 shells in the calculation of ΔH_{av}^2.

b) Experimental results and discussion. As already mentioned, the EPR line shape and line width were investigated for different donors by a stationary method. The experimental results are listed in Table I. The experimentally measured line widths $2\Delta H_{obs}$ were corrected in accordance with (2.4) for the line broadening in the AFP. Under the experimental conditions ($\Delta H/H_1 \approx 300$), the observed widths were approximately 10% larger than those corresponding to the true distribution of the spin packets ($2\Delta H_{corr}$, Table I). The Gaussian line shape for shallow donors was confirmed in the course of estimating the values of Γ (see Table I; M_2 and M_4 were determined graphically from the experimental resonance curves), which turned out to be close to unity. A considerable deviation is observed for arsenic donors, which have the highest ionization energy and whose wave function consequently spans a small number of Si^{29} nuclei (Kohn's theoretical estimate gives for the arsenic donors $\Gamma \approx 1.25$). A considerable deviation of Γ from unity is observed also for samples of silicon enriched with Si^{28}.

The experimental line widths ($2\Delta H_{corr}$) coincide with the theoretical ones calculated from (3.6). The results disagree for the same arsenic donor, which is understandable since the effective-mass approximation is less accurate for impurity centers with large ionization energies. The good agreement between the theoretical and experimental results shows that the passage effects have been correctly taken into account, and that there is no spin diffusion.

The observed EPR lines were symmetrical and had no odd moments.

3. Hyperfine Interaction. The investigation of the hyperfine interaction of a donor electron, with both donor and Si^{29} nuclei, yielded much valuable information on the investigated samples. The ENDOR method was used for the purpose. In many investigations, the samples were mechanically stressed. The hyperfine interaction with the Si^{29} nuclei was used to determine the spatial distribution of the wave function of the donor electron, thus yielding k_0. In investigations of the variation of the hyperfine interaction with the donor nucleus under shear deformations, the spacing E_{12} between the singlet and doublet was measured for different impurities and the deformation potential constant Ξ_u was determined.

a) Spatial distribution of wave function. Theoretical premises. It was noted above that the wave function of the donor electron in the ground state is a linear combination of six wave functions corresponding to six energy minima at the bottom of the conduction band and equal at $r = 0$ (on the donor nucleus) [see (1.6)]. With increasing distance from the donor, interference takes place between the different components of the wave function; this interference depends on the position (k_0) of the energy minima at the bottom of the conduction band in wave-vector space. Because of this, the wave function does not decrease monotonically with increasing distance to the donor nucleus, and the largest hyperfine interaction will therefore be observed for the donor nucleus, the hyperfine interaction with the Si^{29} nuclei being smaller and not decreasing in proportion to the distance r_i from the donor nucleus. Thus, the hyperfine interaction between the As and the Si^{29} in the site 440 (Fig. 3) is much larger than with the 220 silicon, although the latter are closer to the donor (see Table II). In order to determine the spatial distributions of the wave function of the donor electron, the theoretical values of the hyperfine interactions with the Si^{29} nuclei, calculated on the basis of the Kohn and Luttinger theory, were compared with the experimental values measured by the ENDOR method. The isotropic hyperfine interaction with the Si^{29} nuclei in sites l is proportional to[12]

$$|\Psi_{01}(\mathbf{r}_l)|^2 = \frac{2}{3}\eta\,[F^{(x)}(\mathbf{r}_l)\cos k_0 x_l + F^{(y)}(\mathbf{r}_l)\cos k_0 y_l + F^{(z)}(\mathbf{r}_l)\cos k_0 z_l], \qquad (3.7)$$

where x_l, y_l, z_l—coordinates of the site l, and η—ratio characterizing the degree of localization of the function $u_j(r)$ in the lattice site l, with a value 186 ± 18[27];

TABLE I

Donor	Concentration, cm^{-3}	$2\Delta H_{obs}$, Oe	$2\Delta H_{corr}$, Oe	$2\Delta H_{theor}$, Oe	$\Gamma = \frac{M_4}{(3M_2)^2}$
Antimony	$2.5\cdot10^{16}$	2,6±0.1	2.3	2.3	1.0±0.1
Phosphorus	$1.5\cdot10^{16}$	2.8±0.1	2.5	2.5	1,0±0.1
Arsenic	$1.8\cdot10^{16}$	3.2±0.1	2.9	3.1	1.3±0.1
Phosphorus in Si containing ≈ 99.88% Si^{28}.	$4\cdot10^{16}$	0.24±0.02	—	—	1.8±0.1

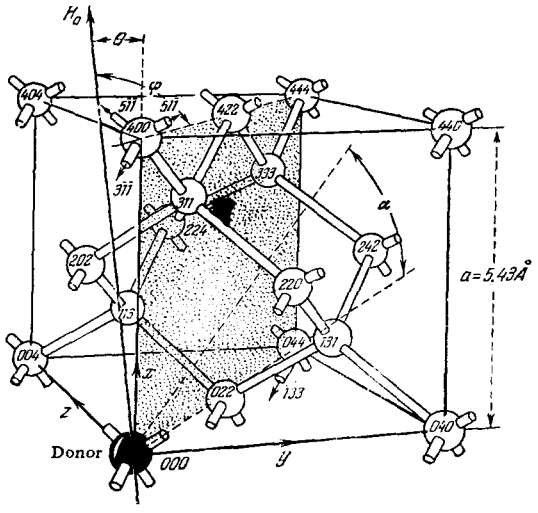

FIG. 3. Unit cell of silicon crystal with substitutional donor. The magnetic field was rotated in the crystal plane (110) (see shaded plane).

the expressions for the components of the anisotropic envelope function $F^{(x)}(r_l)$, $F^{y}\ldots(r_l)$, $F^{(z)}(r_l)$ are given in[12]. For different donors the isotropic hyperfine interaction with the Si^{29} nuclei located in different sites l of the silicon lattice (see Fig. 3) was calculated as a function of the quantity k_0/k_{max}. Corresponding curves were plotted and used to interpret the lines by comparing each measured a_l with the theoretical value.

Experimental results and discussion. As already noted, the hyperfine interactions with the donor nuclei and with the Si^{29} nuclei, which cause broadening of the EPR lines, were investigated by the ENDOR method (see Ch. II). We shall not stop here to discuss this method in detail, since it is thoroughly described in[12] and[24], but consider only briefly the interpretation of the lines[12] and the experimental results.

A part of the ENDOR spectrum for arsenic donors is shown in Fig. 4. The figure shows the lines due to the hyperfine interaction with the nearest Si^{29} nuclei, located in different lattice sites l (see Fig. 3), for three different orientations of the magnetic field—

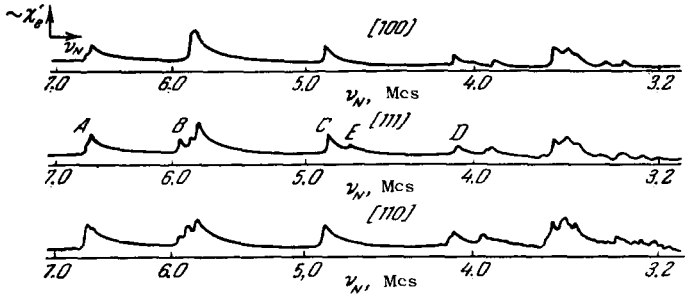

FIG. 4. ENDOR spectrum for silicon with arsenic concentration 8×10^{16} cm^{-3} for three orientations of the magnetic field (T = 125°K, $H_0 \approx 3000$ Oe). The resonance lines correspond to the hyperfine interaction of the donor electron with Si^{29} nuclei located in different lattice sites.

along the [100], [011], and [111] axes. It is seen from Fig. 4 that the line structure depends noticeably on the direction of the magnetic field, thus indicating anisotropy of the hyperfine interaction with the Si^{29} nuclei. The ENDOR lines are designated A, B, C, and D; the line A corresponds to the largest hyperfine interaction, etc. The lines are not symmetrical. Their steep slope on one side is due to the fact that the natural line width of the spin packets is very small; the slow decrease in the line intensity following the passage is connected with the fact that the EPR signal is saturated at a finite rate, which is inversely proportional to the relaxation time (nonstationary method of observation, see Ch. II). Inasmuch as interference takes place between the components of the wave function, a comparison of the theoretical and experimental data for only the isotropic part of the hyperfine interaction does not lead to any interpretation. Therefore, in order to identify the silicon lattice sites of the Si^{29} atoms causing a particular ENDOR line, Feher[12] used two additional factors:

1) Anisotropic hyperfine interaction, which causes the structure of the ENDOR lines to depend on the orientation of the crystallographic axes of the sample relative to the magnetic field H_0. To interpret any particular line, the experimentally determined dependence of its structure on the angle of rotation of the magnetic field was compared with the theoretical expression (3.4) or with an analogous expression. The form of the expression for $h\nu_l^{\pm}$ was determined from an examination of the symmetry of the individual lattice point r_l relative to the donor atom. (For example, the site 333, as can be readily seen from Fig. 3, has axial symmetry and expression (3.4) holds for it.)

2) The relative amplitudes of the ENDOR lines, which are determined by the number of equivalent lattice sites occupied by the Si^{29} nuclei. (Thus, for example, from symmetry considerations it turned out that the lines C and D can be due to any of the sites 333, 444, or 555. An investigation of the relative amplitudes of these lines has shown that site 444 must be excluded from consideration, since there are eight 444 sites, and only four 333 sites and four 555 sites.)

After line A was interpreted from the symmetry investigation, the theoretical curves for a_l versus k_0/k_{max} were used to obtain the approximate value of

TABLE II

Line, site			
A (400)	B (440)	C (333)	D (555)
$a_l/3$ (Mcs)	$a_l/2$ (Mcs)	$a_l/2$ (Mcs)	$a_l/2$ (Mcs)
3.86	3.00	2.04	1.29

k_0/k_{max}, and these curves were then used to interpret the remaining lines.

The experimental results of the interpretation of the ENDOR lines for the As donor are listed in Table II.

We do not list here the constants of anisotropic hyperfine interaction. We note only that they are much smaller than the constants of isotropic hyperfine interaction. Thus, for example, in the case of As donors, the constant $b_l/2$ is equal to 0.023 Mcs for the 400 site and 0.004 Mcs for the 333 site.

Thus, while interpreting the ENDOR spectrum we determined the spatial distribution of the wave function of the donor electron: the electron is localized to a greater degree near the 400 sites, then near the 111 sites, etc. Summation of the hyperfine interactions corresponding to the lines A, B, C, and D shows that these interactions with the Si^{29} nuclei determine the greater part (up to 80%) of the EPR line width. Analogous results were obtained for the donors P and Sb.

The identification of the lines makes it possible to determine the value of k_0/k_{max}. There is no single value of k_0/k_{max} for which the experimentally measured hyperfine splittings for different sites coincide best with the theoretical ones. Thus, for the A line, the best fit is obtained if a_l is calculated with $k_0/k_{max} \approx 0.8$, for the B line—≈ 0.9, etc. Therefore, the actual value of k_0/k_{max} was obtained by averaging these quantities obtained from comparison with experiment over different r_l:

$$k_0/k_{\max} = 0.85 \pm 0.03.$$

This value agrees well with the values of k_0/k_{max} obtained by other methods[28].

There is still no theory by which to calculate the anisotropic hyperfine interaction accurately. It is possible (in Anderson's opinion) that the main factor influencing the anisotropy of the hyperfine interaction is nuclear orientation.

b) Effect of mechanical axial stress on the hyperfine interaction. Theory. An investigation of the variation of the hyperfine interaction in a crystal subject to a force acting along one of its axes and causing shear deformation has made it possible to determine the distance E_{12} between the singlet and the doublet for different impurities, and the shear deformation potential constant Ξ_u[29]. If we apply to the crystal a mechanical compression or tension force along one of its axes, the crystal symmetry will be disturbed and the six energy minima in the Brilluoin zone [the corresponding equal-energy surfaces near k_0 are ellipsoids, see (1.3)] will no longer be equivalent. The energy of some minima will decrease and that of others will increase. Because of this, the relative populations of the ellipsoids will change in accordance with the Boltzmann distribution and the ground state will no longer be a pure singlet, for wave functions of the doublet state will be mixed in with it. (No triplet state is added by such static deformations.)

It was assumed that the action of a mechanical axial stress is manifest only by a change in the relative populations of the ellipsoids. The change in the energy of the ellipsoids relative to the change in the energy of their center of gravity $\Delta\epsilon_j$ was calculated on the basis of the Herring deformation-potential theory[30]. It can be assumed with good approximation[13] that the relative changes in the energies of the ellipsoids are equal to the changes in the energy of the ground state and, in addition, it can be assumed that the off-diagonal matrix elements of the Hamiltonian $\mathcal{H}_{e0}$, which characterizes the spacing between the singlet and the doublet (see Ch. I), do not change when the stress is applied. The changes in the energies of the ellipsoids enter as diagonal terms in the matrix of the Hamiltonian $\mathcal{H}_{e0}$, which is transformed into $\mathcal{H}^*_{e0}$. It is shown in[29] that when this modified matrix $\mathcal{H}^*_{e0}$ acts on several transformed linear combinations of the wave functions (1.8), a change takes place in the wave function of the singlet state and in one of the two functions of the doublet state, i.e., the result of the stress is a mixing of the singlet (Ψ_{01}) with one of the components of the doublet (Ψ_{02}). The remaining states remain unperturbed. Inasmuch as it has been assumed that the only consequence of the deformation is the change in the populations of the ellipsoids, the wave functions corresponding to the mixed states will differ from Ψ_{01} and Ψ_{02} only in the coefficients $\alpha_i^{(j)}$ of the expansion in the basis functions χ_j. These new linear combinations are characterized by coefficients $\alpha_1^{(j)*}$ and $\alpha_2^{(j)*}$, which are determined by solving the Schrodinger equation $\mathcal{H}^*_{e0}\Psi = E_{e0}\Psi$ and normalizing. The coefficients $\alpha_1^{(j)*}$ and $\alpha_2^{(j)*}$ are expressed in terms of some quantity x which characterizes the relative change in energy of an electron located at the minimum point, equal to

$$x = \frac{\Xi_u S'}{6\Delta_c} = \frac{\Xi_u S'}{E_{12}}. \qquad (3.8)$$

Here Ξ_u—deformation-potential constant which characterizes the change in energy due to the axial displacement produced by tension along the ellipsoid axis and compression along the two perpendicular directions; $S' = 2(S_{11} - S_{12}T)$, where S_{11} and S_{12} are the moduli of elasticity and T is the stress. In the case of shear deformation, the energy of the two ellipsoids decreases, and of the four others increases. In the case of strong compression ($-x \gg 1$), the electron in the ground state spends most of the time in the two ellipsoids whose energy decreased. Since the influence of the stress is accounted for in the coefficients $\alpha_i^{(j)*}$, the ratio of the value of the hyperfine splitting in the presence of deformation $(\Delta H)^*$ to the corresponding value in the absence of deformation (ΔH) [see (1.9)] is

$$\frac{(\Delta H)^*}{(\Delta H)} = \frac{1}{6}\left|\sum \alpha_1^{(j)*}\right|^2$$

and assumes upon substitution of $\alpha_1^{(j)*}$ the form

$$\frac{(\Delta H)^*}{(\Delta H)} = \frac{1}{2}\left[1+\left(2+\frac{1}{3}x\right)\left(x^2+\frac{4}{3}x+4\right)^{-1/2}\right]. \quad (3.9)$$

In the case of strong compression ($-x \gg 1$) this expression is equal to 1/3, and in the case of strong tension ($x \gg 1$) we have $(\Delta H)^*/(\Delta H) = 2/3$, i.e., the hyperfine interaction is proportional to the number of occupied ellipsoids in these two limiting cases.

Experimental results. The experiments were made with silicon samples obtained by the Czochralski method, with donor (P, As, Sb) density 10^{16} cm^{-3}, at a temperature 1.25°K. All the measurements were made with AFP, and the bridge was tuned for dispersion.

The dependence of $(\Delta H)^*/(\Delta H)$ on the values of $x = \Xi_u S'/E_{12}$ was investigated for different donors (S_{11} and S_{12} are known for silicon). The values of $(\Delta H)^*/(\Delta H)$ measured experimentally for different S' lie near the theoretical curve calculated from expression (3.9) using the experimental values of E_{12}/Ξ_u.

The experimental results were presented in a different manner. The values of $x = \Xi_u S'/E_{12}$ were calculated from the known experimental values of $(\Delta H)^*/(\Delta H)$ on the basis of expression (3.9). Figure 5 shows the dependence of x on the elastic deformation $S' = 2(S_{11} - S_{12})\tilde{T}$ in the case of arsenic, phosphorus, and antimony donors. It can be seen that the experimental values of x lie near straight lines whose slopes are determined by E_{12}/Ξ_u (see Table III), thus confirming the correctness of expression (3.9), i.e., the change in $|\Psi_{01}(0)|^2$ is due to a change in the populations of the ellipsoids.

To determine the splitting between the doublet and the singlet E_{12} it is necessary to know the deformation potential constant Ξ_u,* which experiments have shown to be positive. Since the wave function of the doublet vanishes on the nucleus, the position of the corresponding level will not depend on the type of impurity, and its energy should be close to the value obtained by

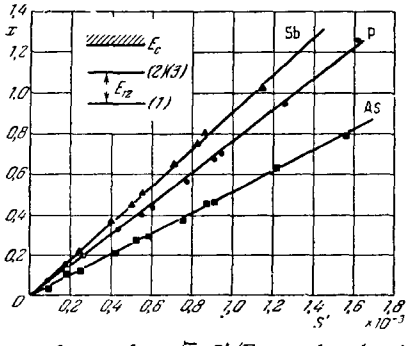

FIG. 5. Dependence of $x = \Xi_u S'/E_{12}$ on the elastic deformation $S' = 2(S_{11} - S_{12})\tilde{T}$ for arsenic, phosphorus, and antimony donors ($T = 1.25$°K, $H_0 \approx 3000$ Oe, donor concentration $\approx 10^{16}$ cm^{-3}).

* A theoretical calculation of this constant, made by Herring [30, 31], gives an incorrect and unusable value of Ξ_u in the interval from 7 to 11 eV.

Table III

Donor	Ionization energy, eV	E_{12}/eV	E_{12}, cm^{-1}
P	$44.6\cdot10^{-3}$	$(1.32\pm0.08)\cdot10^{-3}$	$15\cdot10^{-3}$
As	$52.5\cdot10^{-3}$	$(1.98\pm0.12)\cdot10^{-3}$	$22\cdot10^{-3}$
Sb	$43\cdot10^{-3}$	$(1.10\pm0.07)\cdot10^{-3}$	$12\cdot10^{-3}$

the effective-mass method. Then, taking this into account, Feher obtained the value of Ξ_u by trivial calculations based on known values of the ionization energy for the different donors (see Table III) and the experimental values of E_{12}/Ξ_u. It was found in this way that $\Xi_u = 11 \pm 1$ eV. The values of E_{12} for P, As, and Sb are listed in Table III. Thus, the doublet level lies $(30.0 \pm 1.0) \times 10^{-3}$ eV below the conduction band, in good agreement with the energy (29×10^{-3} eV) obtained by the effective-mass method. The value of E_{12} for the phosphorus donor (15×10^{-3} eV) agrees with the corresponding quantity obtained from measurements by the Hall effect[32].

4. The g-factor. a) Theory of g-factor. At the present time the most complete theory of the g-factor of shallow donors in silicon and germanium is given in the papers of L. Roth[33], Hasegawa[34] and Liu[35]. Inasmuch as the wave functions of the donor electrons are mapped out from functions for the conduction electrons, the authors first estimate the g-factor for the conduction electrons. In calculating this quantity, Roth uses the effective mass method developed by Kohn and Luttinger[36] for the case of degenerate bands and spin-orbit interaction. The problem is solved by perturbation theory (the spin-orbit interaction and the interaction with the external magnetic field are regarded as first-order perturbations relative to the ordinary Hamiltonian, written in the effective-mass approximation). We shall not present the general expression which Roth obtained for the g-factor in tensor form. It follows from the crystal symmetry that the only g-tensor components are

$$g_{zz} = g_{\parallel}, \qquad g_{xx} = g_{yy} = g_{\perp}, \quad (3.10)$$

where z—axis of the ellipsoid.

In calculating the g-factor for Si and Ge, Roth used the energy band structure and the terminology of Herman[37,38] and Phillips[39].

From Roth's calculations it follows that $g_{\parallel} = 0.9$ and

$$g_{\perp} - 2 \approx 0.04 \pm \Delta g'_{\perp}. \quad (3.11)$$

Roth assumes that the value of $\Delta g'_{\perp}$ is of the order of 0.01 and its sign in (3.11) is not known. Phillips[39] has shown that this term is indeed very small.

Thus, the g-factor is anisotropic for the conduction electrons. For each individual ellipsoid, the g-factor is determined from the expression

$$g^2 = g_{\parallel}^2 \cos^2\theta + g_{\perp}^2 \sin^2\theta, \quad (3.12)$$

where θ—angle between the magnetic field and the axis of the ellipsoid. In the case of donor electrons, all the ellipsoids are intermixed and the g-factor for the electron in a singlet donor state is equal to

$$g=\frac{1}{3}g_{\parallel}+\frac{2}{3}g_{\perp}, \qquad (3.13)$$

i.e., an isotropic g-factor should be observed in EPR experiments. In the case of silicon it follows from Roth's estimates that $g_{\parallel}-2=0.01$ (differing from the experimental value -0.003). However, Elliot has shown that the spin-orbit splitting at the edge of the silicon valence band is very small and can reduce $g_{\parallel}-2$ by a factor of 3. This agrees with the experimental value.

As to the estimate of $g_{\perp}$, Roth assumes that the main contribution to $g_{\perp}$ is made by the edge of the valence band. Then $g_{\perp}-2$ should have an approximate value $(g_{\parallel}-2)/6$. Experiments have shown[29] that the Roth model cannot be used for silicon. Liu calculated the g-factor using wave functions, and showed that the greatest contribution to the change in the g-factor is made by the band corresponding to the 2p states of the silicon atom. These states were not taken into account by Roth. As a result, $g_{\parallel}$ and $g_{\perp}$ have nearly equal values in Si. The theoretical values of $g_{\parallel}-2$ and $g_{\perp}-2$, which are -0.0027 and -0.0036 respectively, are close to the experimental values (-0.0028 and -0.0040).

b) Effect of axial stress on the electronic g-value of donors in silicon. Experiments on the influence of the axial stress on the value of the electronic g-value of donor impurities in Si[29] have made it possible to determine $g_{\parallel}$ and $g_{\perp}$, on the basis of which conclusions were drawn with respect to the correctness of the Roth and Liu theory. The change in the g-value in response to an axial stress is brought about by two causes. One is connected with the addition of a doublet state to the singlet one, i.e., with a change in the populations of the ellipsoids. The other is that crystal deformation results in mixing of Δ_1 (of the band closest to the bottom of the conduction band) and Δ_2'* (for which the corresponding matrix elements vanish under the usual conditions). Both effects were investigated separately, since they come into play at different axial-stress orientations relative to the crystallographic axes. No change is produced in the g-value by the first cause if the force is applied along the [111] axis, for identical changes take place in the energies of all the ellipsoids, so that their populations do not vary. On the other hand, Roth has shown that the g-value can not be changed by the mixing-in of the Δ_2' band if the force is applied along the [100] axis.

Let us consider first the change in the g-value due to the change in the ellipsoid populations[29]. Let g* be the g-value in the presence of deformation. In order to take into account the effect of the change in the ellipsoid population when the crystal is compressed along the [100] axis, the product $g(SH_0)=\langle Sg^jH_0\rangle_{av}$ was averaged over new wave functions, characterized by coefficients $\alpha_i^{(j)*}$. An expression was written down for g^{*2} in analogy with (3.12), and the result of some transformations was

$$g^*-g=\frac{1}{6}(g_{\parallel}-g_{\perp})\left(1-\frac{3}{2}\sin^2\theta\right)\times\left[1-(3x+2)\left(x^2+\frac{4}{3}x+4\right)^{-1/2}\right]. \qquad (3.14)$$

Thus, the mixing-in of the nonisotropic doublet state with the isotropic singlet state makes the g-value of the ground state also anisotropic. In the case of strong compression ($-x\gg 1$) expression (3.14) takes the form

$$g^*-g=\frac{2}{3}(g_{\parallel}-g_{\perp})\left(1-\frac{3}{2}\sin^2\theta\right), \qquad (3.15)$$

from which we readily see that the g-value is $g^*=g_{\parallel}$ when $\mathbf{H}_0\parallel\widetilde{T}$, and becomes equal to $g_{\perp}$ when $H_0\perp T$. This result is understandable, for the electrons are situated at all times in the two ellipsoids with lower energy in the case of strong compression along the [100] axis.

The mixing-in of the Δ_2' band upon deformation causes changes in $g_{\parallel}$ and $g_{\perp}$. Roth has shown that the corresponding change in the g-value is

$$g^*-g=\frac{1}{3}A(\widetilde{T}/C_{44})\left(1-\frac{3}{2}\sin^2\theta\right) \qquad (3.16)$$

(the elasticity constant C_{44} of Si is known[40]), where the expression for the matrix element A is given in[35]. No such change in g-value occurs if the stress is applied along the [100] axis of the crystal.

c) Experimental results and discussion. The g-values were determined from formulas which took into account the Breit-Rabi corrections. The experimental g-values for the donors As, P, and Sb are listed in Table IV. Experiments have shown that the g-value for these donors is isotropic, in agreement with the theory considered above.

Table IV

Donor	$g=\frac{1}{3}g_{\parallel}+\frac{2}{3}g_{\perp}$	$g_{\parallel}-g_{\perp}$	$\Delta g=g_D-g_{c.e.}$
As	$1.99837\pm1\cdot10^{-4}$	$(1.10\pm0.05)\cdot10^{-3}$	$-(3.8\pm0.1)\cdot10^{-4}$
P	$1.98850\pm1\cdot10^{-4}$	$(1.04\pm0.05)\cdot10^{-3}$	$-(2.5\pm0.1)\cdot10^{-4}$
Sb	$1.99858\pm1\cdot10^{-4}$	$(1.13\pm0.05)\cdot10^{-3}$	$-(1.7\pm0.1)\cdot10^{-4}$

As can be seen from (3.14) for the g-value under change in the ellipsoid populations, the quantity g^*-g can be determined in two ways: either by varying x at constant θ, or by varying the angle θ between the direction of the force and the magnetic field at constant x. Experiments of both types were made. In these, $\widetilde{T}$ was directed along the [100] axis of the crystal, making it possible to exclude the second cause of the change in the g-value under deformation. Figure 6 shows the de-

*The band designations are those of Herman [37, 38].

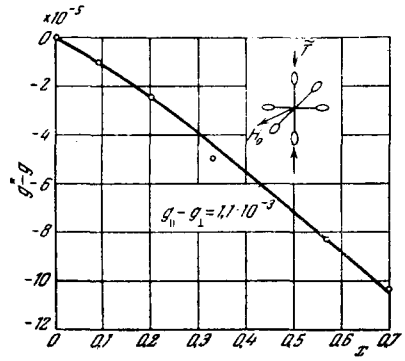

FIG. 6. Dependence of the change in the g-value, $g^* - g$, on the value of $x = \Xi_u S'/E_{12}$($T = 1.25°K$, $H_0 \approx 3000$ Oe). The compression of the crystal was along the [100] axis.

pendence of the experimentally measured $g^* - g$ on x for silicon doped with phosphorus at a concentration of 10^{16} cm^{-3} (the magnetic field H_0 is perpendicular to $\tilde{T}$). The solid line is the theoretical curve, calculated from (3.14) with $g_{\parallel} - g_{\perp} = 1.1 \times 10^{-3}$. The experimental points lie close to this curve, thus confirming the correctness of (3.14) in that the change of the g-value is due only to the change in the ellipsoid populations. The decrease in the g-value with increasing deformation implies that $g_{\parallel} < g_{\perp}$. The values of $g_{\parallel} - g_{\perp}$ (see Table IV) for different donors were determined from (3.14), in which the experimentally measured $g^* - g$ for known x were substituted. As can be seen from Table IV, the values of $g_{\parallel}$ are close to those of $g_{\perp}$ for all three donors, in agreement with the theory of Liu and in contradiction to the theory of Roth. The theoretical results of Liu agree with the experimental data within approximately 10%.

An investigation of the dependence of $g^* - g$ on the angle θ for different values of x has shown that when H_0 is parallel to the [111] axis the g-value is equal to g, i.e., to the corresponding value in the absence of deformation.

Table IV lists also quantities characterizing the deviation of the donor g-factor from the g-value for conduction electrons ($g_{c.e} = 1.99875 \pm 1 \times 10^{-4}$), obtained in [12]*. As can be seen from Table IV, this deviation is larger for donors with higher ionization energy. In the limit (at very low ionization energies), g_D should approach $g_{c.e}$. However, since the values of Δg are very small and close to one another for all three donors, we can assume that the contribution made to the g-value by the spin-orbit coupling due to the impurity atom itself is very small. Thus, the g-value is determined by the spin-orbit interaction due to the silicon atoms; this in fact is taken into account in the Roth and Liu theory.

Experiments were also made on the g-value variation occurring under deformation and due to the mixing in of the Δ_2' band. In these experiments the force was applied along the [111] crystal axis. The dependence of $g^* - g$ on the angle θ between the magnetic field and the direction of the force was investigated experimentally for three different values of x. When the magnetic field is directed along the [100] crystal axis, the g-value is equal to g. The deviation of g^* from g was the same for all three donors. This signifies that this experiment indicates the presence of states much farther from the bottom of the band than the splitting E_{12} between the singlet and the doublet. This corresponds to the assumption made by Roth that the mixed-in band Δ_2' is located approximately 0.5 eV from the bottom of the conduction band.

With the measured values $g^* - g$ substituted in (3.16), the value of the matrix element A was found to be

$$A = 0.44 \pm 0.04.$$

The experiments have shown that the changes in the g-value ($g^* - g$) due to mixing-in of either the doublet state or the Δ_2' band are quantities of the same order. This is attributed by Feher [29] to the closeness of the Δ_2' band to the conduction band and to the fact that the quantity $g_{\parallel} - g_{\perp}$, which causes the change in the g-value when the ellipsoid population changes, is very small for silicon.

2. Electron Spin Resonance of Shallow Donors in Ge. The EPR of shallow donors in silicon has been investigated by now in sufficient detail. The resonance of the shallow donors in germanium was not observed until 1959 when Feher and his co-workers succeeded in doing so [41] by the ENDOR technique.

Data for comparison with silicon, obtained in that investigation (for $H_0 \parallel$ [100]), are listed in Table V.

From these data one can draw certain conclusions on the causes of failure to observe resonance in germanium.

First, the donor hyperfine structure is observed in germanium at donor concentrations that are one or two orders of magnitude lower than in silicon. The reason is that these electrons are easier to delocalize, owing to the large Bohr radius of the donor electrons in germanium. Second, the lines are broader in germanium than in silicon. Third, the deviation of the g-value from the value for the free electron in germanium is approximately two orders of magnitude larger than in silicon. In the discussion of the Kohn and Luttinger theory [8,10], it was shown that the wave functions of the ground state can be represented as linear combinations of four wave functions corresponding to four energy minima in the conduction band. For the combinations corresponding to the degenerate triplet state, the value of $|\Psi(0)|^2$ is zero, so that no isotropic hyperfine splitting can be observed. The singlet state is formed by a linear combination with a finite value of $|\Psi(0)|^2$, and should consequently lead to hyperfine splitting. Thus, an experimental study of the hyperfine

*The anisotropy of the g-value for the electrons in the conduction band, which follows from the Roth theory [33], was not noted in the experiments described in [12].

TABLE V

Donor	Donor concentration cm^{-3}	g-value	Line width ΔH, Oe	Donor	Donor concentration cm^{-3}	g-value	Line-width ΔH, Oe
Germanium				Silicon			
P	$8 \cdot 10^{14}$	1.5631	10	P	$1.5 \cdot 10^{16}$	1.9985	2.8
As	$8 \cdot 10^{15}$	1.5701	11	As	$1.8 \cdot 10^{16}$	1.9984	3,2

splitting shows that the ground state of the phosphorus and antimony electrons in germanium is singlet.

In the case of resonance of the bound electrons, in germanium the line width is anisotropic. The smallest line width occurs when $H_0 \| [100]$. The line shape is Gaussian.

Feher also investigated[41] resonance in germanium at high donor concentrations, when the electron is no longer localized on the impurity, but moves through the entire crystal (impurity conductivity), even at the very lowest temperatures. A single resonance line is then observed. In germanium such a line turns out to be anisotropic. Its width is minimal (~ 4 Oe) and $H_0 \| [100]$; the maximum value (~ 65 Oe) is observed when H_0 makes an angle 70° with [100] in the (110) plane. The experiments have shown that the line width depends on the temperature. The line shape is Lorentzian. In germanium doped with phosphorus and arsenic, the g-value for the nonlocalized electrons is isotropic and is approximately equal to the g-value of the bound electrons, from which we can conclude that at these concentrations the electron spends most of the time near the impurity atom.

Germanium doped with antimony was investigated at concentrations from 10^{15} to 3×10^{16} cm^{-3}. The line shape was found to be extremely asymmetrical, and the g-value was found to be anisotropic and to fluctuate from 1.6 when $H_0 \| [100]$ to 1.9 when $H_0 \| [110]$.

It was reported in[42] that in antimony-doped germanium one can observe, in addition to the lines observed by Feher[41], four other lines with an anisotropic g-value. The principal values of g coincide with the theoretical and experimental values of g for electrons at the minimum of the conduction band. The widths and shapes of these lines do not depend on the temperature in the interval from 1.2 to 5° K. The number of paramagnetic centers responsible for this spectrum is likewise practically independent of the temperature. The line intensity is proportional to the antimony concentration. No such lines were observed in arsenic-doped germanium. The line intensities are not affected by exposure of the specimen to light with a wavelength in the far infrared, from which we can conclude that this spectrum cannot be caused by electrons excited in the impurity band through the forbidden band. The nature of the spectrum is still unclear at present. However, Keyes and Price[43] made an attempt to explain some features of the observed spectrum (coincidence of the values of the g-tensor, the absence of a similar spectrum in germanium doped with arsenic, weak temperature dependence, etc.) by assuming that it may be connected with the presence of local deformations in the germanium crystal, which exert a particular influence on the structure of the impurity band of antimony.

3. Paramagnetic Absorption in Acceptor Resonance in Silicon. Until 1960, all attempts to observe EPR of acceptors in silicon were unsuccessful. The reason for this failure, as indicated by Kohn[10], was the degeneracy of the valence band in silicon. Feher and his co-workers[44] succeeded in observing paramagnetic absorption in a p-type silicon sample previously compressed along one of the crystallographic axes.

Figure 7 shows the structure of the valence band in silicon. In the absence of deformation, the band is degenerate at k = 0, and the equal-energy surfaces are curved (Fig. 7a). Compression along one of the axes lifts the degeneracy, and at sufficiently large deformations the band splits with the corresponding equal-energy surface becoming ellipsoidal (Fig. 7b). Local stresses connected with dislocations, defects, and lattice vibrations are always present in the sample. This leads to a splitting of the valence band by an amount ΔE.

In an external magnetic field, the spin degeneracy is also lifted, and each band splits by an amount $g_h \beta H_0$, where g_h—spectroscopic-splitting hole factor. The following two cases can be singled out:

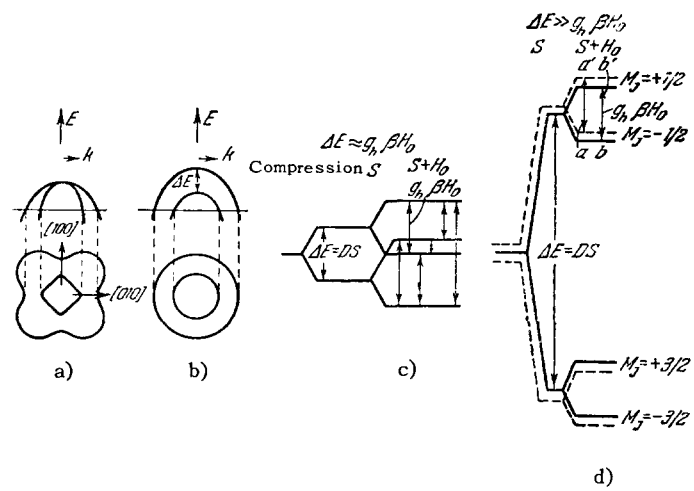

FIG. 7. Valence band in silicon. a) In the absence of compression, b) in the presence of unilateral compression, c) energy levels at $\Delta E \approx g_h \beta H_0$, d) energy levels for $\Delta E \gg g_h \beta H_0$.

1) $\Delta E \ll g_h \beta H_0$. In this case all six quantum transitions are allowed. In a specimen with random stress distribution, a broad spectrum of values of ΔE, together with a large set of transitions corresponding to different effective g-values, is possible. As a result, the resonance line becomes so broad that it cannot be observed.

2) $\Delta E \gg g_h \beta H_0$. Such a set can be readily obtained by compressing the specimen along one of the axes. Figure 7b shows the case when the compression is along the [100] axis. The possible transitions are $m_J = \pm 1$. Local stresses influence little the width of the resonance line. It then becomes possible to observe the acceptor EPR.

In[44] the experiments were made with p-type Si at 1.3° K and 9000 Mcs. They showed that the line disappears when the compression is equal to zero.

The hole g-value is anisotropic. In the boron concentration range from 5×10^{15} to 2×10^{17} cm^{-3} the g-value is independent of the concentration and when a compression of 800 kg/cm^2 is applied in the [100] direction its values become

$$g_\perp = 2.43 \pm 0.01, \qquad g_\parallel = 1.21 \pm 0.01.$$

Paramagnetic absorption of the acceptors was observed in silicon doped with aluminum, gallium, and indium. The behavior of the g-value under variation of the compression direction was studied, and the values of g_h were found to differ from the foregoing values of $g_\perp$ and $g_\parallel$ by several percent.

IV. SPIN LATTICE RELAXATION IN SEMICONDUCTORS

The problem of the relaxation mechanisms in semiconductors is very complicated, both theoretically and experimentally. Consequently the present ideas concerning these mechanisms are still far from complete or clear.

As applied to a system of paramagnetic centers, including the case when their concentration is small and classical statistics are applicable, the relaxation time is the time when the system reaches thermal equilibrium with the crystal lattice. This equilibrium is independent of the initial state, and the electron levels have a Boltzmann distribution, i.e., the populations are proportional to $\exp(E_n/kT)$, where E_n is the energy of the given level and T is the lattice temperature. Such a distribution is the result of interaction between the paramagnetic centers and the thermal lattice vibrations. We shall consider below the possible mechanisms of this interaction.

If two level energies E_{n_1} and E_{n_2} are specified then, for a given coupling mechanism between the spin system and the lattice, we can calculate the probabilities W_1 and W_2 of the direct and inverse transitions induced by the lattice. If we take the latter to be a reservoir that remains at constant temperature all the time, then the ratio of these probabilities is

$$\frac{W_1}{W_2} = \exp\left(\frac{\Delta E}{kT}\right), \tag{4.1}$$

where $\Delta E = E_{n_2} - E_{n_1}$. For convenience we introduce the quantity $W = \sqrt{W_1 W_2}$. By solving the simplest differential equation for the population change of levels n_1 and n_2, we obtain

$$\frac{n(t) - n(\infty)}{n(0) - n(\infty)} = e^{-2W \operatorname{ch}\left(\frac{\Delta E}{2kT}\right) t}, \tag{4.2}*$$

where n(t)—difference in the populations of levels n_1 and n_2, n(0)—initial difference of the populations of these levels, and $n(\infty)$—equilibrium population difference.

It is clear therefore that the rate at which the system enters equilibrium is determined by the relaxation time T_1, which equals, in accordance with (4.2),

$$T_1 = 2W \operatorname{ch}\left(\frac{\Delta E}{2kT}\right). \tag{4.3}$$

It follows from (4.2) and (4.3) that

$$n(\infty) = N \operatorname{th}\left(\frac{\Delta E}{2kT}\right), \tag{4.4}\dagger$$

where $N = n_1 + n_2$.

The very first experiments[2,3,6,45] have shown that the relaxation times in semiconductors depend strongly on the temperature, impurity concentration, magnetic field, number of free carriers present in the sample, etc. The character of the dependence differs with the range of each parameter. This indicates that different relaxation mechanisms are present.

Most published papers deal with the simplest impurity center, phosphorus, which has electron and nuclear spins 1/2. The four energy levels corresponding to such a system are shown schematically in Fig. 8. The possible transitions between these levels are indicated by arrows. The relaxation processes corresponding to these transitions will be denoted T_X, T_X', T_S, and T_N.

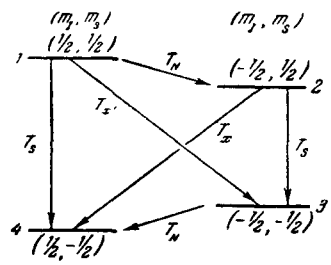

FIG. 8. Types of spin-lattice relaxation in silicon doped with phosphorus.

The designated T_X pertains to crossing relaxation, in which the orientations of the electron and nuclear spins, which have opposite directions, change simultaneously ($\Delta m_S = \pm 1$, $\Delta m_I = \pm 1$); T_S denotes the process of "vertical relaxation," in which only the

*ch = cosh

† th = tanh

electron spin orientation changes ($\Delta m_S = \pm 1$, $\Delta m_I = 0$); T_N corresponds to a process in which only the nuclear spin orientation changes ($\Delta m_S = 0$, $\Delta m_I = \pm 1$), while $T_{X'}$ corresponds to a process in which, as in the case of T_X, both electron and nuclear spins flip, but have the same direction ($\Delta m_S = \pm 1$, $\Delta m_I = \pm 1$).

The processes T_X, $T_{X'}$ and T_N are frequently called "horizontal relaxation processes", since the nuclear spin must change orientation in these processes. It must be emphasized that the notation T_X, T_S, etc. pertains not to some definite mechanism of energy exchange between the spin system and the lattice, but to the entire process that leads to a change in the orientation of the spins in accordance with the given selection rules. This process can be the result of many relaxation mechanisms that accompany one another.

1. Theory of Spin-Lattice Relaxation in Semiconductors. There is no theory as yet providing a more or less full explanation of relaxation processes in semiconductors. However, attempts were made at calculating the spin-lattice relaxation time of electrons on shallow donor levels in silicon and germanium[46,47,33,34,48]. These calculations were based principally on the notions of Kroenig[49] and Waller[50] concerning the possible mechanisms of energy exchange between a system of paramagnetic centers and a crystal lattice. According to these notions, the thermal vibrations of the lattice can influence the magnetic dipole interaction of the spins, and also modify the intracrystalline electric fields, which in turn leads to a perturbation of the energy levels of the paramagnetic center. In the latter case, the change in orientation of the spins which cannot interact with the electrostatic fields directly is due to the spin-orbit coupling. The spin system and the lattice can exchange energy either in discrete quanta equal to the lattice-vibration energy quantum (phonon) at the corresponding frequency (the so-called resonance or direct single-phonon process), or by scattering of a phonon with a change of its energy (combination scattering or the two-phonon Raman process).

1. **Direct phonon process.** Pines, Bardeen, and Slichter[46] estimated the relaxation times for the T_S and T_X processes under the assumption that the energy exchange between the spin system and the lattice is resonant at a frequency ω_0, and that the state of the donor electron changes adiabatically. Such an assumption is valid so long as $\hbar\omega_0$ is small compared with the electron binding energy, and makes it possible to employ with assurance the deformation-potential method[51] proposed earlier by Bardeen and Shockley. In[46], as in all the subsequent papers[33,34,47,48], the state of the donor electron is described with the aid of the wave functions (1.6), but in[46] a simplified wave function is used, corresponding to a single energy minimum, for which the average effective mass of the electron is 0.31m. Only longitudinal phonons are considered in[46] although, as will be shown below, transverse phonons are essential for the understanding of many of the observed variations.

In[46] Ψ_0^+ denotes the wave function describing the state of an electron with spin parallel to the constant magnetic field, while Ψ_0^- describes the state of an electron with antiparallel spin; the transition from the second state into the first is then characterized by the matrix element

$$(\Psi_0^-,\ (\delta V + \delta\mathcal{H}_I)\,\Psi_0^+) = (\Psi_0^-,\ \varepsilon_+'\Delta\Psi_0^+) + (E_{0_+} - E_{0-})\,(\Psi_0^-,\ \delta\Psi_0^+). \tag{4.5}$$

Here Δ—exchange broadening (no other types of deformation was considered), δV and $\delta\mathcal{H}_I$—change in the electrostatic potential and hyperfine interaction, ϵ_+'—change in the total energy of an electron with spin parallel to the field, and $\delta\Psi_0^+$—corresponding change in the electron wave function. The volume broadening Δ is written in[46] in the form

$$\Delta = \sum_{\mathbf{q}} \frac{i\mathbf{q}b_{\mathbf{q}}}{\sqrt{\rho}}\, e^{-i\mathbf{q}\mathbf{r}}, \tag{4.6}$$

where $\mathbf{q}$—phonon wave vector and ρ—silicon density.

a) The T_X process. One of the possible relaxation mechanisms is connected with the fact that the lattice vibrations modulate the hyperfine interaction between the donor electron and the impurity nucleus, producing an energy-level change corresponding to the reorientation of the electron and nuclear spins. The paper presents an estimate of the matrix element (4.5) for this mechanism. The first term of (4.5) vanishes, since the spin parts of the wave functions of electrons having opposite spin orientations are orthogonal. The second term of (4.5) is

$$(E_{0_+} - E_{0-})\,(\Psi_0^-,\ \delta\Psi_0^+) = \frac{1}{2}\,\delta A. \tag{4.7}$$

Here δA—change in the hyperfine interaction constant under volume broadening, which can be represented in the form

$$\delta A = \tilde{\gamma} A \Delta(0),$$

where $\tilde{\gamma}$—is a factor characterizing the degree of distortion of the energy bands upon deformation. This factor can be estimated if one knows the wave functions and the structure of the energy bands. It is assumed in[46] that $10 \leq \tilde{\gamma} \leq 100$ in the case of silicon. The relaxation time T_X is found from the expression

$$\frac{1}{T_x} = \frac{2\pi}{\hbar}\int \frac{dq}{(2\pi)^3}\,\delta(\hbar sq - \hbar\omega_0)\left(N_q + 1\left|\frac{1}{2}\,\delta A\right|N_q\right)^2. \tag{4.8}$$

The last factor under the integral sign is the square of the matrix element for the electron-phonon interaction, N_q—number of phonons with wave vector q, s—speed of sound, k—Boltzmann constant, and T—lattice temperature.

In the general case, when the nuclear spin is equal to I, we have

$$T_x = \frac{4\pi\hbar^2 s^5 \varrho}{\omega_0^3 kT I \tilde{\gamma}^2 A^2}. \quad (4.9)$$

For $\tilde{\gamma} \approx 50$, $(\omega_0/2\pi) = 9000$ Mcs, and $T = 1.2°K$ we have $T_X = 3.6 \times 10^6$ min for Si doped with lithium. For silicon doped with phosphorus, arsenic, and antimony T_X is equal to 560, 56, and 41 min, respectively.

b) The T_S process. In[46] is given an estimate of the relaxation time for the T_S process. The matrix element (4.5) was calculated for this process primarily under the assumption that spin reorientation is due to modulation of the spin-orbit coupling of the donor electron by the lattice vibrations. It is shown in the paper that the main contribution to this process should be made by the first term of the matrix element (4.5), which does not vanish in this case, since the spin-orbit coupling causes mixing of the states corresponding to the different spin orientations. The energy of the spin-orbit interaction depends on the gradient of the periodic potential produced by the silicon atoms, and on the gradient of the potential produced by the impurity atoms. The degree of mixing of the states can be approximately characterized by the change in the g-value relative to its value for the free electron (Δg). We shall denote by Δg_{Si} the change in the g-value due to the silicon atoms and by Δg_{imp} the g-value change connected with the impurity atom.

If we assume that the mixing of the states is due to spin-orbit interaction caused only by the silicon atoms, then the first term of the matrix element (4.5) turns out to be

$$(\Delta g_{Si})\, \varepsilon'_+ q_0^2 b_{q_0} (3a^*). \quad (4.10)$$

It is assumed here that the volume broadening (4.6) is produced only by one resonant phonon q_0.

On the other hand, if we consider only the spin-orbit interaction connected with the impurity atoms, then this term of the matrix element is approximately equal to

$$(\Delta g_{imp})\, \varepsilon'_+ q_0^2 b_{q_0} r_{n0}, \quad (4.11)$$

where r_{n0}—dipole matrix element for the transition from the n-th excited state to the ground state.

The relaxation time T_S, calculated in the ordinary manner and corresponding to the first term of the matrix element (4.5), is given by the expression

$$\frac{1}{T_s} = \frac{(\varepsilon'_+)^2 \omega_0^4 kT}{2\pi\hbar^2 \varrho s^7} [(\Delta g_{imp})^2 \langle r_{n0}\rangle^2 + (\Delta g_{Si})^2 (3a^*)^2]. \quad (4.12)$$

Assuming that $\omega_0/2 = 9000$ Mcs, $\varepsilon'_+ = 14$ eV, $\langle r_{n0}\rangle = 2.4 \times 10^{-7}$ cm, $T = 1.2°K$, and $\Delta g_{imp}/\Delta g_{Si} = 0.1$ we get $T_S \geq 75$ min.

The second term of (4.5) for this mechanism is calculated first for the conduction electrons at helium temperatures. It corresponds to a relaxation time $T \approx 10^{-5}$ sec, which coincides with the experimental value[52]. The ratio of the matrix elements for the bound and conduction electrons is very low; in[36] this ratio is assumed to be $\hbar\omega_0/1\ \text{eV} \sim 10^{-5}$. If we take also account of the difference in the effective densities of the conduction-electron states and of the bound electron states, then we obtain for the bound electrons a relaxation time so long that it cannot be measured experimentally.

In[46] there is considered still another mechanism of relaxation of donor electrons for the T_S process, in which the lattice oscillations modulate the hyperfine interaction between the donor electron and the Si^{29} nuclei. The relaxation-time ratio for this mechanism to T_X is of the order of 100—2000 for phosphorus, arsenic, and antimony impurities; for lithium this ratio is smaller than unity.

From the theory of Pines, Bardeen, and Slichter follows the conclusion that the shortest relaxation time corresponds to the T_S process for the relaxation mechanism in which the lattice oscillations modulate the spin-orbit coupling of the donor electron. However, this conclusion, which is confirmed by experiment, is based on an inaccurate estimate of the second term of the matrix element (4.5).

Abrahams[47] made a more rigorous calculation. Unlike in[46], he uses in his theory not simplified wave functions with a single minimum, but the wave functions (1.6) which take into account the spin-orbit coupling in the Bloch functions:

$$\Psi_0 = A|\pm\rangle + M^{\pm}B^{\pm}|\mp\rangle, \quad (4.13)$$

where A—the wave functions (1.6) and

$$B^{\pm} = \frac{1}{\sqrt{6}} \sum_{j=1}^{6} F_j \varphi_j^{\pm}.$$

Here $M^{\pm}$—matrix element characterizing the degree of mixing of the states, and $\varphi_j^{\pm}$—Bloch function for the excited state. The second term of (4.5) takes the form

$$G(N_q+1)^{1/2} q^{1/2} [M^-(A, e^{iqr}B^-) + M^+(B^+, e^{iqr}A)], \quad (4.14)$$

where $G = i\varepsilon'_+ (\hbar/2\rho Vs)$ and V—volume of the silicon.

Van Vleck has shown[55] that if $M^- = M^+$ with $(B^-)^* = -B^+$, then such a matrix element is equal to zero (the Van Vleck "cancellation"). The matrix element (4.14) then becomes equal to

$$G\left(\frac{2g\beta H_0}{E_{0n}}\right)(N_q+1)^{1/2} q^{1/2} M(B^+, e^{iqr}A), \quad (4.15)$$

i.e., an account of the Van Vleck "cancellation" leads to the appearance of a factor $2g\beta H_0/E_{0n}$, where E_{0n}—energy difference between the ground and excited states. The last factor of (4.15) can be written, with account of (4.12), in the form

$$(B^+, e^{iqr}A) = \frac{1}{6} \sum_{ij} \int F^2(\mathbf{r}) (\varphi_j^+)^* e^{iqr} \Psi_i\, dr. \quad (4.16)$$

The anisotropy of the effective mass is neglected here, so that the function $F^2(\mathbf{r})$ is the same for all the energy minima. The slow variation of $F^2(\mathbf{r})$ causes the terms of the matrix element with identical summation indices, i.e., those relating identical minima, to be equal

to zero; the matrix elements relating different minima tend to zero as a result of interference of the Bloch functions.

Thus, the Abrahams calculations, in which account is taken of the Van Vleck "cancellation," which leads to the appearance of a factor $2g\beta H_0/E_{0n}$, and of the "phase cancellation," which leads to a decrease in the second term of the matrix element (4.5) by approximately 10^4 times, show that the estimate given for the matrix element in[46] is too low, and that in fact this matrix element corresponds to a relaxation time $T_S \sim 10^9$ sec, which cannot be measured experimentally.

The spin-lattice relaxation time of the donor electrons in silicon and germanium was also calculated for the T_S process by Hasegawa[34]; he considers a relaxation mechanism in which the lattice vibrations modulate the value of the singlet-doublet splitting in the silicon and of the singlet-triplet splitting in germanium. This mechanism leads to a time variation of the population of the different energy minima and is therefore manifest in a change in the g-value. The appreciable difference between the calculations of Hasegawa[34] and the calculations of Pines, Bardeen, and Slichter[46] or of Abraham[47] is due to the following:

1) Hasegawa[34] uses the Herring and Vogt deformation-potential theory[30], which is a generalization of the theory of Bardeen and Shockley[51] to the case of multivalley semiconductors. Both the isotropic dilatation of the lattice and the uniaxial strain characterized by Ξ_u and determined experimentally in[53,54] are considered here. The isotropic dilatation was considered in[46,47]. The contribution made by the uniaxial strain to the spin-lattice relaxation process is indicated in[34].

2) Hasegawa chose for the excited states that mix in with the ground state as a result of spin-orbit interaction the states (1.7) that are produced as a result of the splitting of the ground state.

Let us dwell briefly on some results of the Hasegawa theory. We denote by Ψ_n the donor-electron wave functions satisfying the Schrödinger equation with Hamiltonian

$$\mathcal{H} = -\frac{p^2}{2m} + \tilde{V}(\mathbf{r}) + \frac{\hbar}{2m^2c^2}(s \operatorname{grad} \tilde{V}), \qquad (4.17)$$

where $\tilde{V}(r)$—sum of the periodic and impurity potentials. (We note that the third term of (4.13) expresses the energy of the spin-orbit interaction.) Inasmuch as each level is at least doubly degenerate in the absence of a magnetic field, the symbol Ψ_n denotes two series of eigenfunctions, Ψ_n^+ and Ψ_n^-, corresponding to the eigenvalues ϵ_n^*.

Hasegawa considers in[34] the interaction of the electron with a constant magnetic field H_0 ($\mathcal{H}_Z = \beta H_0 (1 + gs)$) and with the crystal lattice ($\mathcal{H}_{e-L} = -Q(\mathbf{r}) \operatorname{grad} V_{period}$).

The change in the ground-state energy due to this interaction is

$$\Delta\mathcal{H} = (\Psi_0, \mathcal{H}_z\Psi_0) + (\Psi_0, \mathcal{H}_{e\text{-}L}\Psi_0) + \sum_n{}' \frac{1}{E_0 - E_n}[(\Psi_0, \mathcal{H}_z\Psi_n)(\Psi_n, \mathcal{H}_{e\text{-}L}\Psi_0) + (\Psi_0, \mathcal{H}_{e\text{-}L}\Psi_n)(\Psi_n, \mathcal{H}_z\Psi_0)]. \qquad (4.18)$$

Here Ψ_0 denotes the wave function of the ground state. The second term of (4.18) represents a first-order interaction between the electron and the lattice. However, as shown by Abrahams[47], this term does not make any appreciable contribution to the relaxation, owing to the Van Vleck cancellation and the phase cancellation. Hasegawa[34] estimates the contribution of the third term of (4.18) to the spin-lattice relaxation process. The summation is carried out, generally speaking, over all the excited states, but Hasegawa confines himself only to those states which were produced as a result of the splitting of the ground state. The energy of interaction with the lattice is small in comparison with this splitting, so that perturbation theory can be used.

Hasegawa considers both longitudinal and transverse phonons with wave vector q. The relaxation time T_S is determined from the expression

$$\frac{1}{T_s} = \frac{4}{5\pi}\left(\frac{g'\Xi_u}{3gE_{0n}}\right)^2\left(\frac{1}{\varrho v_1^5} + \frac{2}{3\varrho v_2^5}\right)\left(\frac{2\beta H_0}{\hbar^2}\right)^4 kTf(\theta, \varphi),$$

where

$$\varrho v_1^2 = c_{11} - \frac{2}{5}c^*, \quad \varrho v_2^2 = c_{44} + \frac{1}{5}c^*, \quad g' = \frac{1}{3}(g_{\parallel} - g_{\perp}), \qquad (4.19)$$

$g = (1/3)(2g_\perp + g_\parallel)$ (see above concerning the g-value anisotropy). The energy difference between the ground and excited state is $E_{0n} = E_{12}$ for silicon and $E_{0n} = E_{13}$ for germanium; c_{11}, c_{44}, and c^* are elastic constants. It follows from these expressions that $1/T_S$ is proportional to the first power of T and to the fourth power of H_0. This relation is due to the fact that 1) the matrix element $\langle\mathcal{H}_{e-L}\rangle$ is proportional to H_0^2, 2) the principal term in the expression for the density of states for acoustic phonons is proportional to ω^2, 3) the mean value of the square of the dynamic strain is proportional to kT and does not depend on H_0. Substituting the numerical values in (4.19), and assuming that the magnetic field H_0 lies in the (110) plane (for in which case we have $f(\theta) = \cos^4\theta + (1/2)\sin\theta$ for germanium and $f(\theta) = (3/4)\sin^2\theta\,(1 + 3\sin^2\theta)$ for silicon), we obtain the data listed in Table IV at $T = 1.25°$ K for different donors and different directions of the field $H_0 = 3000$ Oe.

The anisotropic properties of the relaxation time are due to the geometrical structure of the edge of the conduction band.

It must be noted that the main results of[34], which we cite here, have been obtained under the following assumptions: 1) the state of the electron is described by the wave functions of Kohn and Luttinger (1.6); in

Table VI. Theoretical values of T_S, calculated by Hasegawa[34]

	$H_0 \parallel [111]$			$H_0 \parallel [100]$	
		Ge	Si	Ge	Si
$1/T_s$, sec^{-1}	P	$4.4 \cdot 10^2$	$9 \cdot 10^{-5}$	$1.3 \cdot 10^3$	0
	As	$2.4 \cdot 10^2$		$7.3 \cdot 10^2$	0

the case of silicon and $H_0 \parallel [100]$, the matrix element for the transition between the states with reversed spin, described by (1.7), tends to zero, making $1/T_S = 0$; 2) the spin-orbit interaction due to the impurity can be neglected; 3) the contribution of the higher excited states can likewise be neglected.

The correctness of the latter assumption is confirmed by the fact that the only excited states leading to the H_0^4 dependence, which is confirmed experimentally, are those due to splitting of the ground state.

Results analogous to[34] were obtained also by L. Roth[33]. Let us stop to discuss briefly these results. It is shown in[33] that the g-factor for the electrons in Si and Ge is anisotropic (see Ch. III). In experiments on the EPR of donor electrons one usually observes an isotropic g-factor, because these electrons are in the singlet state, which is described by wave functions which constitute a linear combination of the wave functions corresponding to different ellipsoids, such that the effect becomes averaged. The g-value anisotropy characteristic of the conduction electrons in Si and Ge, is manifest for donor electrons in the singlet state by the strong interaction between the electrons and the waves due to the uniaxial strains in the crystal lattice. The ground states of the donor electrons in Si and Ge, as indicated above, are singlet; Roth, like Hasegawa, define the two-fold and three-fold degenerate levels produced as a result of the splitting of the {1s} level as excited. Inasmuch as for an arbitrary magnetic field direction the interaction $g\beta H_0$ is different for electrons with values of k_j that lie on different ellipsoids, a mixing of the singlet and excited donor states is possible; the latter, in particular, can also differ from the ground state in the spin orientation. Therefore interactions with the crystal-lattice waves capable of changing the orientation of the donor-electron spin are possible. The usual Van Vleck cancellation used in[47] cannot be employed here. It is due to the invariance of the operator under time reversal, which is impossible if an interaction with the magnetic field is also included.

The calculation given in[33] for the direct phonon process is essentially analogous to the calculation of Hasegawa[34]. We shall not repeat here the cumbersome expressions for the relaxation time of the donor electrons. We merely note that these expressions give the same dependence of the relaxation rate on the temperature and on the magnetic field as (4.19). These calculations also lead to the anisotropic properties of the relaxation rate, and in particular to the small value of this rate for $H_0 \parallel [100]$ in the case of silicon. For some averaged direction of the magnetic field at $H_0 = 9000$ Oe and $T = 1.25°K$ we have $T_S \sim 1000$ sec.

2. Raman process. A second-order interaction between the phonons and the donor electrons leads to a process of the Raman type. Such a process comprises phonon scattering with a transition from the q-state into the p-state, with simultaneous electron spin flipping. An estimate of the spin-lattice relaxation time of the donor electrons in silicon and germanium in the Raman process was made by Abrahams[47] and by Roth[33]. Let us discuss first the first paper. The calculation procedure is the same as for the direct phonon process. The effective matrix element characterizes a transition to an excited orbital state with emission or absorption of a phonon, and then the inverse transition, likewise with absorption or emission of a phonon. The electron spin flip can occur either in the first or in the second transition.

We shall not stop to calculate the matrix element for such a process, presenting only the final result:

$$T_s \approx 10^{15} T^{-13}. \tag{4.20a}$$

In calculating this expression we neglect the energy $g\beta H_0$ compared with $\hbar sp$ and $\hbar sq$; therefore in the final analysis T_S is independent of the magnetic field.

It follows from (4.28) that at helium temperatures the relaxation time for this process is very large, but it is already of the order of 1 second at 14°K. A different dependence of the relaxation time on the temperature and on the field was obtained for the two-phonon process in[33]. Like Hasegawa[34], Roth uses the Herring and Vogt deformation-potential method[30] in the calculations, which are confined to an estimate of the contribution made to the matrix element by the transverse waves produced in the case of axial shears of the crystal lattice. In[33] the value obtained for silicon is

$$\frac{1}{T_s} = \frac{9\pi^3}{175}\left(\frac{\sigma}{E_{12}}\right)^4\left(\frac{\Delta g}{g}\right)^2 \omega^2 \frac{(kT)^7}{\hbar^5 \varrho^2 c_t^{10}}\left\{\frac{H_x^2 H_y^2 + H_x^2 H_z^2 + H_y^2 H_z^2}{H_0^4}\right\}. \tag{4.20b}$$

Here E_{12}—splitting between the singlet and the doublet, equal to 10^{-2} eV, $\Delta g/g = 1.5 \times 10^{-3}$, $\sigma = 11$ eV, and $c_t^5 = 5 \times 10^{28}$. At 4.2°K, the relaxation time for such a two-phonon process in silicon is 60 seconds. The relaxation rate, as can be seen from (4.20b), is proportional to the 7th power of the temperature and to the square of the field.

3. Exchange interaction between neighboring impurity centers. As will be shown presently, the relaxation mechanisms considered above can be used to explain, with one degree of accuracy or another, the experimentally observed relaxation times and their dependence on the magnetic field and on the temperature. However, it was impossible to explain by means of these mechanisms the sharp decrease in the relaxation time with increasing concentration of the doping impurity, a decrease observed even in the first experiments of Feher (when the phosphorus concentra-

tion was increased from 10^{17} cm^{-3} to 4×10^{17} cm^{-3}, the relaxation time decreased from several seconds to 10^{-5} sec). So far there is no theory capable of answering this question.

In [46] an attempt was made to relate the decrease in the relaxation time with the occurrence of groups consisting of several impurity atoms. A calculation was made for groups made up of two closely-lying impurity atoms. It was assumed there that the lattice vibrations modulate the exchange interaction between these atoms. The calculation is essentially analogous to the calculation of the relaxation time for the process due to the modulation of the hyperfine interaction of the electron with the impurity nucleus. If the energy of the exchange interaction is JS_1S_2 (where J is the exchange-interaction constant, which depends on the distance between the impurity atoms, i.e., in final analysis, on the impurity concentration), then the ratio of the relaxation time T_{exch} for this process to T_x is equal to

$$\left(\frac{2r}{3a^*}\right)^2\left(\frac{J}{\hbar\omega_0}\right)^2. \qquad (4.21)$$

At an impurity atom concentration 3×10^{16} cm^{-3}, the most probable distance to the nearest neighbor r is approximately 87 Å, and in this case the value of the exchange integral J, expressed in Oersteds, is approximately 0.88; consequently $T_{exch} = 4 \times 10^5\ T_x$ at $H_0 = 3000$ Oe and $T_{exch} \sim 225\ T_x$ at a concentration 10^{17} cm^{-3}. Thus, the relaxation time for this mechanism is very large.

4. Interaction between the donor electrons and the conduction electrons. If the conduction band contains electrons, we may encounter a new mechanism for the relaxation of the donor electrons. Pines et al [46] considered exchange scattering of electrons whereby the impurity electron and the conduction electron exchange places, after which a very rapid relaxation of the conduction electrons takes place. Let us dwell briefly on the main results. We assume that n—number of conduction electrons and N—number of donor electrons. If W^+—velocity of the conduction electrons and U—probability of exchange transition, and if W^+ is large, calculations show that the relaxation rate of the electrons is equal to nU, i.e., to the number of collisions experienced by the donor atoms per unit time. This quantity can be estimated, since $U/2 = \sigma_{0p} v_e$, where σ_{0p}—cross section of spin exchange and v_e—velocity of conduction electron. The cross section can be determined from the formula for the exchange scattering of electrons from hydrogen atoms:

$$\sigma_{0p} = \frac{144\pi\hbar^4}{m^2e^4},$$

After which account is taken of the dielectric constant of silicon; then $\sigma_{0p} = 3 \times 10^{-12}$ cm^2. If we assume $v_e = 10^6$ cm/sec, then $U = 6 \times 10^{-6}$ sec and $nU = 6 \times 10^{-6}$ n. When $n = 10^8$, the donor electron relaxation rate should be 6×10^2 sec^{-1} (relaxation time 1.6×10^{-3}), if the relaxation rate of the conduction electrons is sufficiently large. Actually, however, this requirement is very difficult to satisfy, since it signifies that $W^+ \gg NU$. When $N = 10^{16}$ cm^{-3}, W^+ should be considerably larger than 6×10^{10}. At room temperature, W^+ is equal only to 10^9, and at helium temperature it is even smaller, since the relaxation rate of the donor electrons can be assumed to be approximately equal to W^+n/N. Portis and his co-workers [1] have found that the line width at resonance of the conduction electrons is equal to 2 Oe, which corresponds to a relaxation rate of 4×10^7 sec^{-1}. If $n/N = 10^{-12}$, then the relaxation time is of the order of 400 minutes. So large a value of n/N cannot result from thermal ionization and helium temperatures, although at 20° K such an excitation is possible. As will be shown later, such a value of n/N, and an even higher value at helium temperatures, can be produced by optical excitation.

In addition to this mechanism, others are also possible, as shown by Abrahams [47], viz., Coulomb scattering of the conduction electrons and of the bound electrons, which can lead to flipping of the spins of the latter; flipping of the donor spins under the influence of magnetic fields produced by the motion of the conduction electrons; dipole-dipole interaction between the bound electrons and the conduction electrons, in which spin flip of both types of electrons takes place. It turned out that none of these mechanisms is as effective as exchange scattering.

5. Influence of acceptor impurity on the relaxation rate of donor electrons. Experiments show that in phosphorus-doped silicon containing an acceptor impurity the rate of relaxation is the larger, the larger the acceptor impurity content. V. I. Avdeev [48] attempted to estimate the effect of the acceptors on the relaxation rate of the donor electrons.

Avdeev considers as a possible mechanism the following: the electron from the neutral donor atom (i) goes over to the next ionized atom (j), and such a transition is accompanied by absorption or emission of a phonon. The considered transitions $i(+) \rightarrow j(-)$ are due only to the modulation by the lattice vibrations of the hyperfine interaction of the electron with the impurity nucleus. Since interatomic transitions are important in this case, the overlap integral should not be very small. On the other hand, to resolve the hyperfine structure it is necessary that the integral not be very large. In germanium, the latter condition is satisfied at a concentration 4×10^{16} cm^{-3}, and the overlap integral has a value on the order of 10^{-2}; for silicon under the same conditions, the overlap integral is approximately equal to 10^{-5}.

We shall not repeat the expression obtained in [48] for the relaxation times T_x, but it follows from it that the relaxation rate for this process depends little on the field and is proportional to T^5. The relaxation rate for the given mechanism is proportional to the

product of the probability of spin flip in the single-phonon process and the probability of the transition of the electron from one atom to the other. The first probability, as follows from the theory of the single-phonon process, is proportional to T, while the second, as follows from semiconductor theory, is proportional to T^4 at low temperatures.

In calculating T_X for germanium, Avdeev found that the relaxation rate decreases with decreasing concentration of the donor impurities and does not depend on the nature of the acceptor impurity. For germanium at an arsenic donor concentration $(1-4) \times 10^{16}$ cm^{-3} and at an acceptor concentration half as large we have $1/T_X = 0.3-3$ sec^{-1}. For silicon at a donor concentration $(4-3) \times 10^{16}$ cm^{-3} and at an acceptor concentration half as large we have $1/T_X = 10^{-2}-10^{-3}$ sec^{-1}. The accuracy of the calculation is less reliable, since the overlap integral is small.

2. Experimental Methods of Determining the Relaxation Time

The first measurements of the spin relaxation time were made by Honig [45], who obtained very large relaxation times (tens of seconds at 4° K), he assumed that he dealt in this case with nuclear relaxation processes. Subsequent experimental and theoretical investigations [46,47,33,34] have shown that large electron relaxation times are involved in this case. Of all the experimental papers on the determination of the spin-lattice relaxation time, the most complete are those of Feher and Gere [20], Honig and Stupp [56], and Wilson and Feher [29].

There are several methods of measuring relaxation time. In all methods it is first necessary to disturb the thermal equilibrium between two levels. This is done either by completely saturating the spin system, or by level inversion under adiabatic fast passage (see above).

When measuring large relaxation times, such as encountered in semiconductors, it is necessary to prevent light from striking the sample and to protect the sample against thermal radiation from the waveguide elements which are at room temperature. This is done by wrapping the cavity with several layers of aluminum lined with carbon paper. The waveguide connected to the cavity is filled on the inside with foamed styrene [20], and in addition, a glass plate 1 mm thick is inserted in it to absorb the thermal radiation of the waveguide elements that are at room temperature. As indicated above, there are different relaxation processes in silicon doped with phosphorus. In order to investigate them in detail it is necessary to be able first to separate experimentally each of these processes, and then to be able to understand which mechanism (or mechanisms) leads to a given relaxation process.

1. Study of the T_S process. a) Case of strong field. Honig and Stupp [56] measured T_S in the case of a strong field (above 1500 Oe) in the following fashion. They saturated the "vertical" levels by multiple passage through resonance so that the fast-passage signal became equal to zero. Then the amplitude of the signal (difference in level population) was measured at definite time intervals t. Since dispersion is observed under the condition of adiabatic fast passage, and since field modulation and narrow-band detection circuits are used in addition, the signal has a complicated dependence on such parameters as the microwave power, the rate of change of the constant magnetic field, the velocity and amplitude of the modulating field, etc. However, when all these parameters were maintained constant, then the signal amplitude (which is proportional to the population difference) could be reproduced in [56] with accuracy of 3% for many hours.

As follows from (4.2), the relaxation time can be calculated from the slope of the plot of

$$\frac{n(t)-n(\infty)}{n(0)-n(\infty)}$$

against t (Fig. 9). The quantities n(0) and n(t) in this expression can be measured, but it is quite difficult to determine $n(\infty)$ if we deal with very large relaxation times. To determine this quantity one usually employs a feature of the "vertical" relaxation process, whereby T_X becomes small in very strong fields. (Thus, for example, at $H_0 = 10{,}000$ Oe, $T_S < 7$ min in all phosphorus-doped samples.) Consequently, in a field $H_0 = 10{,}000$ Oe it is possible to measure simultaneously $n(\infty)$ and T_S with great accuracy.

b) Case of weak field. In the case of a weak field T_S is measured essentially by the same method. However, inasmuch as the Zeeman splitting of the levels, and consequently also the population difference between them (the amplitude of the signal) are small, it is difficult to obtain a good signal/noise ratio, and this lowers the measurement accuracy. In order to overcome this difficulty, the following procedure is used: the equilibrium magnetization of the sample and the level inversion are effected in a strong field, while the

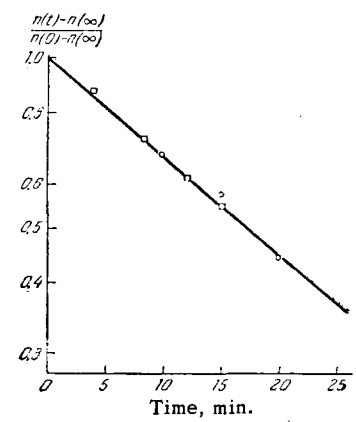

FIG. 9. Dependence of $[n(t) - n(\infty)]/[n(0) - n(\infty)]$ on the time. The ordinate scale is logarithmic.

rate of the change of the signal is measured in the investigated weak field. This yields a good signal/noise ratio even in the weakest fields. The correctness of this was confirmed by the agreement between the results of this method and others. It must be noted that the described method of determining T_S cannot be used if the dominating process is T_X and not T_S. However, there are other methods which make it possible to determine which of the processes predominates. One of the most widely used methods, also used by Honig and Stapp[56], is the method of "forbidden transitions." This method consists in first establishing the equilibrium population difference between the levels (1 ↔ 4) and (2 ↔ 3), and then rotating the waveguide through 45°. The microwave field H_1 will then have a component along H_0. As a result, the transition ($m_I = 1/2$, $m_J = -1/2$) ↔ ($m_I = -1/2$, $m_J = +1/2$) will be saturated. This forbidden transition can be realized only when there is a sufficiently strong microwave field parallel to H_0. After saturation of this transition, the waveguide is set in its initial position and the signal intensity is measured. If the T_S process predominates, then the amplitudes of the resonance lines have the same magnitude, equal to half the amplitude which they would have if the forbidden transition were not saturated. If the T_X process predominates, the amplitudes are equal to zero.

2. Measurements of T_X, T_X', and T_N. The processes T_X, T_X', and T_N are considered together, since the experiments yield unavoidably a combination of these processes. In the study of the processes of "horizontal" relaxation one usually uses two measurement methods. Each gives a distinct relaxation time, which has a different dependence on T_X, T_X', and T_N. The two methods complement each other, and taken separately neither can give an idea of the relative importance of the processes T_X, T_X', and T_N.

The first method is based on the application of the Overhauser effect to the discrete hyperfine structure lines; this method was used in several different variants by Pipkin[57], Feher[58], and Honig[56]. Let us stop to discuss the last variant, which has several advantages over the others.

In this method the transitions 1 ↔ 4 and 2 ↔ 3 are first saturated quasi-continuously (see Fig. 8), and passage through the line is with a speed such as to make the period of the passage small compared with T_X and T_S. Let us assume that the only horizontal-relaxation process is T_X. When t = 0 the populations of all four levels are equal ($n_1 = n_2 = n_3 = n_4 = N/4$). After some definite time interval, an equilibrium population difference is established between levels 2 and 4, and this difference can be measured in the following fashion: the "vertical" transitions are saturated first, then the transition 2 ↔ 4, followed by measurement of the signal amplitudes. They are equal in magnitude and proportional to $(n_4 - n_2)/2$; the relaxation time T_X can be determined from the formula

$$(n_4 - n_2)(t) = \frac{N}{2} \operatorname{th}\left(\frac{\beta H_0}{kT}\right)(1 - e^{-t/2T_X}). \qquad (4.22)$$

In the case when alongside with T_X there are present also the T_X' and T_N processes, formula (4.22) becomes more complicated (see[56]) and takes the form*

$$(n_4 - n_2)(t) \approx \frac{N}{2} \operatorname{sh}\left(\frac{\beta H_0}{kT}\right)[1 - \exp(-\langle\langle 2W\rangle\rangle t)],$$

where "2W"—effective probability;

$$\langle\langle 2W_{Over}\rangle\rangle = \left(\langle\langle \frac{1}{T_1}\rangle\rangle\right)_{Over} = (W_x - W_{x'})[1 - (W_{x'} + W_N)t]. \qquad (4.23)$$

The difference $W_X - W_{X'}$ can be determined directly from the experimental data if the time t is small. If the measurements are sufficiently accurate, $W_{X'} + W_N$ can be determined. In the experimental determination of the times of horizontal relaxation, measures must be taken to exclude "forbidden" transitions that lead to the same effect as the T_N process. This is accomplished by accurate orientation of the waveguides in such a way as to make the component H_1 along H_0 minimal.

The second method of determining the times of "horizontal" relaxation, that of depolarization of the nuclei, consists in producing a definite nuclear polarization, which is then varied (the nuclei are depolarized) as a function of the magnetic field and the temperature. The nuclear depolarization is caused by the relaxation processes T_X, T_N, and T_X', and the depolarization can be determined by measuring the ratio of the amplitudes of two hyperfine structure lines. Assuming that $\cosh(\beta H_0/kT) \approx 1$ and $W_S > W_X$, $W_{X'}$, and W_N, we get

$$T_{1\,dep} = \left[\frac{W_x + W_{x'}}{\operatorname{ch}(\beta H_0/kT)} + 2W_N\right]^{-1}. \qquad (4.24)$$

The expressions (4.23) and (4.24) for T_1 show that in medium fields (for which the relation $\cosh(\beta H_0/kT) \approx 1$ holds), the relaxation time measured by the depolarization method is always smaller than the time measured by the Overhauser method. Estimates of the relative importance of each of the horizontal-relaxation processes will be presented below.

3. Main Experimental Results

1. T_S process. The T_S process was investigated in detail in[20,56] over a wide range of magnetic fields (from zero to 11,000 Oe), temperatures (from 1.25 to 4.2° K), and impurity concentrations (from 10^{14} to 5×10^{18} cm^{-3}). The first striking fact is the sharp dependence of the relaxation time on the donor concentration. Figure 10 shows the experimental dependence of the relaxation rate $1/T_S$ on the phosphorus concentration, obtained by Feher[20]. It is seen from this curve that at concentrations below 10^{16} cm^{-3} the

*sh = sinh

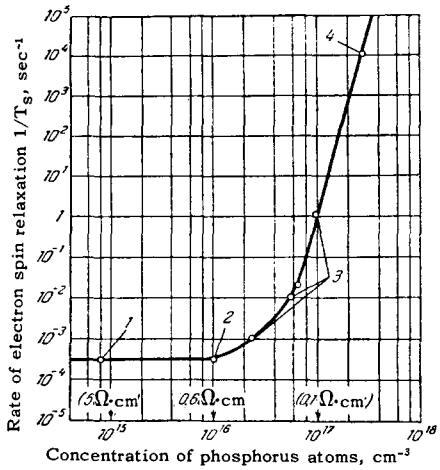

FIG. 10. Dependence of the spin-lattice relaxation time on the concentration of phosphorus in silicon (T = 1.25°K; $H_0 \approx 3200$ Oe). 1 – Sample Si VIII-58, boron concentration 3×10^{14} cm^{-3}; 2 – sample Si VIII-64, boron concentration 3×10^{14} cm^{-3}; 3 – sample Si VIII-230, boron concentration 2×10^{14} cm^{-3}; 4 – sample Si VIII-215, B concentration $\leq 10^{15}$ cm^{-3}.

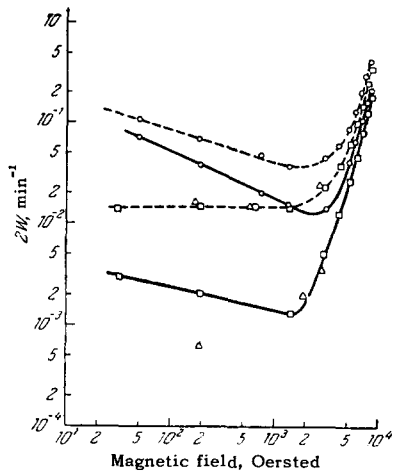

FIG. 11. Dependence of the relaxation probability 2W on the magnetic field for three samples: o – sample with phosphorus concentration 1.1×10^{16} cm^{-3}; □ – 10^{15} cm^{-3}; Δ – 10^{14} cm^{-3}; measurements made at 1.25°K (continuous curves) and 2.16°K (dashed).

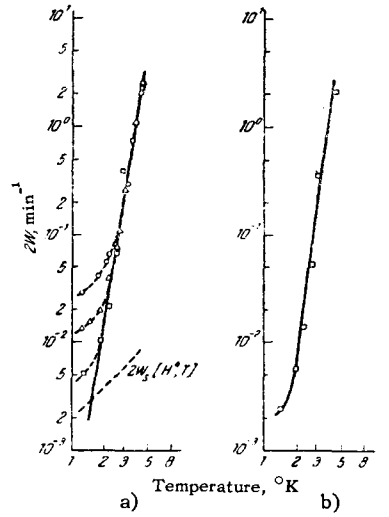

FIG. 12. Dependence of relaxation probability 2W on the temperature: a) Samples B, C, F (points o, Δ, and □, respectively), b) sample F after subtracting from the relaxation probability the values of $2W_s(N_p)$ and $2W_s(H^4, T)$, which are connected respectively with the concentration-dependent and with the H^4 relaxation mechanisms, and also the transition probability for horizontal relaxation; H_0 = 3400 Oe.

relaxation time is practically independent of the concentration; at concentrations above 10^{16} cm^{-3}, the dependence is very sharp. Therefore Feher distinguishes between two relaxation mechanisms, one dependent on the concentration and one independent. However, such a subdivision is apparently inaccurate. As shown by Honig and Stupp [56], in this case there are in effect at least three mechanisms, each of which predominates in a definite range of values of the field, temperature, and donor concentration, but makes a contribution to the T_S process even outside this region.

The first mechanism, called by Honig and Stupp the H^4 mechanism, predominates in strong magnetic fields and at temperatures lower than 2.5°K. This mechanism, as follows from the figure, is characterized by the fact that the relaxation rate is proportional to H^4 and depends linearly on the temperature. The greatest deviations for samples with different concentrations are due to the fact that even in strong fields some contribution is made by the concentration-dependent mechanism. At 3,000 Oe and 1.25°K, Honig and Stupp obtained $1/T_S = (2.63 \pm 0.1) \times 10^{-5}$ sec^{-1}.

The second mechanism, the T^7 mechanism, predominates at high concentrations for temperatures above 2.5°K, and at low concentrations over the entire temperature range. This mechanism is characterized by the fact that the relaxation rate does not depend on the donor concentration or on the magnetic field, but depends very strongly (in proportion to T^7) on the temperature. The exponent of T is 7.5 ± 0.3 at 4.2°K and 7 at 2°K. Honig and Stupp found that at 2°K

$$\frac{1}{T_s} = (1.65 \pm 0.15) \cdot 10^{-4} \text{ sec}^{-1}.$$

The third, concentration-dependent mechanism, acts in weak fields at low temperatures and at large concentrations. The relaxation rate is proportional to $H^{-1/2}$ and to T. At 3,000 Oe, T = 1.25°K, and a concentration 5×10^{15} cm^{-3} we have

$$\frac{1}{T_s}(\text{conc.}) = (3.3 \pm 0.4) \cdot 10^{-4} \text{ sec}^{-1}.$$

The experimental curve shown in Figs. 11–12 also receives a small contribution, other than from these three mechanisms, from the "horizontal relaxation." To explain all the experimental points on these curves it is necessary to use in addition to the relaxation mechanisms a fifth mechanism, which acts on samples with low donor concentration for fields from 2000 to 3000 Oe at 1.25°K. This mechanism is characterized by a small relaxation rate, $1/T_1 \sim 2 \times 10^{-5}$ sec^{-1}. The properties of this mechanism were investigated very

little. We can assume, however, that in this field interval the relaxation rate does not depend on the magnetic field (or depends on it little), but depends on the concentration of the compensating impurity. This deduction was arrived at by Honig and Stupp on the basis of the following considerations. They investigated the dependence of the relaxation rate on the phosphorus concentration in silicon (see below and Fig. 13). The regular variation of the relaxation rate with the concentration is violated only for sample E. This sample was cut from silicon obtained by crucible melting, in which a high degree of impurity compensation is possible. The dependence of the relaxation rate on the magnetic field for this sample is analogous to the dependence obtained for the "fifth" relaxation mechanism. The tests that suggested to Honig and Stupp the existence of a "fifth" mechanism were repeated on samples with low donor concentration, obtained from the same initial material as sample E. It was therefore concluded that the "fifth" mechanism is connected with the degree of compensation of the sample.

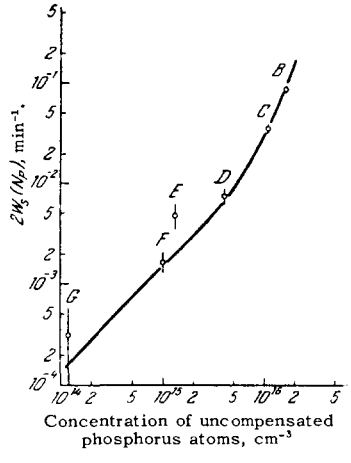

FIG. 13. Dependence of the relaxation probability $2W_s$ (N_p) on the concentration of the uncompensated phosphorus atoms for the concentration-dependent relaxation mechanism. (H_0 = 200 Oe, T = 1.25°K).

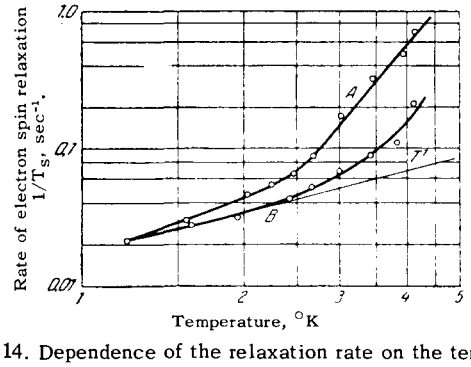

FIG. 14. Dependence of the relaxation rate on the temperature in two samples with different degrees of compensation (T = 1.25°K, $H_0 \approx$ 3200 Oe). Curve A – sample Si IX-99, phosphorus concentration 4×10^{16} cm^{-3}, boron concentration 1×10^{16} cm^{-3}; curve B – sample Si VIII-230, boron concentration 2×10^{14} cm^{-3}, phosphorus concentration 7×10^{16} cm^{-3}.

Feher[20] made special investigations of the influence of acceptors on the relaxation rate of donor electrons. Figure 14 shows the temperature dependence of the relaxation rate for silicon samples having the same donor concentration but different degrees of compensation. The relaxation time in the compensated samples is smaller than in the uncompensated ones.

Let us stop to discuss in somewhat greater detail the dependence of the relaxation rate on the donor concentration. Honig and Stupp determined the experimental relaxation probability for the concentration-dependent mechanism. This probability is obtained by excluding from the observed relaxation probability the relaxation probabilities connected with the H^4 mechanism, the T^7 mechanism, the "fifth" mechanism, and the "horizontal" relaxation. As a result they obtained the curve of Fig. 13, which shows that at phosphorus concentrations below 10^{16} cm^{-3}, the relaxation rate increases linearly with the concentration; at concentrations above 10^{16}, the dependence is much steeper. Such a dependence was observed also by Feher (see Fig. 10), but it was connected only with the concentration-dependent-mechanism. He therefore found that at low phosphorus concentration the relaxation rate is practically independent of the concentration. On the other hand, at high concentrations he found that the relaxation time decreases sharply from $3 \times 10^{+3}$ sec (concentration 10^{16} cm^{-3}) to 10^{-4} sec (concentration 3×10^{17} cm^{-3}).

Feher and Gere[20], and also Honig and Stupp[56], investigated the dependence of the relaxation rate for this process on the temperature and on the magnetic field. They found that in the low temperature region (< 2.50° K), the dependence is the same as for the direct phonon process. At higher temperatures, the dependence is not so strong as for the T^7 mechanism.

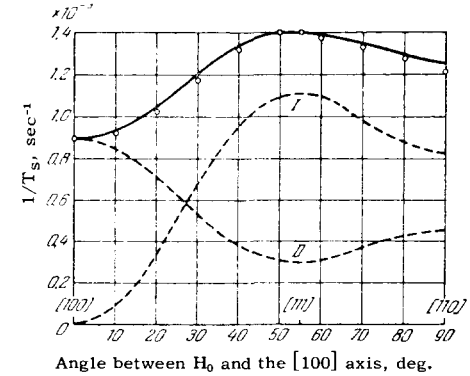

FIG. 15. Dependence of the relaxation rate on the angle between the magnetic field and the [100] axis for silicon doped with phosphorus; T = 1.25°K; ν_e = 9000 Mcs. o – Experimental points; dashed curve – theoretical; I – for the mechanism connected with the change in the populations of the different minima; II – for the mechanism connected with the modulation of the g-value for one energy minimum. Continuous curve – theoretical, obtained by summation of I and II.

Feher and Gere found that the relaxation rate for this mechanism does not depend on the magnetic field. Honig and Stupp observed a weak dependence on the magnetic field (for details see below).

We note still another interesting feature—the anisotropy of the relaxation time for the T_S process. Prior to the publication of the papers of Hasegawa[34] and Roth[33], which pointed to the anisotropy of T_S, experiments on the study of relaxation were made at arbitrary orientation of the sample relative to the magnetic field. Honig and Stupp made a series of experiments on the anisotropy of the relaxation time already following the publication of[56], in view of the publication of the papers by Hasegawa and Roth, and in a postscript to[56] they reported observation of anisotropic effects. Detailed investigation of this question, however, was made by Wilson and Feher[29]. Figure 15 shows the dependence of the relaxation rate on the angle between the magnetic field and the [100] axis. A noticeable anisotropy is seen.

2. Horizontal relaxation processes. Honig and Stupp measured the horizontal relaxation time ($\Delta m_I = \pm 1$). These measurements were made by the Overhauser method and by the nuclear depolarization method. An important factor in the first method, as follows from (4.23), is the time t, reckoned from the instant of saturation of the "vertical" levels. The results obtained by the two methods are quite close. Thus, for example, for $H_0 = 3400$ Oe, $T = 1.25°$ K, and a phosphorus concentration 1.1×10^{16} cm^{-3}, the horizontal relaxation time is $T_{Over} = 38^{+10}_{-6}$ hr (at t = 5 hr), while $T_{dep} = 32^{+6}_{-4}$ hr. The errors in these measurements are very large and are connected with the large relaxation times, the poor signal/noise ratio, etc. Honig and Stupp believe that at 2.15° K

$$0 \leqslant W_{x'} \leqslant 0{,}2,$$
$$0 \leqslant W_N \leqslant 0{,}1.$$

Here $T_X = 3 \pm 0.4$ hours. The T_X process is apparently the dominating "horizontal" relaxation process at higher temperatures, too. In the opposite case, the relaxation rate corresponding to the other processes should increase more rapidly than T^{10}.

At 1.25° K, the following relations hold true, in the opinion of Honig and Stupp, for the relaxation probabilities:

$$0 \leqslant W_{x'} \leqslant 0.2,$$
$$0 \leqslant W_N \leqslant 0.2,$$

i.e., at this temperature T_X exceeds 16 hours, $T_{X'} > 80$, and $T_N > 80$. The data of Honig and Stupp do not confirm the quadratic field dependence obtained by Feher and Gere[20] for the relaxation rate of the T_X process. The latter obtained $T_X = 30$ hr at $H_0 = 3200$ Oe and $T = 1.25°$ K and $T_X = 5$ hr at $H_0 = 8000$ Oe and $T = 1.25°$ K. Feher and Gere state also that $T_N > 10$. The large discrepancy in the experimental results for T_X, in the opinion of Wilson and Feher, is connected with the fact that local stresses are possible inside the crystalline specimen. Wilson and Feher[20] made a series of experiments on the influence of stresses on the relaxation time T_X. They measured T_X for silicon samples doped with As ($\sim 10^{16}$ cm^{-3}) in compression. In the absence of compression the value of T_X (at $H_0 = 3000$ Oe and $T = 1.25°$ K) is approximately 3×10^3 sec.

When the crystal is compressed along the [100] axis, T_X drops to 10^2 sec.

3. Effect of light on the relaxation time. In the first experiments of Feher and Fletcher[59] it was noted that the relaxation time was strongly influenced by light. Honig[60] has shown that the greatest decrease in the relaxation time is produced by light with a wavelength from 2 to 25 microns.

Feher and Gere[20] investigated the dependence of the relaxation rate on the wavelength of the light illuminating the object. The factor influencing the relaxation time is not the number of incident photons, but the number of free carriers (and the sign of their charge) excited by these photons. Figure 16 shows the results of these measurements for a silicon sample doped with phosphorus at a concentration $7 \times 10^{+15}$ cm^{-3}.

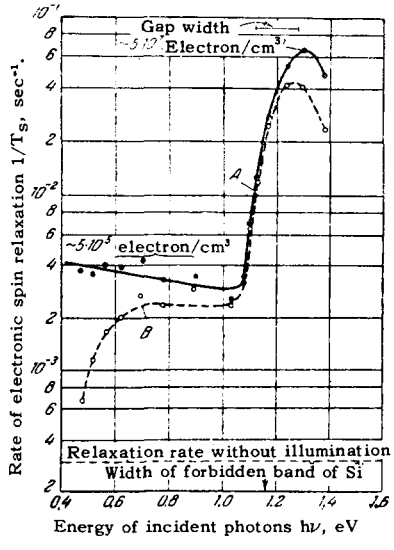

FIG. 16. Dependence of the relaxation rate in phosphorus-doped silicon on the wavelength of the incident light (phosphorus concentration 7×10^{15} cm^{-3}). Curve A – flux $\approx 3 \times 10^{13}$ photon/sec, curve B – observed increase in relaxation rate ($T = 1.25°$K, $H_0 \approx 3200$ Oe).

One curve shows a decrease in the relaxation time with increasing frequency of the incident light, while the other is normalized to a constant photon flux (approximately 3×10^{13} photons/sec) incident on the sample. This curve was calculated under the assumption that the decrease in the relaxation time is proportional to the number of incident photons. The dependence of the number of electrons excited by the light on the light energy follows the normalized curve up to energies below 1.15 eV. The sharp jump in the relaxation time

near approximately 1.15 eV is due to the fact that electron-hole pairs are produced near this energy. The majority carriers are still electrons with a mobility approximately equal to the mobility of the electrons in the photon-energy region corresponding to the ionization of the impurity atom.

4. Discussion of Results and Comparison with the Theory. Our explanation of the experimental results will begin with the single-phonon T_S process. According to the experimental data one should observe for this process a linear connection between the relaxation rate and the temperature, and a proportionality of this rate to H^4. As can be seen from the theory, such a dependence was obtained by Pines, Bardeen, and Slichter[46] (see (4.12)). However, as indicated by Abrahams[47], an allowance for the Van Vleck cancellation leads to the appearance of a factor proportional to H^2 in the expression for the relaxation rate $1/T_S$, i.e., $1/T_S \sim H^6$. In addition, the relaxation mechanism considered by Pines, Bardeen, and Slichter[46] and by Abrahams for the single-phonon T_S process corresponds to very large relaxation times ($\sim 10^9$ sec), whereas the experimentally observed times are much smaller (see Sec. 3, heading 1).

The experimentally observed dependence of T_S on the temperature and on the field in the single-phonon process is obtained from the calculations of Hasegawa[34] and Roth[33] [see (4.19)].

The relaxation rate (for $H_0 \parallel [111]$, $H_0 = 3000$ Oe, and $T = 1.25°$ K) obtained from Hasegawa's calculations for phosphorus-doped silicon (see Table VI) is equal to 9×10^{-5} sec^{-1}, whereas the experimental value of $1/T_S$ obtained by Honig and Stupp for the same field value but for arbitrary field orientation (and the same temperature) is 2.63×10^{-5}. Such an agreement of the theoretical and experimental values is very good. From the theory of Hasegawa and Roth follows also the anisotropy of the relaxation times [see (4.19)]. These effects were investigated in detail by Wilson and Feher[29]. However, before we compare experiment with theory, let us stop to discuss some of Feher and Wilson's considerations.

As indicated above, the relaxation mechanism proposed by Hasegawa and Roth[33,34] consists in the modulation of the singlet-doublet splitting by the lattice vibrations, i.e., it is a time dependent change in the populations of the different energy minima, and is therefore manifest in the modulation of the g-tensor. However, this mechanism yields $1/T_S = 0$ for $H_0 \parallel [100]$.

Roth[33] considered a different mechanism, which results from modulation of the variation of the g-value corresponding to one energy minimum. This change is due to the shift of the bands under periodic lattice deformation even when all the electrons are at one minimum.

To compare theory with experiment it is necessary to consider the effect of both mechanisms simultaneously.

At $H_0 = 8000$ Oe and $T = 1.25°$ we get according to theory $1/T_S = 0.45 \times 10^{-3}$ sec^{-1} for the first mechanism and 0.16×10^{-3} sec^{-1} for the second. For the same field orientation ($H_0 \parallel [111]$) and the same values of H_0 and T, the experimental values of $1/T_S$ are respectively 1.1×10^{-3} and 0.3×10^{-3} sec^{-1}, i.e., approximately twice as large. Such an agreement between the theoretical and experimental values can be regarded as very good.

For a Raman type process it was found in the experiments of Honig and Stupp[56] that the relaxation rate $1/T_S$ is proportional to T^7 and does not depend on the magnetic field or on the impurity concentration. The theory for this process was developed by Abrahams[47] and Roth[33]. As was indicated above, the results obtained in[33] were in poor agreement with experiment. According to Roth's calculation [see (4.20)] the relaxation rate $1/T$ for this process is proportional to T^7 and to H^2. However, no quadratic dependence on the field was observed experimentally in the range from 3000 to 8000 Oe. Nor was anisotropy of T_S observed in analogy to the anisotropy for the single-phonon process. The experimental value of T_S and that predicted by the Roth theory likewise diverge. The reason for this divergence is not clear.

As regards the concentration-dependent mechanism, we can state that there is no theory of this mechanism which agrees to any degree with experiment. As indicated above, the exchange interaction process considered by Pines, Bardeen, and Slichter[46] (see Sec. 1, heading 3) does not reflect the laws observed experimentally. Honig and Stupp have proposed a qualitative interpretation of the experimental results. Their idea[56] is that the relaxation of the main mass is realized by spin diffusion from the rapidly relaxing centers. Such centers may be pairs of impurity atoms. The pairs may comprise ionized and neutral phosphorus atoms or two phosphorus atoms. Honig and Stupp proposed that the T_S(conc.) process is due to pairs consisting of two neutral phosphorus atoms. The electron wave functions should be determined for such a pair with allowance for the Coulomb interaction of the electrons with both phosphorus nuclei, and also with account of the exchange interaction between the electrons. As noted above, the relaxation time due to modulation of the exchange-interaction constant is very large. However, owing to the absence of spherical symmetry of the Coulomb potential, and also owing to electron correlation effects, the spin-orbit coupling can, in the opinion of Honig and Stupp, change in such a way that the electrons connected with such a pair begin to relax rapidly. On the other hand, the electrons connected with the isolated phosphorus atoms relax as a result of spin diffusion from the same centers.

Honig and Stupp have shown that the number of pairs produced by two neutral atoms increases linearly with increasing impurity atom concentration. The

probability of relaxation due to the relaxation of only the electrons connected with the pair (in the absence of spin diffusion) should also depend linearly on the impurity concentration, as was indeed observed experimentally by Honig and Stupp in some regions of phosphorus concentration (see Fig. 13).

It must be noted, however, that the relaxation mechanism proposed by Honig and Stupp does not reflect completely the regularities that are observed experimentally (dependence of the relaxation rate on the field and on the temperature, and the dependence on the concentration in the concentration region above 10^{16} cm^{-3}).

A theoretical calculation of the relaxation time for the T_X process was made by Pines, Bardeen, and Slichter[46] and also by Hasegawa[34]. The former have found that the relaxation rate $1/T_X$ is proportional to H^2 and T. However, the experiment of Honig and Stupp[56] for 1.25°K, when the mechanism proposed by Pines, Bardeen, and Slichter should be effective, has shown that low quadratic dependence in the field is observed. Such a dependence was observed, to be sure, in the experiment of Feher and Gere[20] (see Section 3, Heading 2).

As indicated earlier, Pines, Bardeen, and Slichter derived expression (4.9) assuming a linear variation of $|\Psi(0)|^2$ under isotropic dilatation. The value of $\tilde{\gamma}$ was estimated in[46] to be on the order of 50. Recently Paul measured the ionization energy and the dielectric constant under compression, and it can be concluded from his results that $\tilde{\gamma}$ is at least two orders of magnitude smaller. Therefore the agreement between the theoretical and the experimental values of T_X is purely accidental. Feher and Wilson[29] made additional measurements of T_X with the crystal compressed along the [111] axis, and observed changes in the hyperfine splitting. It follows from these experiments that $\tilde{\gamma} < 2$, in agreement with Paul's theory.

Feher and Wilson conclude[29] from the foregoing that in the temperature and magnetic-field ranges in question the T_X process cannot be due to single-phonon relaxation. Hasegawa calculated T_X under the assumption that a process of the Raman type is effective at 1.2°K, and obtained good agreement with experiment at these temperatures.

5. Conclusion

Thus, a review of the theoretical and experimental results on relaxation effects in silicon doped with elements of the fifth group disclosed that these phenomena have a complicated pattern. Many experimental regularities, such as a dependence on the field and on the temperature at T < 2°K, a dependence on the temperature at 2°K ≤ T ≤ 4.2°K, and many others can be explained by the theory of relaxation mechanisms for single- and two-phonon processes. On the whole, however, the relaxation picture is not yet clear. In particular, there is no explanation for one of the most interesting relaxation phenomena—the sharp increase in the relaxation rate with increasing impurity concentration and exposure to light. The proposed relaxation mechanisms do not lead to good agreement between theory and experiment. The relaxation effects of shallow donors in germanium and deep donors in silicon and germanium, and also in irradiated systems, have not been investigated so far.

V. ELECTRON PARAMAGNETIC RESONANCE OF IMPURITIES PRODUCING DEEP LEVELS

In the last few years EPR and ENDOR methods were used to investigate centers that produce deep impurity levels in silicon and germanium. The main investigations in this field were made by Ludwig and Woodbury, who studied the resonance of various charged states of transition metals in silicon and nickel in germanium. The impurities that produce deep levels were investigated to a lesser degree than shallow donors in silicon; for example, no investigation of the relaxation time was made for the former. However, even the available data lead to a certain rule that explains well the electronic configuration of the substitutional and interstitial ions of the transition elements of the iron group in silicon. The investigations in question concerned the electron configurations of deep impurities in different charge states and their interaction with vacancies. The EPR of Ni^- and Mn^{2-} ions in germanium was investigated. In silicon, the EPR spectra of different charged states of the ions of the iron group (unfilled 3d shell), palladium (unfilled 4d shell), and platinum (unfilled 5d shell) were investigated along with the spectra due to groups of four atoms of manganese with pairs consisting of a transition-metal atom and an acceptor (boron, aluminum, indium, gallium, gold).

1. EPR of the Ions Ni^- and Mn^{2-} in Germanium. The EPR of the ions Ni^- in germanium was considered in[63,64,65]. Germanium crystals doped with nickel (7×10^{15} cm^{-3}) by diffusion at a temperature of 850°C were studied[62]. The nickel atom acts like a double acceptor in germanium. It has two corresponding levels—0.30 eV below the conduction band and 0.22 eV below the valence band[61]. These acceptor levels were filled with electrons by introducing into the crystal a donor impurity (such as arsenic). When only the lower acceptor level is filled, the nickel is in a charged state Ni^-, the spectrum of which was analyzed in detail in[64].

At 20.4°K, the EPR spectrum of the Ni^- ion in germanium, with arbitrary orientation of the magnetic field, consists of six principal lines with an anisotropic g-value. From the symmetry of the spectrum and from the equality of the intensities of its lines it follows that each nickel atom gives only one resonance transition (effective spin S = 1/2), but that this atom

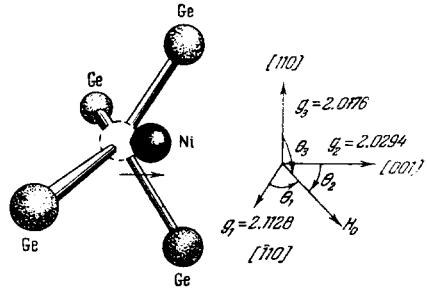

FIG. 17. Location of a Ni^- ion in the germanium lattice. Owing to the Jahn-Teller effect, the nickel atom is displaced from the lattice site along the edge of a cube, for example in the direction indicated by the arrow; θ_1, θ_2, θ_3 – angles between the directions of the magnetic field and the axes of the g tensor.

can be located in six geometrically non-equivalent sites of the lattice, distributed with equal probability over the entire crystal. A model of the lattice site containing the Ni^- ion and explaining the resonant spectrum is shown in Fig. 17. The electron configuration of the Ni^- is not known exactly (the configuration of atomic nickel is $3d^84s^2$). However, the resonant spectrum can be explained by assuming that the configuration is $3d^8$ with a "bound hole" in the valence shell. Then the spin of the 3d shell should be equal to unity, the spin of the valence shell to 1/2, and consequently the total spin should be 1/2, as is observed in the experiment. Such a configuration should lead to orbital degeneracy of the wave function of the ground state of the Ni^- ion. Then, in accordance with the Jahn-Teller theorem, the system should experience a perturbation that lifts the degeneracy. The Ni^- ion shifts from the lattice site along one of the six directions corresponding to the edges of the unit cell. This shift determines the observed spectrum of six lines, for each of which the g-value is determined by the expression

$$g = (g_1^2\cos^2\theta_1 + g_2^2\cos^2\theta_2 + g_3^2\cos^2\theta_3)^{1/2}. \qquad (5.1)$$

Here θ_1, θ_2, θ_3—angles between the direction of the magnetic field H_0 and the principal axes of the g-tensor, which constitute the edges of the cubic cell along which the ion is displaced, and two mutually perpendicular axes [110] (Fig. 17). The correctness of (5.1) for the Ni^- ion was confirmed by the good agreement between the experimental values of the g-value with the theoretical curves obtained by substituting in (5.1) the experimental principal values of the g-tensor ($g_1 = 2.1128$, $g_2 = 2.0294$, $g_3 = 2.0176$). An investigation was made of the temperature dependence of the spectrum of Ni^-. At 20°K the total line widths (between the extrema of the absorption derivative) are equal to 4.2 Oe, and the distance between the extreme lines is ~ 200 Oe. The lines have a Gaussian shape. With increasing temperature, the lines broaden, and at 30°K they begin to overlap. After a complete merging, the resultant single anisotropic line (with Lorentz shape) becomes narrower, reaching a minimum width of 28 Oe, and then, at temperatures above 50°K, it again broadens. This behavior of the spectrum was explained in the following fashion. The Ni^--ion shift, which is "frozen-in" at sufficiently low temperatures, causes a change in its position in the lattice with increasing temperature—a reorientation. The higher the temperature, the higher the reorientation frequency. When this frequency reaches a value corresponding to the width of the individual line at low temperature, the lines broaden; when it reaches a value corresponding to the total splitting between the extreme lines, the individual lines overlap. The different lines broaden at unequal rates. This is caused by the fact that in certain directions of the magnetic field some reorientations do not change the g-value, and because there are also two possible methods of thermally-excited reorientation: inversion and rotation.*

The temperature dependence of the correlation time was investigated for different lines and was calculated from the line broadening; as a result, threshold energies for inversion and rotation were determined. The threshold energy for rotation is approximately 0.018 eV, while for inversion it is ~ 0.022 eV. The latter quantity can be regarded as an approximate estimate of the perturbation energy of the system, leading to the displacement of the ion. In the temperature range from 20 to 40°K, in spite of the somewhat larger threshold energy, the reorientation by inversion takes place to the same degree as reorientation by rotation.

The hyperfine structure of the principal lines, due to the atoms Ge^{73} (I = 9/2) in the two sides closest to the Ni^- ion was also resolved. The best agreement between the theoretical and experimental values of the corresponding hyperfine interaction occurs if one assumes that the Ni^- ion is displaced from the lattice site by 0.2 Å.

The hyperfine interaction due to Ni^{61} was resolved in samples doped with nickel enriched with Ni^{61} (83%) (see [65,64]). The spin of the Ni^{61} nucleus was determined for the first time (3/2).

Watkins observed EPR in Ge doped with manganese in the charged state Mn^{2-} [66]. Investigations of the spectrum at 77° and 1.5°K have shown that the Mn^{2-} ion is in the state $^6S_{5/2}$. The measurements yielded $g = 2.0061 \pm 0.0002$, $A = -45.6 \pm 0.3$ G, $a = +9.5 \pm 0.5$G (A—constant of hyperfine interaction due to Mn^{55} (I = 5/2), a—constant of splitting due to the cubic field). Manganese enters into the lattice in the form of a substitution center, and the degree of occupation of its 3d shell is not changed thereby, and the two positive electrons are captured by the 4s4p shell. No hyperfine interaction with Ge^{73} was observed.

2. EPR of Transition Metals in Silicon. The tran-

*Thus, for example, the shift in the [001] direction as a result of inversion is transformed into a shift along the $[00\bar{1}]$ axis, while rotation results in a shift along the axes [100], $[\bar{1}00]$, [010], and $[0\bar{1}0]$.

sition elements can exist in silicon as isolated atoms that are in different charged states. In addition, transition metal and acceptor pairs can be produced, as well as more elaborate complexes, such as groups of four impurity atoms.

The charged state of the transition metal atom was varied by introducing into the crystal an acceptor impurity, which can gather electrons, or a donor impurity, which can give up electrons[16]. The transition metal molten into the sample was made to penetrate in it by diffusion, the sample being heated to 1300° C, at which the solubility of the transition metals in silicon is close to maximal.

The sample cooling rate after diffusion has an appreciable influence on the arrangement of the impurity in the lattice and on its charged state. Thus, after diffusion of iron in p-type silicon, iron-acceptor pairs are produced in the sample following slow cooling, but rapid cooling causes the production of positively charged isolated iron ions.

1. EPR of transition metals of the iron group. a) Hamiltonian. In elements of the iron group the unfilled shell is 3d. It is known that the EPR and ENDOR methods make it possible to determine the electron orbits and the energy levels of the ion from measurements of the values of the constants contained in the spin Hamiltonian, i.e., to determine the electron configuration and the types of ionic bonds.

In silicon, which has a diamond-type lattice, each substitutional atom and each interstitial atom located at a point with maximum-order symmetry are surrounded by four nearest neighbors on the [111] axis. Therefore both the substitutional and the interstitial atoms are in a crystal field with tetrahedral symmetry.* In both cases the tetrahedral field of the crystal lattice lifts partially the five-fold orbital degeneracy of the 3d shell, as a result of which there are formed triply degenerate t_2 and doubly degenerate e states[67]. However, as shown by experiments (see below), the triplet and doublet levels for the interstitial and substitutional atoms are arranged in an unequal fashion. If we neglect the displacement of the impurity atom from the point with maximum-order symmetry (no such displacement was observed for the elements in question), then the spin Hamiltonian[16] of the isolated impurity atom, whether in the site and in the interstice, can be written in the form

$$\mathcal{H} = g\beta \mathbf{H}_0 \mathbf{S} + A\mathbf{S}\mathbf{I} + \frac{1}{6}a\left[S_x^4 + S_y^4 + S_z^4 - \frac{1}{5}S(S+1)(3S^2+3S-1) - g_I\beta_N \mathbf{H}_0 \mathbf{I}\right]. \quad (5.2)$$

Here ASI characterizes the hyperfine interaction with the nucleus of the transition-metal atom (the hyperfine interaction with nuclei of the isotope Si^{29} is not taken into account). If $S \leq 3/2$, then the term containing the constant a, which characterizes the splitting due to the field of cubic symmetry, is equal to zero.

The frequency of the transition between the electron levels, corresponding to M and M − 1 (the selection rules are $\Delta M = \pm 1$ and $\Delta m_I = 0$) is given by the expression

$$h\nu = g\beta H_0 + Am_I + \frac{[I(I+1) - m_I^2 + m_I(2M-1)]A^2}{2h\nu}. \quad (5.3)$$

Here M—magnetic quantum number characterizing the orientation of the total electron spin, and m_I—quantum number for the nuclear spin.

It is seen from this expression that line splitting should take place in accordance with the term $m_I(2M-1)H^2/2h\nu$. If such a splitting can be resolved, then the total electron spin S can be determined from the number of fine-structure lines (2S).

In the case of double resonance the frequency f of the transition between the nuclear levels (M, m_I) and (M, $m_I - 1$) (selection rules: $\Delta M = 0$, $\Delta m_I = \pm 1$) is equal to

$$f = \left| AM - g_I\beta_N H_0 - \frac{[M(2m_I-1) + S(S+1) - M^2]A^2}{2h\nu} \right|. \quad (5.4)$$

This expression was used both to obtain exact values of the hyperfine interaction constant A, and to determine S. (Owing to the tetrahedral symmetry of the sites the quantities A and the g-value are constants and not tensors.)

b) Experimental results. For some ions of the transition elements under consideration, the experimentally measured constants which enter in the spin Hamiltonian are listed in Table VI, and their configurations are shown in Fig. 19[16]. (More detailed experimental data are given in[81].)

For all the transition-metal ions considered (except iron), the relaxation times in Si at 1.3° K are of the order of seconds and more; the line widths (at T = 10° K) are of the order of one Gauss.

Let us consider some of the resonance spectra.

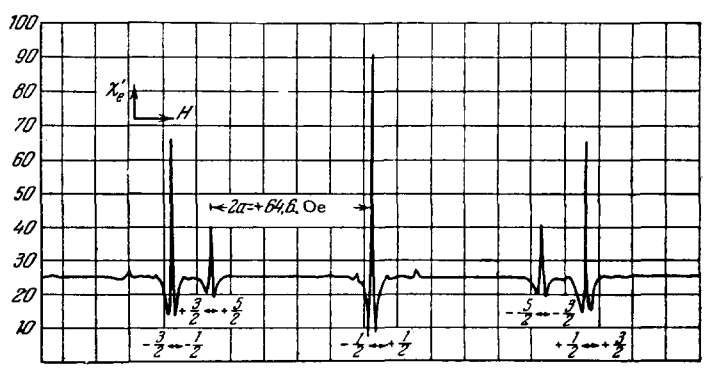

FIG. 18. Spectrum of Cr^+ in silicon at 20.4°K. The magnetic field H_0 is directed along the [001] axis. The corresponding transitions characterized by the quantum number are indicated for the five fine-structure lines.

*Consequently, one cannot determine from the symmetry of the interaction with the crystal field whether the impurity atom causing the resonance is interstitial or substitutional.

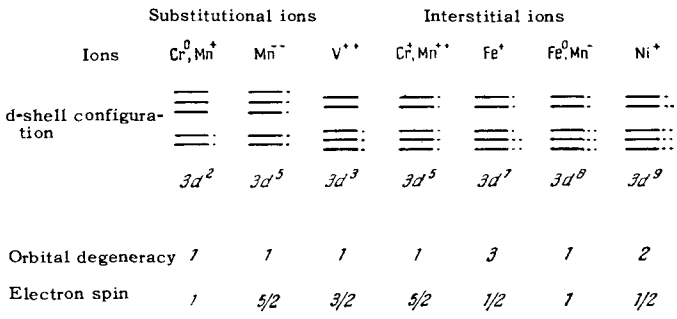

FIG. 19. Electron structure of transition-metal ions (with unfilled 3d shell) in a silicon lattice. Owing to the spin-orbit interaction, the spin of Fe^0 is equal to 1/2.

Table VII

Center	S	g	a, 10^{-4} cm^{-1}	Isotope	I	A, 10^{-4} cm^{-1}
V++	3/2	1.9892		V^{51}	7/2	−42.10
Cr^+	5/2	1.9978	+30.16	Cr^{53}	3/2	+10.67
Mn^-	1	2.0104		Mn^{55}	5/2	−71.28
Mn++	5/2	2.0066	+19.88	Mn^{55}	5/2	−53.47
Mn_4^0	2	2.0063		Mn^{55}	5/2	−12.8
Fe^0	1	2.0699		Fe^{57}	1/2	6.98

The spectrum of V^{++} (the solubility of vanadium in silicon is $\leq 10^{15}$ cm^{-3}) was observed only in low-resistance p-type crystals. It consists of eight narrow hyperfine structure lines, each of which splits into three lines in accordance with the term $m_I(2M-1)A^2/2h\nu$ (5.3). All the double-resonance lines were resolved for $M = \pm 1/2$.

Assume that we measure experimentally the frequency of one of the double-resonance transitions. Then, inasmuch as the nuclear moment of V^{51} is known (+ 5.139 nuclear magnetons), formula (5.4) was used to calculate the transition frequencies for different values of the total spin. Comparison of the data has then disclosed that only the theoretical value of f obtained for the spin S = 3/2 agrees with the experimental frequency. It was thus determined that the total spin S is equal to 3/2. The remaining values of S listed in Table VII, and the signs of the constants A, were determined analogously.

The chromium atom in acceptor-doped crystals is a double donor with solubility $\sim 8 \times 10^{15}$ cm^{-3}. The spectrum of Cr^+, shown in Fig. 18, consists of five (2S) fine-structure lines the positions of which are characterized by the total spin S = 5/2), and the constant a (see Table VII). The sign of a was determined* from the change in the line intensity with decreasing temperature, after which the transition corresponding to each line was identified. Near each fine-structure line there are four weak hyperfine structure lines, due to the Cr^{53} isotope (natural abundance 9.5%).

*For more details see W. Low, Paramagnetic Resonance in Solids, Solid Physics Suppl. 2, Acad. Press, N.Y., 1960.

At room temperature the state of Cr^+ is unstable. After a time on the order of a week, most Cr^+ ions combine with the acceptor present in the sample to form pairs. The resonance spectrum of chromium-gold pairs was investigated[68]. In such a pair the gold occupies the lattice site and the chromium one of the neighboring interstices on the [111] axis relative to the gold. This pair, which is in a neutral charged state $(CrAu)^0$, has a total electron spin S = 3/2. The interaction of the atoms in the pair leads to a splitting of the levels, which can be described by introducing into the Hamiltonian a term DS_z^2, where z is the pair axis. The value of the constant D, which is equal to 6.7 cm^{-1}, is much larger than the interaction between the spin and the magnetic field (0.5 cm^{-1}), so that only the transition $M = +1/2 \rightarrow M = -1/2$ is observed experimentally. The hyperfine interaction due to Au^{197} (I = 3/2) was investigated by the ENDOR method, on the basis of which the magnetic moment of gold was determined.

Groups of four manganese atoms Mn_4^0, constituting four neutral Mn atoms lying on corners of a tetrahedron[69], are produced when manganese diffuses in crystals of low-resistance n-type silicon, or in crystals of high-resistance silicon which are then slowly cooled. In these crystals, at a definite orientation of the magnetic field (in the absence of splitting due to the cubic field of the crystal), 21 hyperfine structure lines are observed. This corresponds to $m_I = \sum_{k=1}^{4}$, where m_k—magnetic quantum number of the k-th manganese-atom nucleus (I = 5/2) in a group of four atoms. The splitting of the hfs line into four lines, due to the interaction with the crystal field, shows that S = 2.

Slow cooling of a p-type sample results in manganese-acceptor pairs. The EPR spectra due to pairs formed by the manganese atoms with such acceptors as boron, aluminum, and gold were investigated in[69,70]. The spectrum of the MnAu pair[70] has axial symmetry with an axis directed along [111] ($g_{\parallel} = 2.0$, $g_{\perp} = 4.0$). This indicates that, like in the case of the CrAu pair, the MnAu pair is oriented along the [111] crystal axis, and the gold atom is substitutional while the manganese atom is interstitial.

Iron impurities in silicon (maximum solubility 1.5×10^{16} cm^{-3}) correspond to a donor level located 0.4 eV above the valence band[71]. When the Fermi level is located above this level, the iron atoms are neutral. The EPR spectrum of such atoms[16,72] consists of one line, the structure of which is resolved at a high microwave power level. It is possible that this structure is due to the hyperfine interaction with the Si^{29} nuclei. Observation of double resonance at T = 1.3°K has made it possible to determine the total spin (S = 1) and also the magnetic moment of Fe^{57} (see[73]). If the crystal is subjected to uniaxial mechanical compression, which disturbs the tetrahedral

symmetry of the sites, then the single Fe^0 line splits into two fine-structure lines. This confirms that S = 1.

The EPR spectrum of pairs produced by an iron atom with acceptors such as B, Ga, Al, and In was also investigated[74].

As first shown by Bloembergen[75], the electric field exerts an influence on the magnetic hyperfine interaction of the paramagnetic ions that occupy in the crystal lattice positions for which the inversion transformation does not take place. Ludwig and Woodbury observed[76] that the EPR lines of ions of the iron-group-element ions situated in the interstices in a silicon lattice, which had no inversion transformation, were split in the electric field. (Thus, for example, the single Fe^0 line splits in an electric field $\mathbf{E}$ ($\mathbf{E} \perp \mathbf{H}_0$, E = 12 kV/cm) into two components of equal intensity; the splitting is proportional to E and varies sinusoidally when the magnetic field orientation changes relative to the crystallographic axes.) A theoretical estimate of the spin Hamiltonian and of the position of the energy levels of such ions was carried out by Ham[77] for the case of an electric field.

As a result of an investigation of the EPR of the iron-group transition-metal ions in silicon, the following rule governing the electronic configurations of these ions in the crystal lattice was established[67]:

1. For ions replacing silicon atoms in the lattice, the energy of the triply degenerate states t_2 is larger than the energy of the doubly degenerate states e (Fig. 19). The opposite holds true for the interstitial ions.

2. In the substitutional ions, enough electrons go over from the 3d shell to the valence shell to form tetrahedral bonds with the four neighboring silicon atoms. In the interstitial ions, all the electrons go over from the valence band to the 3d shell.

The EPR method was used to investigate the interaction between vacancies and chemical impurities[78] (see also Chapter VI). It was observed that the vacancies are captured by interstitial impurities, which turn into substitutional impurities as a result.

3. EPR of Palladium and Platinum in Silicon. The first reported observation of EPR of the ions Pd and Pt in silicon was in[79]. A more detailed investigation[80] was also devoted to this question.

The transition metals Pd (unfilled 4d shell) and Pt (unfilled 5d shell) are acceptor impurities in silicon.

In samples containing shallow donor impurities, the palladium exists in the form of singly charged negative ions Pd^-, while platinum exists in the form of singly charged and doubly charged negative ions, so that two modifications of platinum centers are observed, Pt(I) and Pt(II), each with its own EPR spectra. In crystals with platinum there are more Pt(I) than Pt(II) centers. The positions of the acceptor levels of the palladium and platinum centers have not been determined exactly. In samples containing Pd or Pt, but containing no donor impurity, no EPR spectra are observed at all. The spectrum of Pd^- in silicon is analogous to the spectrum of Ni^- in germanium. It is obvious that the Pd^- ion is also located at the lattice site (see Fig. 17) and is shifted somewhat along the [100] axis. There are six geometrically non-equivalent sites, and accordingly six independent spectra are observed at arbitrary magnetic-field orientation. The hyperfine interaction with Pd^{105} (I = 5/2) and with the two nearest Si^{29} nuclei was investigated. The hyperfine splitting of the spectral lines, due to the nuclear quadrupole interaction, was investigated in samples with palladium impurity enriched with the Pd^{105} isotope (the EPR and ENDOR methods were used).

A study was made of the temperature dependence of the spectrum of Pd^- usually observed at 20.4°K. At a temperature above 20° the lines broaden and then vanish completely. Unlike the case of Ni^- in Ge, no averaging takes place here of the g-tensor as a result of reorientation of the sites, which leads to the merging of the lines. In the opinion of Ludwig and Woodbury, this is due to the fact that the spin-lattice relaxation broadens the resonance transitions of differently located Pd^- ions before the frequency of the site orientation becomes comparable with the frequency difference between the individual spectral lines. The spectrum of the Pt(I) center is analogous to the spectrum of Pd^-, i.e., it can be attributed to displacement of the platinum ion from the lattice site in one of the six directions [100]. A hyperfine interaction due to the Pt^{195} isotope was investigated (I = 1/2, natural abundance 34%). The spectrum of Pt(I) was observed only at low temperatures. At temperatures above 12°K, the lines of the Pt(I) spectrum broaden and disappear.

When an axial mechanical stress is applied to the samples, the spectra of Pd^- and Pt(I) vary in the same manner.

The spectrum of Pt(II) was observed at temperatures 20°K and above. This spectrum of Pt(II) shows that there are four geometrically nonequivalent sites, in which the center Pt(II) can be located and which are displaced along the [111] axes. The intensity of the spectrum of the Pt(II) center varies from sample to sample, and is connected to a certain degree with the oxygen content in the crystal. It is thus possible that the Pt(II) center is a platinum atom bound to the oxygen atom. The Pt(II) spectrum is not sensitive to axial compression of the crystal. The electron configuration of the Pd^{-1}, Pt(I), and Pt(II) centers is analogous to the configuration of Ni^- in germanium, i.e., the tetrahedral bonds with the four nearest neighbors are filled, but there is a "bound hole" in the corresponding unfilled shells.

VI. ELECTRON PARAMAGNETIC RESONANCE IN IRRADIATED SILICON

In the last decade thorough studies were made of different imperfections produced in silicon and ger-

manium bombarded with neutrons and electrons. In most cases, however, it was impossible to connect the concrete changes in the electric, optical, and mechanical properties of the materials with any particular imperfection produced by bombardment. The use of paramagnetic resonance has cast new light on the nature of the defects produced in irradiated crystals. Much progress was made in the study of radiation defects produced in silicon bombarded with high-energy electrons (0.5—1.5 MeV) and fast neutrons.

EPR of radiation defects in silicon was first observed in 1955 in a sample doped with boron and bombarded with neutrons at room temperature[82]. Later on EPR (and in some cases also the ENDOR method) was used to study in detail the structure of the main paramagnetic centers connected with the defects in silicon bombarded with 0.5, 1, and 1.5 MeV electrons, and a study was initiated of centers produced in silicon bombarded with fast neutrons. In addition to the structure of the centers, studies were made also of other properties, for a better understanding of the production of centers in irradiated materials.

1. EPR of Radiation Defects Produced by Electron Bombardment of Silicon. The EPR spectra of radiation defects in silicon were investigated with the samples bombarded by electrons having energies 0.5 and 1 MeV[83] and 1.5 MeV[84]. In the latter case the electron energy was sufficient to produce simple types of defects: interstitial atoms, vacancies, two vacancies located alongside—divacancies, etc. Depending on the radiation dose, on the position of the Fermi level, on the temperature of the irradiation, on the type of impurity, and on the method of obtaining the crystal, these simple defects can form different paramagnetic centers, each with its own EPR spectrum.* In general, up to 20 individual EPR spectra were observed in electron-bombarded silicon, obviously corresponding to different defects (some represent different charged states of the same defect). We consider here the five principal centers (Si-A, Si-B, Si-C, Si-E and Si-J centers) produced when silicon is bombarded with 1.5 MeV energies, investigated by Watkins and Corbett[85]. We shall consider, using the Si-A center as an example, the procedure for the experimental investigation of the structure and properties of these centers, and also a theoretical estimate of their wave functions, hyperfine interaction, and g-value, obtained on the basis of the molecular-orbital method.

1. Si-A center. a) Experimental method and results. The Si-A center† is the principal center produced when high-energy electrons bombard silicon crystals drawn from a melt.* It was first investigated by paramagnetic resonance by Bemski, Feher, and Gere[86], and was subsequently investigated in detail by Bemski[83] and by Watkins and Corbett[84, 87,88]. Let us discuss briefly the results of these experiments, which have made it possible to construct a model of the A center.

The characteristic EPR spectrum corresponding to the A-center (Fig. 20) is observed by irradiating at room temperature low-resistance crystals of drawn n-type silicon (with doping impurity concentration 10^{15}—10^{16} cm^{-3}) with a beam of 0.15, 1, and 1.5 MeV electrons (the dose was 10^{15}—10^{16} electrons/cm^2).

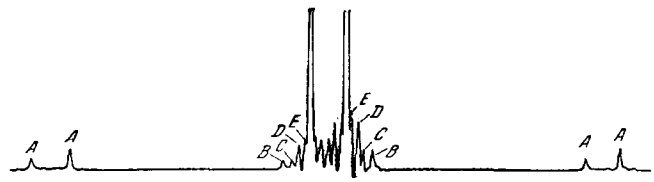

FIG. 20. Spectrum (derivative dispersion) of Si-A center at 40°K. The magnetic field H_0 is directed along the [100] axis of the crystal. The letters A, B, C, D, and E denote the hyperfine structure lines due to the hyperfine interaction with Si^{29} nuclei located in five groups of nonequivalent lattice sites.

No corresponding resonance spectrum was observed when crystals of p-type silicon or of high-resistance n-type silicon were irradiated with an equivalent dose. The EPR spectrum of the A-center does not depend on the sort of doping impurity and is the same for crystals doped with As or with P. The resonance lines disappear almost completely after the samples are heated for several minutes at 750°K.

The formation of A-centers in n-type silicon (with a phosphorus concentration 10^{15}—10^{16} cm^{-3}) was investigated in[84] with the aid of EPR following irradiation at room temperature with 1.5-MeV electrons. The dependence of the concentration of these centers on the radiation dose, determined from the intensity of the corresponding spectrum, was investigated. These experiments have shown that the produced radiation defects capture the phosphorus donor electrons and become paramagnetic as a result; resonance of A-centers is observed only after they have captured electrons.

The A-center is thus an electron trap. A comparison of the EPR experimental results with electrical measurement results[89,90] has shown that the A-center corresponds to an acceptor level 0.17—0.16 eV below the conduction band. In crystals obtained by zone melting, the concentration of the A-centers was only several percent of the corresponding value in

*We shall not emphasize from now on the difference between the concepts "paramagnetic center" and "defect," recalling that we are speaking of a defect which becomes paramagnetic for some reason or another.

†We shall henceforth call it simply the A-center, and the other centers will be called the B-center, C-center, etc. We shall bear in mind that we are dealing with irradiated silicon.

*As is well known, the former crystals contain up to 10^{18} oxygen atoms per cubic centimeter. The oxygen concentration in silicon crystals obtained by zone melting is much lower (10^{15} – 10^{16} cm^{-3}).

crystals grown in quartz crucibles, i.e., a high oxygen concentration is necessary for the formation of A-centers.

An investigation of the rate of A-center formation in different samples[84,88] has shown that the A-center is produced as a result of capture of a primary defect by an electrically neutral admixture of oxygen, which is present in sufficient amounts in silicon grown in quartz crucibles.*

Special experiments were made[84] to show that the A-center is not a primary defect (i.e., one produced immediately after the breaking of the bonds). The samples were irradiated at 20°K, and the resonance was observed after annealing (approximately 30 minutes at each temperature) followed by heating. No A-centers were observed immediately after irradiation. However, even after annealing at room temperature the A-center concentration does not amount to more than 2.5% of the concentration obtained after equivalent irradiation at room temperature. An analogous phenomenon takes place for irradiation at 77 and 90°K[83]. Thus, the A-centers are not primary, and displacement of primary defects is necessary for their formation. The defects are mobile at temperatures below room temperature, and the A-centers are produced as a result of capture of oxygen atoms by the moving defects (vacancies).

Valuable information on the nature of A-centers was obtained from an analysis of the corresponding EPR spectrum (see Fig. 20). The spectrum is described by a spin Hamiltonian

$$\mathcal{H} = g\beta \mathbf{H}_0 \mathbf{S} + \sum_j I_j \mathbf{A}_j \mathbf{S}. \qquad (6.1)$$

The spectrum is characterized by an anisotropic g-value and, depending on the orientation of the magnetic field relative to the crystallographic axes of the sample, it is resolved into a different number of lines (for example, the spectrum for $H_0 \parallel [100]$ (Fig. 20) consists of two principal lines). An investigation of the anisotropy of the g-value has shown[88] that there are six nonequivalent arrangements (orientations) of this defect in the silicon lattice, each of which corresponds to a displacement of the silicon atoms making up the A-center in one of the six [100] directions. The principal axes of the g-tensor are shown in Fig. 21, and its principal values are given in Table VIII. The second term of the Hamiltonian (6.1) describes hyperfine interactions with the Si^{29}, which was resolved for five nonequivalent lattice site groups. The corresponding hyperfine structure lines are denoted on Fig. 20 by the letters A, B, C, D, and E. All these interactions

*Attempts to observe hyperfine interaction with O^{17} in specimens enriched with this magnetic oxygen isotope, and to demonstrate by the same token its presence in the A-centers with the aid of EPR, were not successful because the oxygen atom is at the node of the wave function of the unpaired electron, and only an insignificant hyperfine interaction can occur for it.

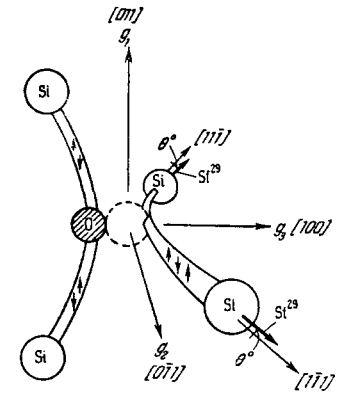

FIG. 21. Model of A-center. The principal axes of the g tensor are denoted g_1, g_2, and g_3. The thick arrows denote the axes of hyperfine interaction with the Si^{29} nuclei. The dashed line denotes a vacancy.

Table VIII

g (±0.0003)	Principal values of the tensor of hyperfine interaction with Si^{29} 10^{-4} cm^{-1}	Number of equivalent Si^{29} atoms and the principal axes of the corresponding hyperfine interaction
$g_1 = 2.0092$ $g_2 = 2.0026$ $g_3 = 2.0033$	$A_\parallel = 153.0 \pm 0.05$ $A_\perp = 128.8 \pm 0.5$	(I) [11$\bar{1}$] (I) [1$\bar{1}$1]

have axial symmetry with axes lying near [1$\bar{1}$1] or near [11$\bar{1}$] (Fig. 21), and can be described with the aid of the quantities $A_\parallel$ and $A_\perp$. For the line A, the quantities $A_\parallel$ and $A_\perp$ and the number of equivalent sites are given in Table VIII. For the line B: $A_\parallel = 16 \times 10^{-4}$ cm^{-1}, $A_\perp = 12 \times 10^{-4}$ cm^{-1}; for the line C: $A_\parallel = 10.6 \times 10^{-4}$ cm^{-1}, $A_\perp = 7.9 \times 10^{-4}$ cm^{-1}. The corresponding quantities for the lines E and D are even smaller. Thus, the greatest hyperfine interaction occurs for the site group A, i.e., the unpaired electron is localized principally near the two silicon atoms that are obviously closest to the defect.

b) Model of A-center. All the experimental results considered above have made it possible to construct the A-center model shown in Fig. 21. The occurrence of the A-center can be explained in the following manner. The irradiation produces four broken bonds around a vacancy, one for each of the surrounding silicon atoms. The oxygen atom captured by the vacancy joins two of the broken bonds, forming a Si-O-Si "molecule." The remaining two silicon atoms with broken bonds are slightly attracted to each other, and this results in a Si-Si "molecule." Such a defect is not paramagnetic in the neutral state, since the spins of all the electrons are paired. The paramagnetism is the result of the additional electron which goes over from the donor and is captured by the Si-Si molecular bond. The wave function of this electron can be constructed in the form of a linear combination of atomic wave functions. Inasmuch as the unpaired electron is

essentially localized near two neighboring silicon atoms (atoms A and A′ on Fig. 22), its wave function can be constructed with good approximation from the wave functions of these two atoms (Ψ_A, $\Psi_{A'}$). In the Si_A-$Si_{A'}$ "molecule," the wave functions Ψ_A and $\Psi_{A'}$ overlap, so that the corresponding energy levels split into two (the distance between them is determined by the binding energy). If the overlap is not very large, then the additional electron with uncompensated spin is described by an asymmetrical linear combination

$$\Psi^*_{AA'}=\frac{1}{\sqrt{2}}(\Psi_A-\Psi_{A'}).$$

This "disintegrating" orbit corresponds to an upper energy level lying 0.17 eV below the conduction band. (The state described by the antisymmetrical wave function $\Psi^*_{AA'}$ is stable. Indeed, according to the model of James and Lark-Horovitz[92] the vacancy is an electron trap. In addition, when the Si_A-$Si_{A'}$ bond captures an additional electron, the stresses resulting in the vacancy region from the attraction of the Si_A and $Si_{A'}$ atoms during the formation of the bond, are appreciably reduced.) The lower level, which can lie in the valence band, corresponds to the symmetrical wave function

$$\Psi_{AA'}=\frac{1}{\sqrt{2}}(\Psi_A+\Psi_{A'})$$

("binding" orbit). At this level are located both electrons with compensated spins, which remain from the broken covalent bond. This A-center model (Fig. 21 and 22) satisfies the following properties, which were determined on the basis of the resonant spectrum: 1) the electron is localized principally near two silicon atoms; 2) the symmetry of the hyperfine interaction tensor, the axes of which are directed towards the center of the vacancy, is representative of the symmetry of the atomic orbits with the bond broken, forming the molecular orbit; 3) the symmetry axes of this molecular orbit correspond to the principal axes of the g-tensor.

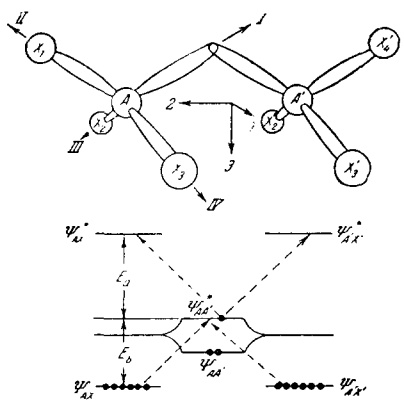

FIG. 22. Arrangement of the Si_A-$Si_{A'}$ "molecule" of the A-center in the silicon lattice. Energy level scheme for such a "molecule.". The dashed arrows indicate the electronic transitions which are taken into account in the calculation of the g-factor. The numbers 1, 2, and 3 denote the three principal axes of the Si-Si "molecule."

The theoretical estimate of the hyperfine interaction and of the g-value, based on the molecular-orbital method[88], is valid for both the A-center and for the remaining four centers under consideration.

c) Theoretical estimate of the hyperfine interaction and of the g-value. The wave function of the unpaired electron was constructed in the form of a linear combination of the wave functions of the atoms contained in the lattice site near the vacancy:

$$\Psi=\sum_j \eta_j\Psi_j, \tag{6.2}$$

where Ψ_j—wave function of the atom in the j-th site, representing the hybrid orbit 3s3p:

$$\Psi_j=\alpha_j(\psi_{3s})_j+\beta_j(\psi_{3p})_j. \tag{6.3}$$

If we neglect the overlap, then these functions are normalized under the conditions

$$\alpha_j^2+\beta_j^2=1, \tag{6.4}$$

$$\sum_j \eta_j^2=1. \tag{6.5}$$

In the case of axial symmetry, the principal values of the tensor of hyperfine interaction with Si^{29} are

$$A_{\parallel}=a+2b, \qquad A_{\perp}=a-b. \tag{6.6}$$

(The expressions for a and b are given in[88].) If we neglect the overlap, then the hyperfine interaction with the Si^{29} nucleus located in the j-th site is determined principally by the atomic wave function Ψ_j in this site. Then

$$a_j\cong\frac{16\pi}{3}\gamma\beta\beta_N\alpha_j^2\eta_j^2|\psi_{3s}(0)|^2,$$
$$b_j\cong\frac{4}{5}\gamma\beta\beta_N\beta_j^2\eta_j\langle r^{-3}\rangle_{3p}. \tag{6.7}$$

Inasmuch as γ is negative for Si^{29} and only direct interaction is taken into account in (6.7),* a_j and b_j are also negative.

The values of a_j and b_j were then determined directly with the aid of expression (6.6) from the experimental values of $|A_{\parallel}|_j$ and $|A_{\perp}|_j$ for different sites A, B, C, and D.

The values of α_j^2, β_j^2, and η_j^2 can be determined from (6.7) and from (6.4)—(6.5) if we know the ratio $|\psi_{3s}(0)|^2/\langle r^{-3}\rangle_{3p}$. A value of 1.4 was obtained for this ratio from an estimate by Hartree et al[93] for Si^{3+}, under the assumption that when the charged state of the silicon atom changes the values of $|\psi_{3s}(0)|^2$ and

*In the general case, in addition to direct interaction between the nucleus and the unpaired electron, account is taken also of the indirect interaction via the other electrons surrounding the nucleus. (In other words, the field acting on the nucleus is due to the magnetic moment of the spin of the unpaired electron and to that magnetization which it produces in the electron shells surrounding it.) The hyperfine interaction was estimated only with account of the direct interaction, but at small interactions such an approach may yield incorrect results.

$\langle r^{-3}\rangle_{3p}$ vary in identical fashion: the value 1.4 was used in this case, too.

Thus, α_j^2, β_j^2, and η_j^2 were determined under the conditions that the wave function is described by (6.2) and (6.3), that $|\psi_{3S}(0)|^2/\langle r^{-3}\rangle = 1.4$, and that only direct interaction takes place. For the sites A: $\alpha^2 = 0.37$, $\beta^2 = 0.63$, and $\eta^2 = 0.36$. The values $|\psi_{3S}(0)|^2 = 24 \times 10^{24}$ cm^{-3} and $\langle r^{-3}\rangle_{3p} = 17 \times 10^{24}$ cm^{-3} were then determined from (6.7). These quantities agree with those estimated theoretically in[94] for the neutral silicon atom.

For the sites B, C, and D we have $\alpha^2 = 0.25$ and $\beta^2 = 0.75$, which corresponds to tetrahedral sp^3 orbits. This physically reasonable result confirms that the values and relative signs (identical) of a_j and b_j are correct.

The wave functions for the atoms A and A′ have a larger S-state admixture (see Table VIII) than the tetrahedral sp^3 orbits—they are more like sp^2 orbits. This character of the wave function is in accord with the fact that the atoms A and A′ are somewhat shifted from their normal position towards the vacancy, owing to the molecular Si_A-$Si_{A'}$ bond.

The value of the coefficient η^2 ($\eta^2 = 0.72$) indicates that approximately 70% of the wave function is due to the Si_A-$Si_{A'}$ diatomic molecule ($\eta_A^2 = \eta_{A'}^2 = 0.36$). The remainder of the wave function corresponds to the other 12–16 atoms (B, C, D, E) in the vicinity of the vacancy. The lattice sites at which these atoms are located have not been established as yet. Accordingly, we cannot construct the remaining 30% of the wave function of the unpaired electron.

Watkins and Corbett assumed that to construct a detailed wave function for either the A-centers or the other centers in question it is meaningless to use a linear combination of those wave functions which are taken into account in the case of shallow donors, and efforts must be continued to apply the molecular-orbital method, supplemented by an analysis of the perturbations in the region of the vacancy.

Nonetheless, even the available wave function, which takes into account the contributions of the two atoms A and A′, makes it possible to explain sufficiently well the observed g-values.

In the first order of the spin-orbit interaction the deviation of the g-value from the corresponding value for the free electron (2.0023) is equal to

$$\Delta g_{ij} = -2\lambda\Lambda_{ij},$$

where

$$\Lambda_{ij} = \sum_n \frac{\langle 0|L_i|n\rangle\langle n|L_j|0\rangle}{E_n - E_0}. \qquad (6.8)$$

The summation must be carried out over all the n excited states. However, since the unpaired electron is localized to a considerable degree near two Si_A sites, we can take into account in first approximation the excitation of the state only for the diatomic Si_A-$Si_{A'}$ molecule. When estimating the g-value, a system of eight atoms was considered: the two atoms A and A′ and six silicon atoms X (Fig. 22). A weak bond exists between the atoms A and A′, whereas their bond to the remaining atoms is strong and covalent.

In the ground state, the corresponding 12 electrons are on filled binding orbits, corresponding to wave functions Ψ_{AX} and $\Psi_{A'X'}$, two electrons are in the state $\Psi_{AA'}$ and one unpaired electron is in a state as described by the antisymmetrical wave function $\Psi^*_{AA'}$. The transitions to the excited state can be described in such a system with the aid of matrix elements of two types. One corresponds to a transition from a level described by $\Psi^*_{AA'}$ to levels characterized by Ψ^*_{AX} and $\Psi^*_{A'X'}$, and causes Δg to be negative (λ is positive); the other corresponds to a transition from levels corresponding to Ψ_{AX} and $\Psi_{A'X'}$ to the $\Psi^*_{AA'}$ level, resulting in positive Δg (λ negative). The total change is due to both effects.

The molecular wave functions $\Psi^*_{AX'}$, $\Psi_{AX'}$, ..., etc. were constructed in the form of linear combinations of atomic wave functions σ^{I}, σ^{II}, ..., σ^{IV*} and were normalized with allowance for the overlap, characterized by the expression

$$S^* = \langle \sigma^{II}(A)|\sigma^{-II}(X_1)\rangle. \qquad (6.9)$$

In estimating the g-value, no account was taken of the weak overlap for the Si_A-$Si_{A'}$ bond, and the matrix elements of the orbital angular momentum L_i were transformed under the assumption that $\sigma^{II}(A)$ is a unique function of the atom A, which overlaps $\sigma^{-II}(A)$ appreciably. As a result it was obtained from (6.8) that the change in the g-value for the three principal axes (1, 2, 3) of the "molecule" (Fig. 22) is:

$$\Delta g_{1,2,3} = \Delta g_{ij} \cong |\lambda| \left\{\frac{1+S^*}{E_b} - \frac{(1-S^*)}{E_a}\right\} \langle \sigma^I(A)|L_i^2|\sigma^I(A)\rangle, \qquad (6.10)$$

where E_a—energy difference between the levels characterized by $\Psi^*_{AA'}$ and Ψ^*_{AX}, while E_b—between the levels described by $\Psi^*_{AA'}$ and Ψ_{AX}. From simple calculations it was found that the matrix elements in (6.8) for these three axes are

$$\left.\begin{aligned} \langle \sigma^I(A)|L_1^2|\sigma^I(A)\rangle &= \beta_A^2, \\ \langle \sigma^I(A)|L_2^2|\sigma^I(A)\rangle &= \tfrac{1}{3}\beta_A^2, \\ \langle \sigma^I(A)|L_3^2|\sigma^I(A)\rangle &= \tfrac{2}{3}\beta_A^2, \end{aligned}\right\} \qquad (6.11)$$

where $\sigma^I(A)$ is given by (6.3). Using the experimental values $\Delta g_1 = \pm 0.0070$ and $\beta_A^2 = 0.63$, taking $|\lambda| = 0.02$ eV and $S^* = 0.7$ from[94,95], and assuming in the solution of (6.10) that $E_a \approx E_b$, Watkins and Corbett found that $E_a \approx E_b = 2.6$ eV. In other words, the energy difference between the disintegrating and binding states is approximately 5 eV, which is physically

*σ^I, σ^{II}, σ^{III}, σ^{IV} – wave functions of the atom A for the binding-force directions indicated in Fig. 22. The wave functions for the opposite directions are σ^{-I}, ..., σ^{-IV}.

quite realistic. It follows from (6.11) that $\Delta g_1 : \Delta g_3 : \Delta g_2 = 3:2:1$. This result differs appreciably from the experimental data, since it was measured that $\Delta g_1 = 0.0070$, $\Delta g_3 = +0.0010$, and $\Delta g_2 = +0.0003$. But the signs of Δg were theoretically determined correctly. Furthermore, the relation $\Delta g_1 > \Delta g_3 > \Delta g_2$ is satisfied, as follows also from experiment. The positive change in the g-value is attributed primarily to the fact that the wave function of the unpaired electron overlaps more strongly the binding AX orbits than the disintegrating AX orbits.

Thus, this simple transition scheme, considered under many simplifying assumptions, makes it possible to determine correctly the signs and the ratio of the values of Δg, in spite of the fact that the wave function of the unpaired electron is not completely determined. This fact can be regarded as rather remarkable if it is recalled that the unpaired electron of the A-center corresponds to a level which is 0.17 eV away from the conduction band, and that no account of the semiconductor property of the material was taken at all in the calculation.

d) Investigation of the A-center structure by EPR observations of a crystal subjected to a force along one of its axes. An important method for the investigation of the structure and properties of defects is to study their motion with the aid of EPR. To this end, a study was made of the line broadening due to the motion of defects with increasing temperature; the preferred defect orientation, the redistribution of the electrons among the defects, etc. were investigated in a suitable temperature range with a mechanical axial stress applied to the crystal.

We stop to discuss briefly the experiments performed to confirm the A-center model considered above [88,85]; they were also carried out in order to investigate the structure and properties of the remaining four centers in electron-bombarded silicon.

An axial mechanical stress disturbs the normal cubic symmetry of the crystal. As a result, the six possible locations of the A center are no longer equivalent, i.e., these centers no longer yield lines of equal intensity. This change in the relative intensities of the spectral lines under deformation of the crystal is due to two mechanisms, which were studied separately, since their influence comes into play in different temperature ranges.

1) Depending on how the A-center is located relative to the direction of the applied stress, the energy of the electron captured by the defect can either increase or decrease. Accordingly, the electrons are redistributed among the traps via thermal ionization, which is manifest in a change in the relative intensities of the resonance-spectrum lines. This mechanism was investigated in the 60—80° K temperature range. The redistribution of the electrons was investigated by measuring the time necessary to restore the initial intensity of the line after removal of the applied stress. An investigation of the temperature dependence of the recovery time (equal to the average time spent by the electron in the trap) in the 60—70° K range has made it possible to determine the activation energy of this process. It characterizes the height of the barrier that must be overcome by the electron in order to leave the defect, and is equal to 0.20 ± 0.03 eV, i.e., it is close to the energy of the disintegrating orbit (0.17 eV). A study was also made of the energy difference (ΔE) between the electron levels corresponding to differently located defects. The signs of the corresponding measured values of ΔE have shown that the trap energy increases when the two silicon atoms come closer together in the Si_A-$Si_{A'}$ molecule. This confirms that the electron captured by the defect is on a disintegrating orbit between the two silicon atoms of this molecule.*

2) At higher temperatures, the defects themselves can become reoriented, i.e., a transition of the oxygen atom takes place from one pair of silicon atoms to another pair of atoms surrounding the vacancy. If a stress is then applied along any of the crystal axes, some defect orientation becomes dominating. This causes an additional change in the relative amplitudes of the spectral lines which, as already stated, can be readily separated from the distribution of the electrons among the defects, which is a process of higher frequency. The activation energy of the defect reorientation process (in the neutral states), measured in the temperature region 120—145° K, in which this phenomenon begins to manifest itself, is 0.38 ± 0.04 eV. The preferred orientation, which is characterized by the relative number of identically oriented defects, is determined principally by the two orthogonal Si-O-Si and Si-Si molecular bonds (see Fig. 21). The energy of each of these bonds decreases when the stress is applied along the direction of the bonds (the intensities of the corresponding lines increase). The relative stability of the different orientations (and, by the same token, the preferred orientation) is determined by the degree (relative ease) to which each of the molecular bonds Si-Si and Si-O-Si is oriented along the direction of the applied stress. The change in energy of each bond is determined by the component of the strain tensor along the direction of this bond. On the basis of the measured values of the preferred orientations and of the energy differences of the electron levels (ΔE), and also on the basis of the magnitude of the stress used in the experiment, the changes in energy of each of the two bonds and of the Si_A-$Si_{A'}$ were calculated per unit change in strain. These were found to be of the order of the deformation potential for silicon, a result which is physically reasonable. It was found at the same time that the change in the bond energy per

*When the two atoms come closer together the energy of the binding orbit decreases and that of the disintegrating orbit increases.

unit change in strain has an opposite sign for the single electron on the disintegrating orbit, and constitutes half of the corresponding change in energy for the two electrons on the binding orbit. This fact is also a very essential confirmation of the A-center model. On the basis of the changes in the bond energies, the signs and magnitudes of the preferred orientations and of ΔE were determined for different directions of force applications. They agree very well with the experimental values, again confirming the correctness of the chosen A-center model.

The location of the oxygen atom, like its very presence in the A-center, cannot be determined directly with the aid of EPR observations. It was found in [91] that infrared absorption at 12μ is observed in the materials considered above, owing to the vibrations of the oxygen atom. By studying the influence of an axial-mechanical stress on the infrared-absorption band and by comparing the results of this experiment with those of analogous experiments on paramagnetic resonance, it became possible not only to prove the presence of the oxygen atom in the A-center, but also to find that its location corresponds to the model considered above.

2. Si-E center. E-centers have been observed only in silicon obtained by zone melting, and are the main centers in such crystals irradiated at the doses in question. Each line of the E-center resonance spectrum is a doublet. This splitting is obviously due to the hyperfine interaction with the phosphorus atoms ($I = 1/2$), which comprise the main impurity in the investigated crystals. The E-center model is shown in Fig. 23. The wave functions of the unpaired electron has a greater p-state content than the hybrid sp^3 orbit ($\alpha^2 = 0.19$, $\beta^2 = 0.81$). This indicates that the silicon atom (denoted by the number 1 in Fig. 23) is drawn away from the vacancy by its three nearest silicon neighbors. A study of the hyperfine interaction with the Si^{29} and P atoms has shown that the unpaired electron is localized principally near one silicon atom, and its state can be described in first approximation by one free orbit remaining from the broken covalent bond. The fact that the coefficient η^2 has a value 0.59 indicates that approximately 60% of the wave function is connected with this orbit. The resonance spectrum of the E-center was observed only when its acceptor level (0.43 eV) was not occupied by electrons. Thus, the E-center is a vacancy in a neutral charged state, near which is located a substituting phosphorus atom. The E-center model shown in Fig. 23 was confirmed in a study of the thermally-activated transition of an unpaired electron from one silicon atom to others with equivalent positions (relative to the phosphorus-vacancy direction) near the vacancy. This transition of the electron from atom to atom, occurring when the temperature is increased, was investigated both by observing the EPR with an axial stress applied to the crystal, and by investigating the line broadening due to this effect. The activation energy for such a transition is ~ 0.06 eV. The E-center model was confirmed also by investigating the preferred orientation arising when the crystal is deformed at room temperature.

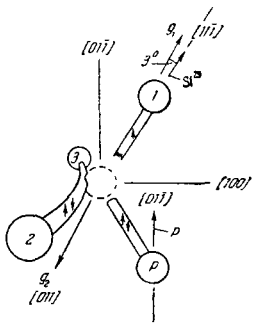

FIG. 23. Model of E-center. The numbers 1, 2, and 3 denote the silicon atoms. The arrow marked P denotes the axis of the hyperfine interaction with the phosphorus atom, while the arrow marked Si^{29} – the axis of hyperfine interaction with the Si^{29} atoms. The dashed line shows the vacancy.

The investigations have thus shown that the same defect, a vacancy, participates in the formation of both A-centers and E-centers, depending on which impurity, oxygen or phosphorus, is captured by the vacancy. In addition, the structure of the E-center, which contains a phosphorus atom, is weighty proof that the vacancies are mobile below room temperatures, a fact demonstrated by experiments on low-temperature irradiation of silicon grown in a quartz crucible.

3. Si-B center. The exact model of the B-center has not yet been determined. An investigation of the g-tensor and of the hyperfine interaction with Si^{29} [83] has shown that the unpaired electron due to the EPR spectrum is localized principally on one silicon atom, and that its state can be described with the aid of the free orbit left after the covalent bond is broken. The fact that the coefficient η^2 is equal to 0.64 shows that approximately 65% of the wave function is connected with this orbit. The values of α^2 and β^2 indicate that the content of the p-state in the wave function is much larger than in the tetrahedral sp^3 orbit. This corresponds to the silicon atom being drawn away from the vacancy by its three nearest neighbors. Their mutual placement thus approaches the planar configuration for which the AX bonds are sp^2 orbits and the free orbit corresponding to the unpaired electron is a pure p orbit. The lines of the B-center spectrum are neither broadened nor narrowed by the motion of defects as the temperature is increased to room temperature. Watkins and Corbett proposed on the basis of their experimental results that the B-center can contain one or more vacancies, with the atoms so arranged around them that one free bond is left. It has not yet been established whether the impurity atom (for example, oxygen) enters into the B-center.

4. Si-C and Si-J centers. These centers are made up of defects of a different kind in irradiated silicon—

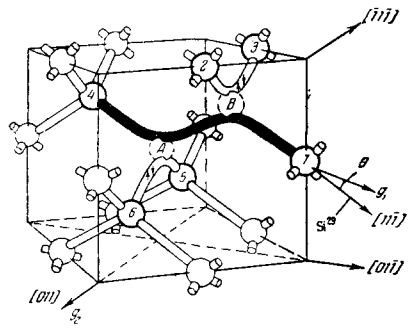

FIG. 24. Divacancy in silicon lattice. The vacancies are shown by dashed lines and are denoted A and B. The orbit on which the electron causing the EPR is situated is shown schematically by a thick black line. The arrow designated Si^{29} shows the axis of the hyperfine interaction with the Si^{29} nuclei.

divacancies consisting of two neighboring empty sites (designated A and B in Fig. 24). Investigations of samples irradiated at 20° K have shown[97] that the divacancy is a primary defect, which is stable at room temperature and is formed immediately upon irradiation. At an electron energy 1.5 MeV, the rate of divacancy formation is approximately 5% of the rate of vacancy formation, as determined from measurements on A centers. It has been observed that the rate of divacancy formation is anisotropic with respect to the direction of the electron flux. In p-type silicon, and in high-resistance n-type silicon, divacancies (Fig. 24) become paramagnetic and produce an EPR spectrum. The corresponding paramagnetic centers are called Si-J and Si-C centers. Their formation is explained in the following fashion. The broken bonds of atoms 5 and 6 and of atoms 2 and 3 (Fig. 24) join to form molecular bonds, and the corresponding electrons are paired. In p-type material, one of the two electrons corresponding to the broken bonds of atoms 1 and 4 goes over to the acceptor, while the remaining unpaired electron is on the orbit between these atoms (black line on Fig. 24) and produces an EPR spectrum (J-center). In this state the divacancy is a singly-ionized donor. The paramagnetic C-center is produced in high-resistance n-type silicon when an additional electron goes over to the divacancy. This electron is on a disintegrating orbit between atoms 1 and 4, and the corresponding binding orbit is filled. In this state, the divacancy is a singly-ionized acceptor. The C-center spectrum is not observed in low-resistance n-type silicon. This is due to the fact that in such a material the divacancy captures one more electron, i.e., becomes a double acceptor. The experimental EPR results which have made it possible to construct the Si-C and Si-J center models are given in[97]. The values of the coefficients η^2 show that in the case of J-centers ($\eta^2 = 0.56$) the disintegrating orbit constitutes only 56% of the wave function, while in the case of the J-center—62% ($\eta^2 = 0.62$). The ratio of the values of the coefficients α^2 and β^2 indicates that the wave function of the unpaired electron, especially for the J-center ($\alpha^2 = 0.16$, $\beta^2 = 0.84$), contains much more of the p-state than the tetrahedral sp^3 orbit. For the C-center we have $\alpha^2 = 0.22$ and $\beta^2 = 0.78$.

The thermally activated transition of an electron between equivalent configurations (see Fig. 24) was investigated for both centers by using EPR observations with the crystal deformed and by studying the line broadening. These experiments have confirmed the C- and J-center models. The activation energy of this motion is ~ 0.06 eV for both centers. The model was also confirmed by investigations of the preferred orientation of the vacancy-to-vacancy direction. The values of the preferred orientation, as well as the kinetics of the reorientation, are identical for both centers. The activation energy of the divacancy reorientation process is ~ 1.3 eV for both centers. This energy can be regarded as the activation energy for the divacancy diffusion. Experiments on the annealing of these centers have shown that the lowest binding energy of the divacancy is $\leq$ 1.5 eV, and that both vacancies diffuse together, the probability of their separation being relatively low.

2. EPR of Radiation Defects Produced by Bombarding Silicon with Fast Neutrons. Compared with electron-bombarded silicon, radiation defects in fast neutron bombarded silicons have been investigated little.

The first experiments on EPR in n- and p-type silicon bombarded with neutrons at room temperature[98] established no connection between the observed spectra and any concrete defects. Only in a recent communication[99] is there a report of a resonant spectrum in silicon bombarded by fast neutrons, due to a definite center called the Si-N center.

The exact structure of this center is still not clear. The experimental data in[99] permit only some assumptions to be made relative to the N-center model.

Bombardment of the crystal with fast neutrons gives rise to a series of all kinds of possible defects. (The total number of displaced atoms is ~ 20 per neutron-cm.) Fast-neutron bombardment increases the resistivity of n- and p-type samples to a value corresponding in the case of prolonged bombardment to the intrinsic conductivity, and the Fermi level shifts towards the middle of the forbidden band. The resonance signals produced were in the main very complicated, and most cases could not be resolved completely. However, none of the spectra produced by bombardment of silicon with 1.5-MeV electrons were observed in this case. The greater part of the investigations was devoted to samples whose resistivity was raised by irradiation to almost the intrinsic value. In these samples, the spectrum did not depend on the neutron dose, and the rate of center formation was 0.1 neutron-cm. Unlike silicon bombarded with electrons, the centers produced were not connected with the chemical impurity. In order to separate individual centers and by the same token simplify the spectrum, several experiments were made in which the investigated crystals

were heated. The resonant spectrum remaining after heating for two hours at 170°C and one-hour at 300°C, and left unaffected by further heating at higher temperatures, was investigated. This spectrum can be separated into two parts which differ in line intensity and in the character of the temperature dependence above room temperature. The more intense part of the spectrum was found to be due to a definite center, called the Si-N center. The EPR spectrum of the N-center was not observed in samples irradiated at 50°C but not heated[100]. Thus, the heating is essential for the formation of the N-center. The defect causing the resonance probably does not contain the impurity atom connected with it, since the N-center spectrum was observed in both chemically pure samples and in samples containing various amounts of different impurities, including oxygen. The EPR spectrum of the N-center was investigated at different temperatures. At room temperature this spectrum is described by the simple spin Hamiltonian

$$\mathcal{H} = \beta H_0 g S, \qquad (6.12)$$

where

$$S = 1/2 \quad \text{and} \quad g = g_1^2 \cos^2\theta_1 + g_2^2 \cos^2\theta_2 + g_3^2 \cos^2\theta_3. \qquad (6.13)$$

There are 24 different equivalent positions of the defect in the silicon lattice, with which 24 expressions of (6.13) can be connected. In accordance with this fact, the resonance spectrum for arbitrary magnetic-field orientation can consists of 24 lines. When the magnetic field is directed along one of the crystallographic axes, some lines (or even all) coincide. For example, for $H_0 \parallel [001]$ the spectrum consists of one line for which g_1 [$1\bar{1}0$] = 2.0126, g_2 = 2.0048, and g_3 = 2.0090.

The EPR spectrum of the N-center was investigated also at low temperatures. The relaxation time of the N center was measured at 77°K and found to be of the order of 10^{-4} sec. At 77 and 4°K it was possible to resolve the hyperfine interaction with the Si^{29} nuclei [in which connection a term IAS must be introduced into the Hamiltonian (6.12)], and an investigation of the hyperfine interaction has shown that at low temperatures the unpaired electron is localized near one silicon atom. The character of the symmetry of the hyperfine interaction and of the g-center indicates that the wave function of the unpaired electron has a slightly perturbed axial symmetry with principal axis along [111]. Accordingly, it can be represented by the free orbit remaining after the tetrahedral bond is broken. A theoretical estimate of this wave function, based on the molecular orbital method, yields $\eta^2 = 0.63$ and $\beta^2/\alpha^2 = 6.4$, i.e., the p-state admixture predominates in the part (63%) of the wave function under consideration.

The temperature dependence of the N-center spectrum was also investigated for different orientations of the magnetic field. The observed vanishing of certain fine-structure lines and the appearance of new lines in the N-center spectrum can be explained by assuming that as the temperature increases the electron is no longer localized on one of the sites, but "jumps" to some neighboring equivalent site within the confines of the defect. The electron cannot "jump" to any site, but only to one whose g-tensor axis has the same direction as the first site. As the temperature is raised above 100°K, the jumping rate increases and the electron becomes localized on two silicon atoms, so that new lines appear. The experiments have shown, however, that the thermally activated electron "jump" is not the only process causing the observed temperature dependence of the N-center. It has been suggested[99] that at T ~ 160°K another mechanism comes into play—thermal averaging of the lattice perturbations in the vicinity of the N-center. However, the existence of this mechanism has not yet been proved experimentally. Thus, whereas the measurements at low temperatures show that the unpaired electron is localized at these temperatures on one silicon atom and can be described by one free orbit, the results of the measurements of the temperature dependence of the spectrum allow us to assume that at higher temperatures the electron is localized on two silicon atoms, and its wave function is represented by two free orbits, for which the g-tensor axes have a definite orientation relative to one another. None of these experiments yielded an exact model of the Si-N center. The experimental temperature dependence agrees with a defect model either in the form of a single isolated vacancy, or a divacancy (Fig. 25). More complicated vacancy groups, which are produced under neutron bombardment, can likewise be identified with the N-center. The hyperfine interaction constants and the g-tensor of the N-center are very close to the corresponding characteristics of the B-center spectrum. However, an analysis of the experimental data shows that in spite of the fact that the N- and B-centers are each described (at T = 77°K) by one free orbit belonging to one silicon atom, these centers are undoubtedly connected with different defects.

3. Conclusion. Thus, the structure of the defect producing the N-center is still not clear, and its determination calls for additional experiments.

The structure and nature of the main centers pro-

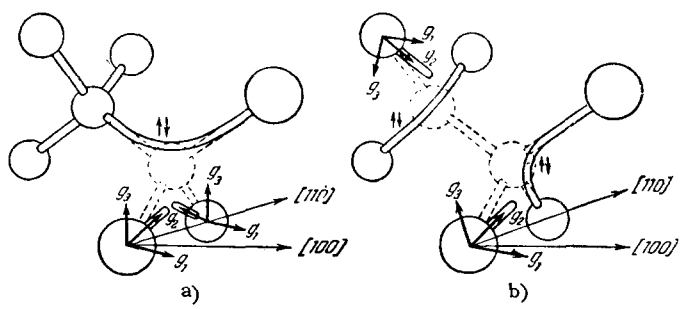

a) b)

FIG. 25. Possible model of Si-N center. a) Single vacancy; b) divacancy.

duced when silicon is bombarded with 1.5-MeV electrons have been investigated in sufficient detail; the Si-A and Si-E centers are each connected with a vacancy. Below room temperature the vacancies are mobile and can be captured by different chemical impurities, resulting in different centers. The activation energy of the vacancy motion is ~ 0.4 eV. The Si-J and Si-C centers are each connected with a divacancy, which is also a mobile defect. Its motion has an activation energy ~ 1.3 eV. The binding energy of the two vacancies forming the divacancy is not less than 1.5 eV. The divacancy is thus a stable defect which moves as one unit, with low separation probability.

[1] Portis, Kip, Kittel, and Brattain, Phys. Rev. **90**, 988 (1953).

[2] Fletcher, Yager, Pearson, Holden, Read, and Merrit, Phys. Rev. **94**, 1392 (1954).

[3] Fletcher, Yager, Pearson, and Merrit, Phys. Rev. **95**, 844 (1954).

[4] A. Honig and A. F. Kip, Phys. Rev. **95**, 1686 (1954).

[5] Feher, Gordon, Gere, and Thurmond, Phys. Rev. **109**, 221 (1958).

[6] Feher, Fletcher, and Gere, Phys. Rev. **100**, 1784 (1955).

[7] C. P. Slichter, Phys. Rev. **99**, 479 (1955).

[8] W. Kohn and J. M. Luttinger, Phys. Rev. **97**, 883 (1955).

[9] W. Kohn and J. M. Luttinger, Phys. Rev. **98**, 915 (1955).

[10] W. Kohn, Solid State Physics, vol. 5 (F. Seitz and D. Turnbull, ed.), New York, 1957.

[11] W. Kohn, Phys. Rev. **105**, 509 (1957).

[12] G. Feher, Phys. Rev. **114**, 1219 (1959).

[13] P. J. Price, Phys. Rev. **104**, 1223 (1956).

[14] G. Feher, Bell Syst. Techn. J. **36**, 449 (1957).

[15] A. M. Portis, Phys. Rev. **91**, 1071 (1953).

[16] G. W. Ludwig and H. H. Woodbury, Phys. Rev. **117**, 102 (1960).

[17] F. Bloch, Phys. Rev. 70, 460 (1946).

[18] A. M. Portis, Phys. Rev. **100**, 1219 (1955).

[19] M. Weger, Bell Syst. Techn. J. **4**, 1013 (1960).

[20] G. Feher, Phys. Rev. **114**, 1245 (1959).

[21] Rabi, Ramsey, and Schwinger, Revs. Mod. Phys. **26**, 167 (1954).

[22] G. Feher, Phys. Rev. **103**, 500 (1956).

[23] G. Feher, Phys. Rev. **103**, 501 (1956).

[24] J. Eisinger and G. Feher, Phys. Rev. **109**, 1172 (1958).

[25] F. M. Pipkin and J. W. Culvahause, Phys. Rev. **106**, 1102 (1957).

[26] Feher, Fuller, and Gere, Phys. Rev. **107**, 1462 (1957).

[27] R. G. Shulman and B. J. Wyluda, Phys. Rev. **103**, 1127 (1956).

[28] Macfarland, McLean, Quarington, and Roberts, Phys. Rev. **111**, 1245 (1958).

[29] D. K. Wilson and G. Feher, Phys. Rev. **124**, 1068 (1961).

[30] C. Herring and E. Vogt, Phys. Rev. **101**, 944 (1956).

[31] C. Herring, Bell Syst. Techn. J. **34**, 237 (1955).

[32] D. Long and J. Myers, Phys. Rev. **115**, 1119 (1959).

[33] L. M. Roth, Phys. Rev. **118**, 1534 (1960).

[34] H. Hasegawa, Phys. Rev. **118**, 1523 (1960).

[35] L. Liu, Phys. Rev. Letts. **6**, 683 (1961).

[36] W. Kohn, Phys. Rev. **97**, 869 (1955).

[37] F. Herman, Phys. Rev. **93**, 1214 (1954).

[38] F. Herman, Revs. Modern Phys. **30**, 102 (1958).

[39] J. C. Phillips, Phys. Rev. **112**, 685 (1958).

[40] H. J. McSkimin, J. Appl. Phys. **24**, 988 (1953).

[41] Feher, Wilson, and Gere, Phys. Rev. Letts. **3**, 25 (1959).

[42] R. E. Pontinen and T. M. Sanders, Phys. Rev. Letts. **5**, 311 (1960).

[43] R. W. Keyes and P. J. Price, Phys. Rev. Letts. **5**, 509 (1960).

[44] Feher, Hensel, and Gere, Phys. Rev. Letts. **5**, 309 (1960).

[45] A. Honig, Phys. Rev. **96**, 234 (1954).

[46] Pines, Bardeen, and Slichter, Phys. Rev. **106**, 489 (1957).

[47] E. Abrahams, Phys. Rev. **107**, 491 (1957).

[48] V. I. Avdeev, FTT **3**, 3480 (1961), Soviet Phys. Solid State **3**, 2525 (1962).

[49] R. L. Kroenig, Physica **6**, 33 (1939).

[50] I. Waller, Z. Physik **79**, 370 (1932).

[51] J. Bardeen and W. Shockley, Phys. Rev. **80**, 72 (1950).

[52] R. J. Elliott, Phys. Rev. **96**, 266 (1954).

[53] Winreich, Sanders, and White, Phys. Rev. **114**, 33 (1959).

[54] H. Fritsche, Phys. Rev. **115**, 336 (1959).

[55] J. H. Van Vleck, Phys. Rev. **57**, 426 (1940).

[56] A. Honig, E. Stupp, Phys. Rev. **117**, 69 (1960).

[57] F. M. Pipkin, Phys. Rev. **112**, 935 (1958).

[58] G. Feher, Physica **24**, 805 (1958).

[59] G. Feher and R. C. Fletcher, Bull. Amer. Soc., Ser. II, **1**, 125 (1956).

[60] A. Honig, Physica, Suppl. **24** (Sept. 1958).

[61] W. W. Tyler, H. H. Newman, and H. H. Woodbury, Phys. Rev. **98**, 461 (1955).

[62] W. W. Tyler, and H. H. Woodbury, Bull. Amer. Phys. Soc., Ser. II, **2**, 135 (1957).

[63] G. W. Ludwig and H. H. Woodbury, Bull. Amer. Phys. Soc., Ser. II, **3**, 135 (1958).

[64] G. W. Ludwig and H. H. Woodbury, Phys. Rev. **113**, 1014 (1959).

[65] H. H. Woodbury and G. W. Ludwig, Phys. Rev. Letts. **1**, 16 (1958).

[66] G. D. Watkins, Bull. Amer. Phys. Soc., Ser. II, **2**, 345 (1957).

[67] G. W. Ludwig and H. H. Woodbury, Phys. Rev. Letts. **5**, 98 (1960).

[68] G. W. Ludwig and H. H. Woodbury, Phys. Rev. **117**, 1287 (1960).

[69] Ludwig, Woodbury, and Carlson, J. Phys. Chem. Solids 8, 490 (1959).
[70] Woodbury, Carlson, and Ludwig, Bull. Amer. Phys. Soc. 4, 22 (1959).
[71] C. B. Collins and R. O. Carlson, Phys. Rev. 108, 1409 (1957).
[72] Ludwig, Carlson and Woodbury, Bull. Amer. Soc. 4, 22 (1959).
[73] G. W. Ludwig and H. H. Woodbury, Phys. Rev. **117**, 1286 (1960).
[74] Ludwig, Carlson, and Woodbury, Bull. Amer. Phys. Soc. 4, 144 (1959).
[75] N. B. Blombergen, Phys. Rev. Letts. 7, 90 (1961).
[76] G. W. Ludwig and H. H. Woodbury, Phys. Rev. Letts. 7 (1961).
[77] F. S. Ham, Phys. Rev. Letts. 7, 242 (1961).
[78] H. H. Woodbury and G. W. Ludwig, Phys. Rev. Letts. 5, 96 (1960).
[79] H. H. Woodbury and G. W. Ludwig, Bull. Amer. Phys. Soc. 5, 158 (1960).
[80] H. H. Woodbury and G. W. Ludwig, Phys. Rev. **126**, 466 (1962).
[81] G. W. Ludwig and H. H. Woodbury, Solid State Physics, vol. 13 (F. Seits, D. Turnbull, ed.), New York, 1962.
[82] E. Schulz-duBois, M. Nisenoff, H. Y. Fan, K. Lark-Horovitz, Phys. Rev. 98, 1561(a) (1955).
[83] G. Bemski, J. Appl. Phys. 30, 1195 (1959).
[84] Watkins, Corbett, and Walker, J. Appl. Phys. 30, 1198 (1959).
[85] G. D. Watkins and J. W. Corbett, Disc. Farad. Soc., No. 31, 86, (1961).
[86] Bemski, Feher, and Gere, Bull. Amer. Phys. Soc., Ser. II, **3**, 135 (1958).
[87] Watkins, Walker, and Corbett, Bull. Amer. Phys. Soc., Ser. II, 4, 159 (1959).
[88] G. D. Watkins and J. W. Corbett, Phys. Rev. **121**, 1001 (1961).
[89] G. K. Wertheim, Phys. Rev. **105**, 1730 (1957).
[90] G. K. Wertheim, Phys. Rev. **110**, 1272 (1958).
[91] Corbett, Watkins, Chrenko, and McDonald, Phys. Rev. **121**, 1015 (1961).
[92] H. H. James and K. Lark-Horowitz, Z. phys. Chem. **198** (1—4), 107 (1951).
[93] Hartree, Hartree, and Manning, Phys. Rev. 60, 857 (1941).
[94] R. G. Barnes and W. V. Smith, Phys. Rev. **93**, 95 (1954).
[95] Atomic Energy Levels (ed. by Moore), National Bureau of Standards, Circular No. 467, U. S. Gov. Printing Office, Washington, 1949.
[96] Mulliken, Rieke, Orloff, and Orloff, J. Chem. Phys. **17**, 1248 (1949).
[97] J. W. Corbett and G. D. Watkins, Phys. Rev. Letts. 7, 314 (1961).
[98] M. Nisenoff and H. Y. Fan, Bull. Amer. Phys. Soc., Ser. II, 4, 159 (1959).
[99] M. Nisenoff and H. Y. Fan, Phys. Rev. **128**, 1605 (1962).
[100] Wun Jung and G. S. Newell, Bull. Amer. Phys. Soc. 7, 186 (1962).

Translated by J. G. Adashko